Dissertation for Doctoral (PhD) Degree

University of Sopron

Faculty of Wood Engineering and Creative Industries

Cziráki József Doctoral School of Wood Sciences and Technologies

Head: Prof. Dr. László Bejó

THE EXAMINATION OF WOODEN PILES OF LAKE-BUILDINGS

Written by:

Brougui Marwa

Supervision:

Dr. Péter Szabó

Dr. habil. Krisztián Andor

Sopron, Hungary

2025

THE EXAMINATION OF WOODEN PILES OF LAKE-BUILDINGS

Dissertation for doctoral (PhD) degree

Written by:

Brougui Marwa

Made in the framework of the University of Sopron József Cziráki Doctoral School of Wood Sciences and Technologies …….…….... programme

Supervisor: Dr. Péter Szabó and Dr. habil. Krisztián Andor

I recommend for acceptance (yes / no) I recommend for acceptance (yes / no)

(signature) (signature)

Final debate:
As assessor I recommend the dissertation for acceptance:

First assessor (Dr. .....) yes/no ……..
(signature)

Second assessor (Dr. .....) yes/no ……
(signature)

(Possible third assessor (Dr. .....) yes/no ……
(signature)

The candidate reached .....% in the public debate of the dissertation

Sopron,

.....
Chairman of the Assessor Committee

Qualification of the doctoral (PhD) degree ….....

.....
Chairman of the University Doctoral
and Habilitation Council (UDHC)

DECLARATION

I, he undersigned Brougui Marwa by signing this declaration declare that my PhD thesis entitled **The examination of wooden piles of lake-buildings** was my own work; during the dissertation I complied with the regulations of Act LXXVI of 1999 on Copyright and the rules of the doctoral dissertation prescribed by the Cziráki József Doctoral School, especially regarding references and citations.[1]

Furthermore, I declare that during the preparation of the dissertation I did not mislead my supervisor(s) or the programme leader with regard to the independent research work.

By signing this declaration, I acknowledge that if it can be proved that the dissertation is not self-made or the author of a copyright infringement is related to the dissertation, the University of Sopron is entitled to refuse the acceptance of the dissertation.

Refusing to accept a dissertation does not affect any other legal (civil law, misdemeanour law, criminal law) consequences of copyright infringement.

Sopron, ... 2025

……..
PhD candidate

[1] **Act LXXVI of 1999** Article 34 (1) Anyone is entitled to quote details of the work, to the extent justified by the nature and purpose of the recipient work, by designating the source and the author specified therein.

Article 36 (1) Details of publicly lectures and other similar works, as well as political speeches, may be freely used for the purpose of information to the extent justified by the purpose. For such use, the source, along with the name of the author, shall be indicated, unless this is impossible.

Acknowledgements

The successful completion of this dissertation would not have been possible without the invaluable guidance, support, and encouragement of numerous individuals and institutions, to whom I hereby express my deepest gratitude.

At the outset, I wish to convey my sincere and profound appreciation to my supervisors, Dr. Andor Krisztián and Dr. Szabó Péter, whose expert guidance, constructive criticism, and steadfast encouragement have been indispensable throughout the entirety of my doctoral studies. Their distinguished scholarship, patience, and mentorship have fundamentally shaped the direction and quality of both my research and academic development.

I am also deeply grateful to my colleagues for their generous assistance, stimulating intellectual exchange, and willingness to share resources and expertise, all of which significantly enriched this research endeavor.

I extend my earnest thanks to Prof. Dr. Zsolt Kovács, the faculty members, instructors, and technical staff of the various laboratories at the University of Sopron. Their professional cooperation and technical support proved essential to the successful execution of the research presented in this work. Furthermore, I wish to acknowledge with gratitude the administrative staff of the University of Sopron for their consistent, efficient support in addressing the official and procedural matters encountered during my studies.

I also wish to express my sincere gratitude to Dr. Tahar Kouider of Robert Gordon University, Scotland, UK, for his invaluable support and guidance throughout my research.

My appreciation further extends to the Hévíz Therapeutic Center, whose personnel graciously provided a conducive environment and appropriate facilities, thereby facilitating the experimental component of this dissertation.

I am also indebted to the Tempus Public Foundation for the financial support rendered through the Stipendium Hungaricum Scholarship (2021), without which the pursuit and completion of my doctoral studies would not have been feasible. Additionally, I wish to express my sincere gratitude to the Algerian Ministry of Higher Education for their continued support throughout my academic journey.

Finally, I wish to express my heartfelt thanks to my family, particularly my beloved mother, and to my friends, whose unwavering love, patience, and encouragement have sustained and motivated me throughout the many challenges of this doctoral journey.

Table of Contents

List of Figures

List of Tables

List of Abbreviations

ASTM	American Society for Testing and Materials
COMSOL	Commercial software for finite element analysis
FEM	Finite Element Modeling
FSP	Fiber Saturation Point
GPR	Ground Penetrating Radar
HF	Hertz Frequency
LMH	Longitudinal Modulus of Elasticity (MOE)
MC	Moisture Content
MOE	Modulus of Elasticity
MSZ EN 338	Hungarian Standard - Structural Timber Strength Classes
NDT	Non-Destructive Testing
NDE	Non-Destructive Evaluation
RT	Radial-Tangential (direction in wood)
TOF	Time of Flight
UT	Ultrasonic Testing

List of Notations

v	Ultrasonic wave velocity (m/s)
L	Length of pile (m)
t or T	Time of flight (wave transit time) (s)
E_{dyn}, E_L	Dynamic modulus of elasticity (longitudinal) (MPa)
ρ	Density (kg/m³)
I	Moment of inertia of cross-section (m⁴)
P_{cr}	Critical buckling load (N or kN)
K	Effective length factor (boundary-condition dependent)
ν_{xy}	Poisson's ratio (subscripts denote directions, e.g., longitudinal–radial ν_{LR})
E_R	Radial elastic modulus (MPa)
E_T	Tangential elastic modulus (MPa)
λ	Load ratio (design-to-capacity ratio)
P	Applied axial load (N or kN)
u_y	Vertical displacement boundary condition (m)
v_L	Longitudinal ultrasonic wave velocity (m/s)
vτ	Shear wave velocity (m/s)
C_D	Dynamic longitudinal stiffness coefficient (Pa or MPa)
G_D	Dynamic shear modulus (Pa or MPa)
PL	Pulse length (ultrasonic signal parameter) (time × voltage²)
IL	Insertion loss (ultrasonic parameter) (dB)
σ	Mechanical stress (axial or bending) (MPa)
δ, d	Lateral displacement (m)

E_{mod}	Modulus of elasticity (general) (MPa)
MC	Moisture content (percentage by dry weight) (%)
FSP	Fiber saturation point (moisture content threshold) (%)
τ	Time constant or characteristic time interval in ultrasonic signal (s)
θ	Grain orientation or wave propagation angle (° or rad)
ν_{MC}	Poisson's ratio at moisture content MC
C_{ν}	Moisture correction factor for Poisson's ratio
Δt	Signal time interval or duration (s)
$E_{95\%}$	95th percentile modulus of elasticity (MPa)
PL_{RT}	Pulse length in radial–tangential direction (time × voltage²)

Abstract

This doctoral research presents a comprehensive investigation into the structural integrity and buckling behavior of submerged timber piles used in lacustrine construction, with emphasis on heritage piles in Hévíz Lake, Hungary. These piles are subjected to long-term immersion in thermally elevated, mineral-rich waters that accelerate biological and chemical degradation, resulting in reductions in stiffness and load-bearing capacity. To address these challenges, the study develops an integrated assessment methodology combining in-situ ultrasonic non-destructive testing (NDT), machine-learning–assisted data interpretation, analytical modeling, and orthotropic finite element simulations. Ultrasonic testing was conducted to measure longitudinal and radial–tangential wave velocities, which were subsequently processed through MATLAB R2023a to derive the dynamic modulus of elasticity (MOE) and to support predictive modeling. Analytical evaluations using Euler–Bernoulli beam theory were employed to estimate critical buckling loads, while orthotropic finite element modeling (FEM) in COMSOL Multiphysics captured submerged and soil-embedded boundary effects with higher fidelity. To situate the research within the broader scientific landscape, a bibliometric analysis was performed to map trends, influential contributions, and existing gaps in submerged timber pile research, guiding both methodological development and scientific contextualization. The results demonstrate an almost perfect linear correlation ($r = 0.998$) between longitudinal ultrasonic velocity and dynamic MOE, confirming ultrasonic NDT as a robust indicator of internal stiffness and structural integrity in submerged timber elements. Building upon this relationship, a predictive buckling model integrating ultrasonic velocity with geometric parameters achieved high accuracy ($R^2 = 0.943$), representing the first field-validated correlation directly linking ultrasonic measurements to buckling stability in long-term submerged heritage piles. Analysis further shows that pile length is the dominant factor governing critical buckling load ($r = –0.73$), while ultrasonic-derived MOE provides a secondary but meaningful contribution ($r = 0.43$), particularly for intermediate-length piles (10–15 m) where stiffness variability significantly influences stability. Comparison of classical Euler–Bernoulli and Granholm-corrected formulations revealed negligible deviation (0.05%), supporting the use of classical beam theory for slender submerged piles. Integrating ultrasonic-based material parameters with geometric characteristics enables reliable, non-destructive prediction of structural stability in submerged timber infrastructure. The research also identifies key limitations in the ASTM D2555 ultrasonic classification system, notably its inability to detect early-stage decay or subsurface defects when ultrasonic velocities remain elevated. A proposed dual-parameter diagnostic framework—combining ultrasonic velocity with dynamic MOE—significantly improves detection sensitivity and accuracy. When further coupled with pile length, the method provides refined risk categorization consistent with observed field deterioration. FEM simulations exhibited strong agreement with ultrasonic-based analytical predictions (correlation coefficient = 0.9998; mean deviation < 5%), confirming the robustness of the integrated methodology. Nonlinear finite element analyses revealed that lateral instability initiates at a reduced load factor ($\lambda \approx 0.8$), preceding classical ultrasonic-based predictions at $\lambda = 1$. This early onset is attributed to nonlinear growth in bending stresses and displacements influenced by geometric imperfections, heterogeneous stiffness fields, and soil–structure interactions. These findings highlight the limitations of purely linear elastic or ultrasonic-based approaches and underscore the necessity of advanced nonlinear modeling to accurately characterize pre-buckling behavior and failure mechanisms. Overall, this dissertation delivers a scien-

tifically rigorous and practically applicable framework for the non-destructive structural assessment of submerged timber piles. The integrated approach advances structural health monitoring, supports targeted maintenance and conservation strategies, and contributes to the sustainable management of heritage aquatic timber infrastructure.

Absztrakt

Ez a doktori kutatás átfogó vizsgálatot nyújt a víz alatti faoszlopok szerkezeti integritásáról és hajlítási viselkedéséről, amelyek tavakban történő építkezés során kerülnek alkalmazásra, különös tekintettel a magyarországi Hévízi-tó örökségi faoszlopaira. Ezek az oszlopok hosszú távon termikusan megnövelt, ásványianyag-tartalmú vizekben merülnek el, amelyek felgyorsítják a biológiai és kémiai lebomlási folyamatokat, a rugalmasság és teherbírás csökkenését eredményezve. A kutatás egy integrált értékelési módszertant dolgoz ki, amely egyesíti a helyszíni ultrahangos nemroncsoló vizsgálatot (NDT), a gépi tanulást alkalmazó adatértelmezést, az analitikus modellezést és az ortotróp véges elem szimulációkat. Az ultrahangos vizsgálatok során hosszanti és sugárirányú–tangenciális hullámsebességeket mértek, amelyeket a MATLAB R2023a programmal dolgoztak fel a dinamikus rugalmassági modulus (MOE) meghatározására és előrejelző modellezés támogatására. Az Euler–Bernoulli gerendamodell analitikus kiértékeléseit a kritikus hajlítási teher becslésére alkalmazták, míg az ortotróp véges elem modellezés (FEM) a COMSOL Multiphysics használatával pontosabban megragadta a víz alatti és talajba ágyazott határokat. A kutatás tudományos környezetbe helyezéséhez bibliometriai elemzést végeztek, amely feltérképezte az iparági trendeket, meghatározó hozzájárulásokat és a faoszlopok víz alatti kutatásának meglévő hiányosságait, segítve a módszertani fejlesztést és a tudományos kontextualizációt. Az eredmények közel tökéletes lineáris korrelációt mutatnak ($r = 0{,}998$) a hosszanti ultrahangsebesség és a dinamikus MOE között, megerősítve az ultrahangos NDT megbízhatóságát a faoszlopok belső merevségének és szerkezeti integritásának jelzőjeként. E kapcsolatra építve egy előrejelző hajlítási modell ultrahang sebességet és geometriai paramétereket integrálva magas pontosságot ($R^2 = 0{,}943$) ért el, amely az első terepi validációjú korreláció az ultrahangos mérések és a tartósan víz alatt lévő örökségi oszlopok hajlítási stabilitása között. Elemzés kimutatta, hogy az oszlop hossza a kritikus hajlítási teher fő meghatározója ($r = -0{,}73$), míg az ultrahang alapján származtatott MOE másodlagos, de jelentős hatással bír ($r = 0{,}43$), különösen a középhosszú (10–15 m) oszlopok esetén, ahol a merevség változékonysága jelentősen befolyásolja a stabilitást. A hagyományos Euler–Bernoulli és Granholm-korrekcióval ellátott formulációk összehasonlítása elhanyagolható eltérést (0,05%) mutatott, támogatva a klasszikus elmélet használatát a vékony víz alatti oszlopok esetében. Az ultrahang alapú anyagtulajdonságok és geometriai jellemzők integrálása megbízható, nem romboló jellegű stabilitás-előrejelzést tesz lehetővé a víz alatti faoszlop-infrastruktúráknál. A kutatás feltárta az ASTM D2555 ultrahangos minősítési rendszer kulcsfontosságú korlátait, különösen az ultrahang sebesség magas értékei esetén az idő előtti korhadás vagy a felszín alatti hibák kimutatásának képtelenségét. Egy javasolt kétparaméteres diagnosztikai keretrendszer – amely az ultrahang sebességet a dinamikus MOE-vel kombinálja – szignifikánsan javítja a detektálási érzékenységet és pontosságot. Az oszlophossz további bevonásával a módszer finomított kockázati kategorizálást biztosít, amely összhangban van a terepi károsodás megfigyeléseivel. A FEM szimulációk erős egyezést mutattak az ultrahang alapú analitikus előrejelzésekkel (korrelációs együttható = 0,9998; átlagos eltérés < 5%), megerősítve az integrált módszertan megbízhatóságát. Nemlineáris véges elem analizisek kimutatták, hogy az oldalsó instabilitás egy csökkentett teherfaktor ($\lambda \approx 0{,}8$) mellett indul, megelőzve a klasszikus ultrahang-alapú előrejelzéseket ($\lambda = 1$). Ez a korai kezdet a hajlítási feszültségek és elmozdulások nemlineáris növekedésének tulajdonítható, amelyet geometriai tökéletlenségek, heterogén merevségértékek és talaj–szerkezet kölcsönhatások befolyásolnak. E megállapítások rámutatnak a tisztán lineáris rugalmas vagy ultrahangos alapú megközelítések korlátaira, és hangsúlyozzák az előbuckling viselkedés és a károsodási mechanizmusok pontos jellemzéséhez szükséges fejlett nemlineáris

modellezés fontosságát. Összességében ez a disszertáció tudományosan megalapozott és gyakorlati alkalmazhatóságot biztosító keretrendszert nyújt a víz alatti faoszlopok nem romboló jellegű szerkezeti állapotértékeléséhez. Az integrált megközelítés elősegíti a szerkezeti egészségmegfigyelést, támogatja a célzott karbantartási és megőrzési stratégiákat, valamint hozzájárul az örökségi vízi fa infrastruktúra fenntartható kezeléséhez.

CHAPTER I: INTRODUCTION AND LITERATURE REVIEW

1.1 Problem statement, Potentiality, Gaps

Wooden piles have been integral to lake-based construction for centuries, serving as foundational supports for structures such as docks, piers, bridges, and elevated platforms (Bouras et al., 2010; Kromoser et al., 2024; J. Zhang et al., 2011). These piles are subjected to a combination of environmental factors (e.g., wave action, wind, hydrodynamic pressures) and mechanical stresses from imposed loads (Kotzamanis & Kalliontzis, 2023; M. Li et al., 2023; Yazdani et al., 2020). Their effectiveness relies heavily on inherent material properties, such as a high strength-to-weight ratio, elasticity, and resilience under both compressive and tensile loading.

However, submerged piles are vulnerable to degradation through biochemical decay (e.g., fungal and bacterial activity), mechanical erosion, and physicochemical transformations (e.g., waterlogging and lignin leaching). These processes lead to significant reductions in material properties (e.g., density, elastic modulus, and tensile strength), which in turn compromise their stability and load-bearing capacity (Jingran et al., 2014; Klaassen, 2014; Martín & López, 2023; Z. Yang et al., 2010). Additionally, the susceptibility of these piles to buckling failure under axial loads remains a critical concern, especially for slender, load-bearing elements subjected to cyclic or fluctuating loads prevalent in aquatic environments (Hassan & Osama A.B, 2021; Kumar et al., 2015; Vukelic et al., 2017).

The heterogeneous nature of wood, along with its exposure to aquatic environments, complicates the assessment of pile stability. Traditional evaluation methods, such as destructive core sampling, are often impractical and costly, especially for in-situ submerged piles(French & Whittaker, 2023; T. Liu et al., 2024; Rajagopalam & Prakash, 1975).

Non-destructive testing (NDT) techniques, especially ultrasonic testing, offer a promising alternative by enabling non-invasive assessment of material integrity and detection of internal defects (Lian et al., 2024; Linpei, 2024; Radha et al., 2021; Tenoudji et al., 2016; Xue et al., 2024). Despite its potential, the application of ultrasonic testing to submerged wooden piles is underexplored. Critical gaps remain in understanding how ultrasonic wave velocity correlates with mechanical properties and how these measurements translate to real-world performance under dynamic loading conditions.

A bibliometric analysis conducted as part of this research (Brougui et al., 2025) substantiates these limitations, revealing that current studies predominantly focus on terrestrial timber or laboratory-scale samples. Systematic investigations of full-scale submerged piles are scarce, and the complex relationships between ultrasonic wave velocity, progressive material degradation, buckling susceptibility, and other mechanical properties are yet to be clearly defined. Furthermore, the influence of environmental parameters—such as high moisture content, saturation levels, and long-term aquatic exposure—on ultrasonic measurements and pile stability remains insufficiently addressed.

To address these gaps, this study systematically investigates the interrelationships among ultrasonic wave velocity, dynamic modulus of elasticity, and the critical buckling load of submerged timber piles. By integrating pile geometry, material degradation, and site-specific environmental factors, the research develops a robust, non-destructive evaluation framework. This framework synergistically combines ultrasonic testing with advanced three-dimensional finite element modeling (FEM) in COMSOL Multiphysics, explicitly incorporating anisotropic wood properties, soil–pile interactions, and submerged boundary conditions, alongside predictive analytical approaches.

Ultimately, the combined experimental and computational methodology aims to enhance the accuracy of structural assessments, establish reliable indicators of pile stability, and inform data-driven maintenance and conservation strategies. These advances will support the extension of service life for submerged timber infrastructure and guide the preservation and safe management of both modern wooden constructions and culturally significant heritage sites.

1.2 Bibliometric Analysis of Timber Mechanical Property Evaluation Research

To systematically delineate the current research landscape and identify critical knowledge gaps in timber mechanical property assessment via non-destructive testing (NDT), a comprehensive bibliometric analysis was conducted (Brougui et al., 2025). This review encompassed 129 peer-reviewed articles indexed in the Scopus database, with a primary focus on ultrasonic wave–based NDT techniques for estimating key mechanical properties, particularly the modulus of elasticity (MOE), in timber structures.

The bibliometric results indicate a steady increase in research output from the early 2000s, with a marked acceleration post-2016, reflecting growing scientific interest in advanced diagnostic methodologies for timber. Thematic analysis revealed that the dominant research cluster centers on “non-destructive testing,” underscoring the sustained emphasis on evaluating structural integrity without material compromise.

Using the bibliometric mapping tool VOSviewer, the analysis delineated seven primary thematic clusters within the literature. These clusters represent concentrated research foci encompassing mechanical characterization of timber, ultrasonic wave propagation mechanisms, the influence of moisture and environmental conditions, quality control methodologies, and hybrid diagnostic approaches (Figure 1.1). The consistent prominence of the keyword “non-destructive examination” reaffirms the centrality of NDT modalities in current timber research.

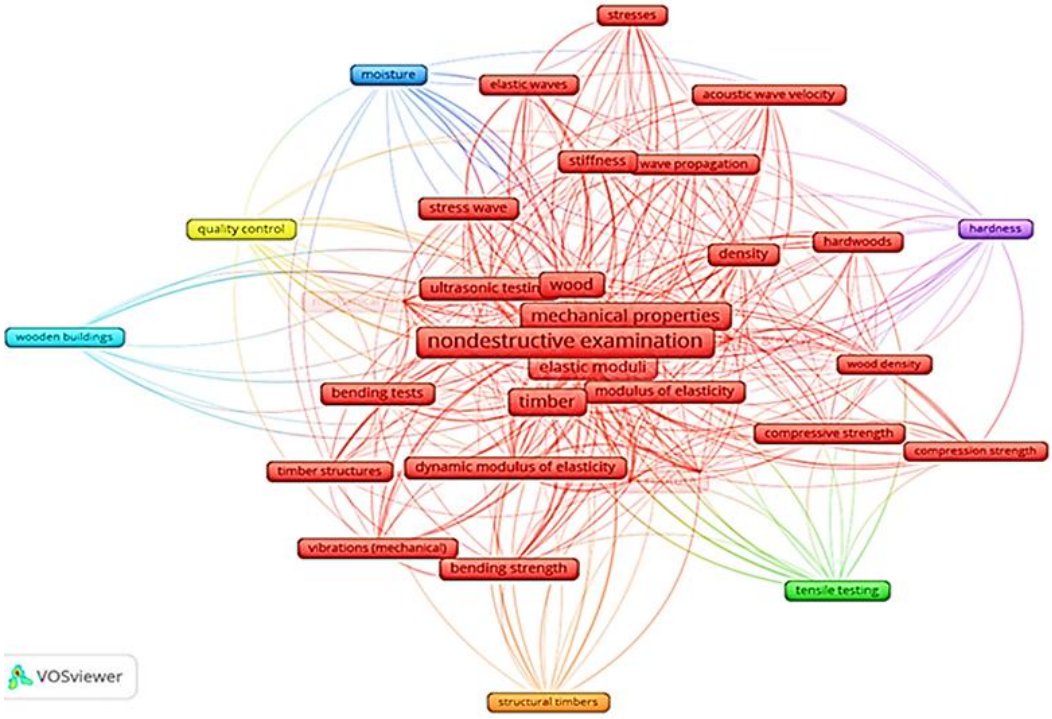

Figure 1. 1 Visualization of VOSviewer on the topics of 'wood' OR 'Timber' AND 'non-destructive testing methods' AND 'mechanical properties'(Brougui et al., 2025).

Despite the expanding literature, several limitations are evident. First, most investigations are confined to terrestrial samples or controlled laboratory conditions, constraining their applicability to in-situ submerged timber piles, which are subject to prolonged water immersion, temperature fluctuations, and biological degradation. Second, the quantitative relationship between ultrasonic wave velocity, progressive material degradation, buckling susceptibility, and other mechanical properties remains inadequately characterized. Although ultrasonic velocity is recognized as a sensitive indicator of stiffness and defect presence, its predictive accuracy is modulated by factors such as moisture content, fiber orientation (anisotropy), and internal decay. Furthermore, the dynamic interplay between material deterioration and structural stability, particularly axial buckling resistance, has not been systematically examined in submerged conditions, highlighting the necessity for integrated experimental and computational analyses.

An additional challenge is the lack of standardized ultrasonic NDT protocols for timber. Substantial variability exists in testing procedures, frequency ranges, and data interpretation methods, limiting cross-study comparability and reducing diagnostic reliability, particularly under variable environmental conditions.

The bibliometric mapping further highlights underexplored but promising avenues for future research. These include:

1. Integration of machine learning algorithms with ultrasonic data to enhance predictive modeling of timber mechanical performance.

2. Development of hybrid diagnostic frameworks, combining ultrasonics with complementary NDT techniques such as acoustic emission and vibration analysis.
3. Application to aged, recycled, or heritage timber, which remains underrepresented despite its practical significance.
4. Validation through computational modeling, particularly finite element modeling (FEM), which enables robust simulation of timber's anisotropic and heterogeneous behavior under varying environmental and loading conditions. Coupling experimental ultrasonic measurements with FEM facilitates more accurate correlation of ultrasonic velocities with mechanical properties and failure modes such as buckling, reduces interpretive uncertainty, and enhances predictive reliability for submerged timber structures.

In summary, this bibliometric analysis not only maps the evolution and thematic focus of ultrasonic NDT research in timber engineering but also delineates four critical gaps: (1) restricted field applicability to submerged timber piles, (2) insufficient characterization of the relationship between ultrasonic velocity and buckling resistance, (3) absence of standardized testing protocols, and (4) limited integration of experimental ultrasonic data with computational modeling and hybrid diagnostic approaches. Addressing these gaps underpins the rationale of the present dissertation, which aims to develop comprehensive, field-applicable ultrasonic testing and modeling strategies for submerged timber piles, thereby advancing sustainable management, structural preservation, and safety assessment of timber infrastructure.

1.3 Thematic literature review

1.3.1 Wooden Piles in Lake-Building Construction

In lake construction, wooden piles serve as fundamental load-bearing elements, transferring structural loads to stable soil or sediment layers beneath the water bodies. This load transfer ensures the durability and resilience of foundations against environmental challenges such as shifting lakebeds and fluctuating water levels (Ceccato et al., 2013; Treu et al., 2019). The use of wooden piles in aquatic structures— including piers, docks, bridges, and elevated platforms—stems from wood's natural abundance, versatility, and favorable mechanical properties (Bouras et al., 2010; Chauhan & Sethy, 2016; Kromoser et al., 2024; J. Zhang et al., 2011).

Compared to alternative materials such as concrete and steel, wooden piles offer greater flexibility, which makes them particularly suitable for unstable or shifting soils. This inherent flexibility enables wooden piles to accommodate lakebed movements, absorb stresses generated by changes in water levels, and thus reduce the risk of structural failure (Chawhan, 2012).

The performance of wooden piles depends on their capacity to sustain both vertical and lateral loads. Vertical loads primarily derive from the weight of the supported structure, whereas lateral loads result from environmental forces such as wave action, water currents, and soil displacement. Together, these dynamic forces impose significant stresses on the piles, demanding high structural resilience to maintain long-term stability (Gerolymos et al., 2014; Ghosh et al., 2023; Stalin et al., 2021; J.-W. G. ; Van De Kuilen et al., 2024).

Over time, however, biological decay and degradation processes gradually diminish the load-bearing capacity of submerged wooden piles, threatening the integrity of the supported structures (Björdal & Dayton, 2020; Elam & Björdal, 2020; Irbe et al., 2019).

Among the various failure modes that can compromise structural integrity, buckling represents a significant risk for slender columns subjected to compressive loads. This phenomenon, characterized by axial compressive forces causing sudden lateral deformation, can lead to catastrophic structural failure. Buckling is particularly concerning slender, load-bearing wooden piles subjected to cyclic or fluctuating loads, conditions prevalent in aquatic environments (Hassan & Osama A.B, 2021; Kumar et al., 2015; Vukelic et al., 2017).

1.3.2 Factors Influencing the Structural Stability and Decay Severity of Timber Piles

The stability and decay susceptibility of timber piles are influenced by a complex interaction of material, environmental, and structural factors. Understanding these influences is critical for accurately assessing pile performance and longevity in aquatic and soil environments.

Structural and Geotechnical Factors

Buckling resistance is a primary mode of failure considered in the structural assessment of slender timber piles subjected to axial compressive forces. When axial loads exceed the pile's critical buckling strength, the pile may experience sudden lateral deflections and catastrophic failure (Hasan, 2019a; Kumar et al., 2015). The critical buckling load depends on several interrelated factors.

Pile diameter substantially affects buckling resistance by influencing the moment of inertia of the cross-section. Larger diameters increase flexural stiffness, thereby elevating the critical buckling load. For instance, Shan et al. (2022) demonstrated that, at a constant excavation depth of 1 m, increasing the pile diameter from 250 mm to 300 mm increased the critical top load by approximately 94% (Fig1.2). This relationship is well supported by multiple studies (J. Liu et al., 2020; R. Zhang et al., 2021a), reinforcing the importance of cross-sectional size and shape on pile stability.

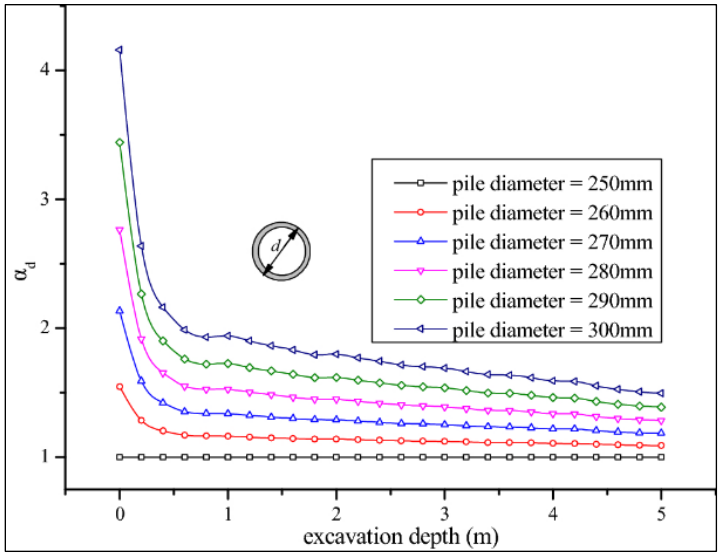

Figure 1. 2 Influence of pile diameter on the critical load at different excavation depths (Shan et al., 2022).

Conversely, pile length exerts an inverse effect on buckling resistance. Hasan (2019) reported that longer piles possess significantly lower critical buckling loads due to increased flexibility and lateral deflections under axial loading, which reduce their load-bearing capacity and buckling resistance. Specifically, increasing the freestanding length of a pile from 2.5 meters to 5.0 meters decreases the critical buckling load by approximately 32.5%. These observations underscore the critical importance of pile length as a key geometric parameter influencing structural stability.

The superior buckling resistance associated with larger diameter and shorter length is further supported by studies emphasizing the advantages of circular pile cross-sections, which offer uniform stiffness distribution (Fenu et al., 2021; Shatri et al., 2013). Standard timber pile diameters are typically between 8 and 18 inches, with Class A piles for heavy loading requiring a minimum diameter of 14 inches as per ASTM standards (Buddy & Showalter, 2012).

Pile length further influences buckling capacity, with shorter piles exhibiting higher critical buckling loads due to reduced effective length and slenderness ratio (Karampour et al., 2020; Tabarestani & Naghipour, 2022). This relationship, predicted by Euler's buckling theory, indicates that even modest reductions in pile length can significantly increase stiffness and lateral load resistance (Fernández-Escobar et al., 2023; Giese et al., 2023; Jais et al., 2024). However, pile length is also constrained by species-specific mechanical properties. For example, *Southern Yellow Pine* piles typically extend up to 70 feet, whereas *Douglas Fir* piles can reach lengths of 120 feet (Buddy & Showalter, 2012; James G. Collin, 2016), illustrating that both geometric factors and material strength must be considered together in evaluating buckling performance.

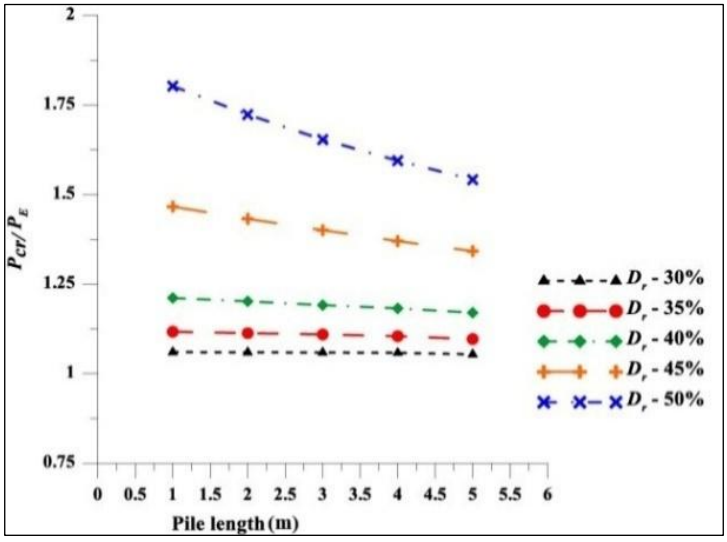

Figure 1. 3 Effect of pile length on critical load across various soil deposits (Praveen & Suresh, 2021).

Lateral support from surrounding soil is another critical determinant of buckling performance. Zhang et al. (2021) report that when embedment depth exceeds 60% of the pile length, the critical buckling load improves appreciably due to enhanced lateral restraint from soil-pile interaction. Conversely, in liquefiable soils, buckling capacity declines exponentially with increasing freestanding pile length, emphasizing the importance of soil characteristics in pile design (Fig1.3) (Praveen & Suresh, 2021).

Boundary conditions markedly influence the buckling behavior and stability of timber piles by altering their effective length and, consequently, their critical buckling load. Constraints applied at the pile's head and base modify the pile's structural response to axial loads (Fig. 1.4) (Gally et al., 2018).

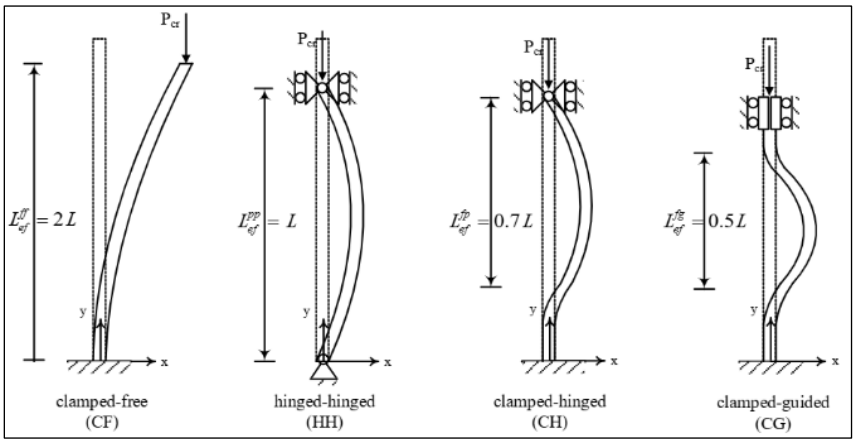

Figure 1. 4 Influence of Support Conditions on Buckling piles (Gally et al., 2018).

Research indicates that free-top piles exhibit lower critical buckling loads compared to pinned or fixed-top piles (Gabr et al., 1997). Fixed-head piles restrain rotation at the head and typically increase critical buckling loads by 20–50% relative to pinned-head piles, especially for longer piles (Hasan, 2019). For instance, a 48-ft fixed-head pile showed significantly higher buckling capacity than an equivalent pinned pile (N. C. Yang, 1966). Load transfer mechanisms—including frictional resistance and end-bearing behavior—further influence the pile's capacity to resist buckling by altering axial load distribution and lateral support characteristics (Hasan, 2019).

The dynamic modulus of elasticity (MOE) reflects material stiffness under fluctuating and dynamic load conditions, making it a vital factor in evaluating timber pile performance in aquatic environments (Chauhan & Sethy, 2016; Dahle et al., 2016; Giaccu et al., 2017). Euler's buckling theory links the critical buckling load directly to flexural rigidity (EI), where E is the elastic modulus and I is the moment of inertia. Materials exhibiting higher MOE values demonstrate increased load-bearing capacity and resilience against buckling failure (Budig & Mlote, 2022; S. Sharma & Bhandari, 2021; F. Wang & Sigmund, 2023).

Figure 1.5 illustrates the relationship between stress and strain during elastic buckling, showing how greater MOE enhances resistance to compressive forces without permanent deformation (Pattillo, 2018).

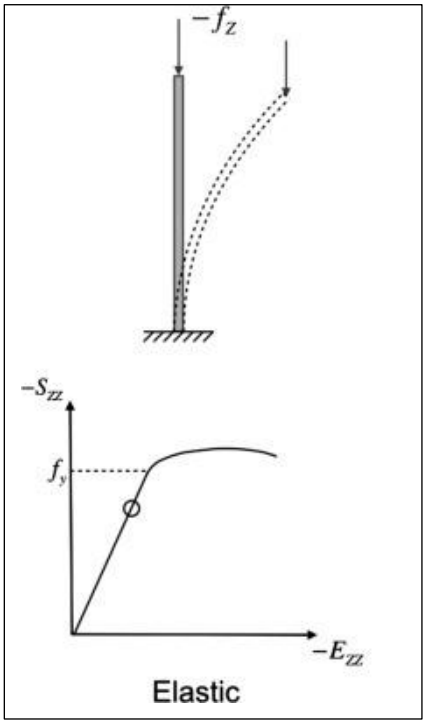

Figure 1. 5 Column Buckling and Material Elasticity (Pattillo, 2018).

Material Factors

The stability and decay resistance of submerged timber piles depend greatly on wood species, as different species exhibit distinct properties affecting performance in aquatic environments. Hardwoods such as oak, larch, and chestnut are preferred for submerged piles due to their high strength-to-weight ratios, natural decay resistance, and durability in waterlogged conditions (Koch et al., 2018; Lynes & Mamaghani, 2021). These species contain elevated levels of lignin, resins, and extractives, which enhance structural rigidity, dimensional stability, and long-term resistance to biological degradation (Deb & Roy, 2021; Santos et al., 2012). Softwoods, though generally less durable, are utilized due to favorable mechanical properties, cost-effectiveness, and broad availability. Their higher permeability and lower extractive content make them more susceptible to decay; however, in submerged anaerobic environments, decay processes slow considerably, allowing softwoods to maintain integrity under specific conditions (Martín & López, 2023; Milke et al., 2010; Morris, 1998; N'Guessan et al., 2023).

Wood properties vary between species and within individual trees, impacting strength and longevity in submerged conditions. Critical distinctions include sapwood versus heartwood, juvenile versus mature wood, and earlywood versus latewood (Gerhards, 1982). Among these, differences between sapwood and heartwood are particularly influential for degradation resistance, mechanical strength, and durability (Fig. 1.6).

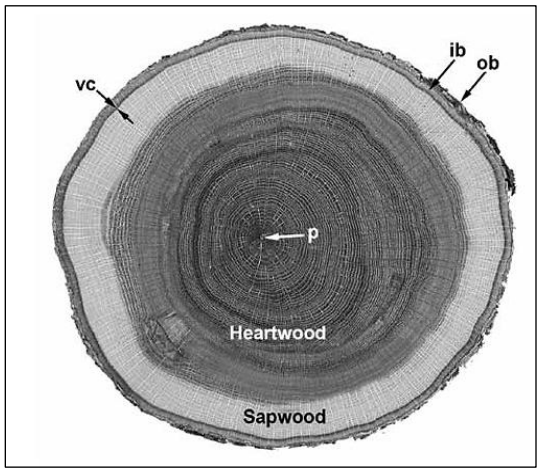

Figure 1. 6 Macroscopic view of a transverse section of a Quercus alba trunk (Forest Products Laboratory - USDA, 2010).

Sapwood, comprising the outer living layers of the tree, has higher moisture content and permeability, making it more vulnerable to decay by fungi, bacteria, and marine borers (Bamber & Fukazawa, 1985; Forest Products Laboratory - USDA, 2010). Over time, sapwood transitions into heartwood through parenchyma cell death and deposition of extractives that boost decay resistance and darken the wood (Taylor et al., 2002). Heartwood exhibits significantly lower permeability and greater resistance to biological degradation, making it the preferred material for submerged piles (Githiomi, J K; Dougal, 2012; J. Wang & DeGroot, 1996). Some species like *Norway spruce* (*Picea abies*) show minimal difference between sapwood and heartwood in decay resistance, underscoring the importance of species selection (Sandberg, 2009).

In addition, Sapwood degrades relatively quickly upon exposure, while heartwood deterioration is delayed, with decay onset estimated around 30 years post-submersion (Giuliana Zelada-Tumialan, 2014) (Fig. 1.7). Bacterial decay progression tends to slow significantly once the decay front reaches heartwood, suggesting a natural limit to cross-sectional degradation, allowing residual heartwood to provide structural support over extended periods depending on mechanical loading (Wang et al., 2008).

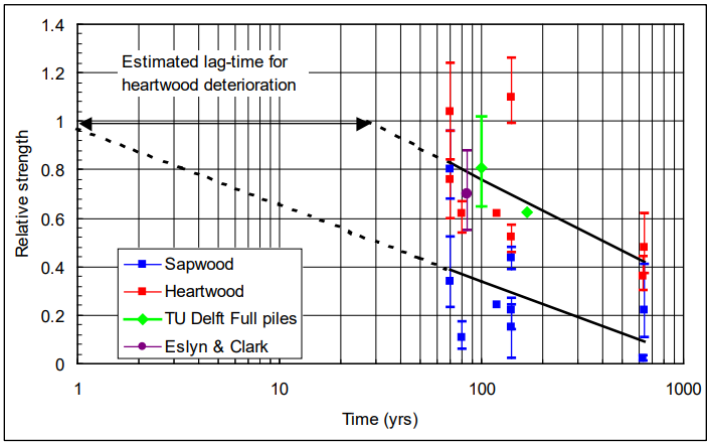

Figure 1. 7 Deterioration of sap and heartwood as a function of age deterioration (Giuliana Zelada-Tumialan, 2014).

Over time, submerged timber piles experience notable declines in compressive strength, closely correlated to the proportion of heartwood present. Piles with higher heartwood-to-sapwood ratios preserve structural stability longer, making them ideal for long-term aquatic foundations (Lynes & Mamaghani, 2021b; Q. Yang et al., 2022). (J. W. van de Kuilen et al., 2021; J. W. G. Van De Kuilen, 2007) found that submerged piles lose compressive strength at an approximate rate of 0.3% per year under load, with residual strength proportional to heartwood cross-sectional area. Heartwood retains approximately 50% of its compressive strength after 300 years, whereas sapwood degrades much faster (see, Fig. 1.8).

Sustained loads exceeding 55% of short-term strength induce creep deformation and potential failure, especially in sapwood-rich sections. However, heartwood's dominant structural role (>90% load bearing) mitigates creep risks (Holzer et al., 1989; P.Morlier, 1994).

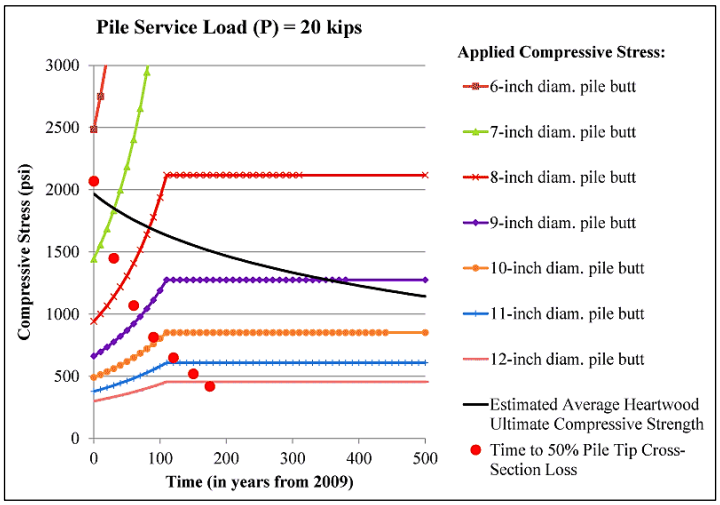

Figure 1. 8 Sample plots of applied compressive stress and estimated heartwood compressive strength vs. time (Giuliana Zelada-Tumialan, 2014).

Wood density is a fundamental factor influencing the mechanical performance and durability of timber piles in aquatic environments. It depends on intrinsic characteristics such as species, age, and cellular structure, as well as extrinsic factors including environmental conditions and growth rates. Generally, hardwoods possess higher density due to their complex cellular makeup and slower growth, resulting in greater strength and longevity. In contrast, fast-growing softwoods like pine and spruce exhibit lower density, which correlates with increased susceptibility to deformation and decay. Table 1.1 summarizes the density values for common submerged wood species as specified by the EN 350:2016 standard, illustrating the typical ranges in density and moisture content for hardwoods and softwoods.

Type	Code acc.to EN13556	Wood Species	Density (kg/m³ at 12% MC)	Moisture Content (% oven-dry	Moisture Content (% after water absorption)	Reference
Hardwood	QCCR	*Oak*	710 – 860	60 – 80	>200	(Roman, Grzegorzewska, et al., 2023)
Hardwood	LADC	*Larch*	470 – 650	50 – 80	150 – 200	(Roman, Grzegorzewska, et al., 2023)
Hardwood	AEHP	*Chestnut*	500 – 590	50 – 80	565 - 607	(Chavenetidou & Kamperidou, 2024)
Hardwood	FASY	*Beech*	690 – 750	50 – 90	>200	(Kazemi et al., 2001a)
Softwood	PCAB	*Spruce*	440 – 470	60 – 120	80 – 150	(Roman, Grzegorzewska, et al., 2023)
Softwood	PNSY	*Scots pine*	520 – 550	60 – 120	>250	(Asante et al., 2022)
Softwood	ABAL	*Fir*	440 – 480	80 – 90	80 – 150	(Kazemi et al., 2001)

Table 1. 1 Physical Properties of Common Submerged Wood Species (Author).

A well-documented positive correlation exists between wood density and structural performance in load-bearing contexts. Higher-density species demonstrate increased compressive strength, tensile resistance, and mechanical stability—key attributes for the long-term integrity of foundation systems in waterlogged environments (Iida et al., 2012; Íñiguez-González et al., 2015; Lucas Filho, 2012; Niemz & Sonderegger, 2003; Wei et al., 2019).

Miyoshi et al. (2018) investigated the effects of density on elastic modulus, strength, and failure strain of hardwoods and softwoods with varying annual ring inclinations. While the expected linear relationship between density and elastic modulus was absent in samples cut at 90° inclination—due to resistance from ray structures—a strong correlation emerged in those cut at 45°, attributable to shearing deformation. Strength also depended on anatomical features such as ray arrangement and vessel orientation, with species-specific exceptions noted (see Fig. 1.9).

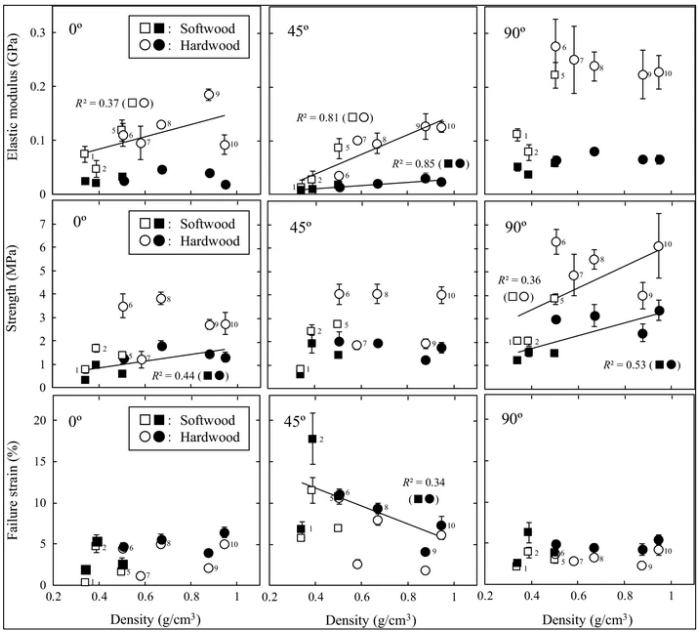

Figure 1. 9 Correlation of hardwood and softwood wood density with mechanical properties (Miyoshi et al., 2018).

The relationship between density and the modulus of elasticity (MOE) in submerged wood is influenced by inherent material properties and the effects of water absorption. Denser species typically exhibit higher MOE because of their richer lignin and cellulose content (Fig. 1.10). Strong correlations have been reported for species such as *Teak* and *Pine* (0.933 and 0.790, respectively)(Izekor, 2010; Missanjo & Matsumura, 2016).

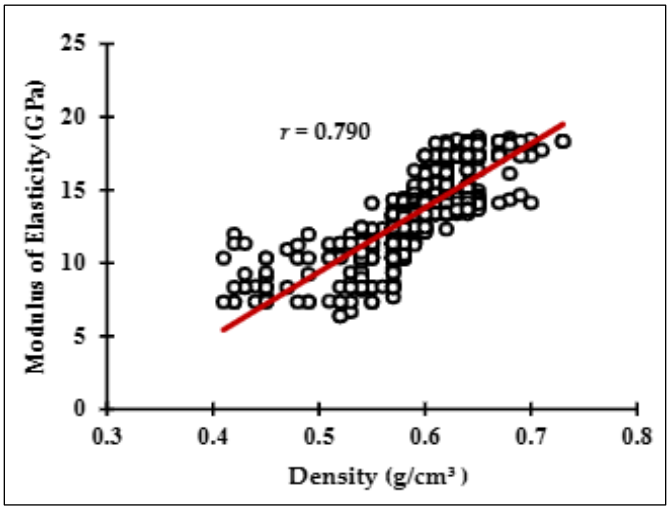

Figure 1. 10 Relationship between Khasi Pine density and MOE (Missanjo & Matsumura, 2016).

However, Baar et al. (2015) observed weaker correlations in some tropical hardwoods, and prolonged submersion has been shown to reduce density by 5–15%, depending on exposure duration and water type. Roman, Leszczyński, et al. (2023) documented a 7.9% density decrease in conifers (*Pine*, *Spruce*, *Larch*) after seawater immersion, accompanied by reductions in MOE due to weakened cell wall structure (J. L. Yang & Evans, 2003).

Figure 1. 11 The higher the wood density is, the smaller the number of voids in the wood is and vice versa (A, C) Cross-sections of the Hevea brasiliensis wood. Scale bars:100 µm (Faria et al., 2021).

Compressive strength is directly proportional to wood density, as denser woods possess a more compact fiber structure with fewer voids or cavities, minimizing stress concentrations and crack propagation (Fig. 1.11). For example, *Red Oak*—a high-density hardwood—has a tip-end crushing strength nearly double that of lower-density *Southern Pine* (3,460 psi and 1,820 psi, respectively) (Thomas Lee Wilkinson, 1968). Increased density also contributes to improved dimensional stability (L. He et al., 2022; Sargent, 2022).

Swelling, especially in the tangential direction, tends to be more pronounced in denser woods and can affect mechanical properties. Hardwoods generally swell more than softwoods, with swelling magnitude positively correlating with density by (Blomberg, 2006; Hernández, 2007; Kretschmann, 2010; Topaloglu & Erisir, 2018).

Moisture content strongly influences wood mechanical properties. Timber absorbs and releases moisture in response to environmental factors such as temperature and relative humidity (Fredriksson, 2019; Glass et al., 2010; W. Simpson & TenWolde, 1999). Moisture uptake occurs in two primary stages: initially (0% to ~30% moisture content, MC), water is absorbed into the cell walls; beyond the fiber saturation point (FSP), which varies by species—22–24% for oak and ash, 26–28% for *Pine*, *Larch*, And *Douglas-Fir*, and 30–34% for *Fir* and *Spruce* (Zelinka et al., 2016)—water fills the cell cavities (Fig. 1.12).

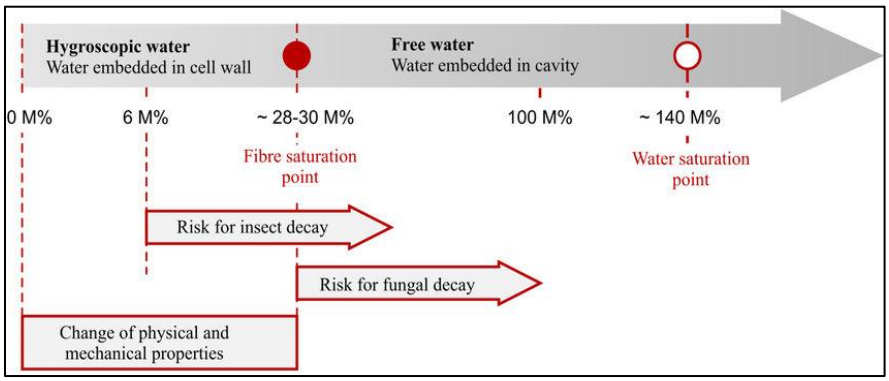

Figure 1. 12 Range of wood moisture content and influence on its properties and vulnerability (Dietsch et al., 2015).

In aquatic environments, timber piles often reach saturation, with MC ranging from 30% to over 200% dry weight depending on species, environmental conditions, and exposure duration (Cao et al., 2023). Moisture fluctuations cause wood to expand and contract primarily along the radial and tangential axes(Glass et al., 2010; Thybring et al., 2022) (Fig. 1.13), as water interacts with cellulose and hemicellulose in the cell walls (Arzola-Villegas et al., 2019; Cai, 2020; Kulasinski et al.,

2017). Significant swelling occurs once MC exceeds 10–15%, affecting wood microfibril bundles (Paajanen et al., 2022).

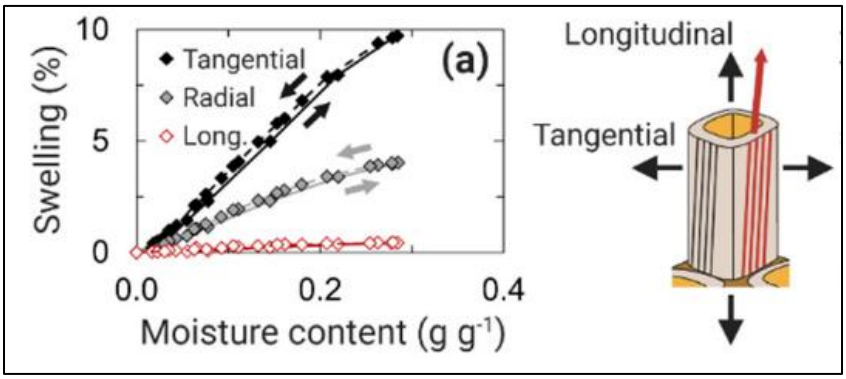

Figure 1. 13 Effect of Moisture Content on Swelling in Wood's Primary Axes (Thybring et al., 2022).

However, in fully submerged conditions, Korkmaz and Büyüksari, (2019) found that timber reaches equilibrium with the surrounding water, with MC surpassing the fiber saturation point (FSP) of approximately 25–30%. At this stage, the cell walls become fully saturated, and any additional moisture accumulates in the cell cavities, resulting in increased weight without further swelling.

Under fully submerged conditions, timber equilibrates with surrounding water, surpassing the FSP (approximately 25–30%); further moisture increases accumulate as free water in cavities without additional swelling (Korkmaz & Büyüksari, 2019). Fluctuations in moisture content, especially when parts of piles are intermittently exposed to air, induce drying shrinkage and cyclic swelling, causing internal stresses, warping, splitting, and gradual loss of structural integrity, as illustrated in Figure1.14 (Dinwoodie, 2000; Fu et al., 2023; Glass et al., 2010).

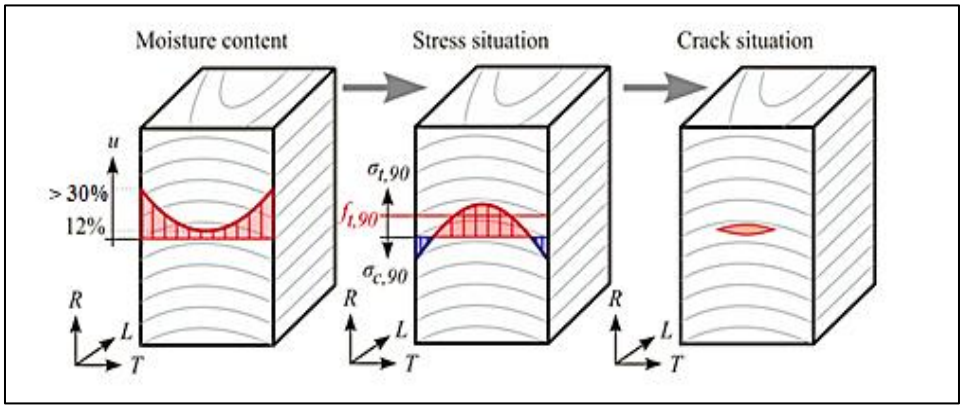

Figure 1. 14 Example of moisture content, corresponding internal stresses, and potential internal crack growth (Dietsch et al., 2015).

Mechanical properties of wood significantly decline as MC increases above the FSP. For example, compressive strength decreases by up to 62.5% when MC rises from 8% to above FSP, with estimated strength reductions of 3.1% per 1% MC increase in *Oak* (Korkmaz & Büyüksari, 2019). Similarly, Güntekin and Aydın (2013) found that compressive strength exhibited the highest rate of change in *Turkish Red Pine*, at 2.3%. Conversely, strength improves when MC decreases below FSP, with increases of 34–35% observed in compressive and shear strength as MC drops from FSP to 12% (Soares et al., 2021).

The modulus of elasticity (MOE), which measures stiffness, decreases with rising MC, with reductions up to 16% when MC increases from 12% to above FSP (Dietsch et al., 2015; Kherais et al., 2024) (Fig. 1.15).

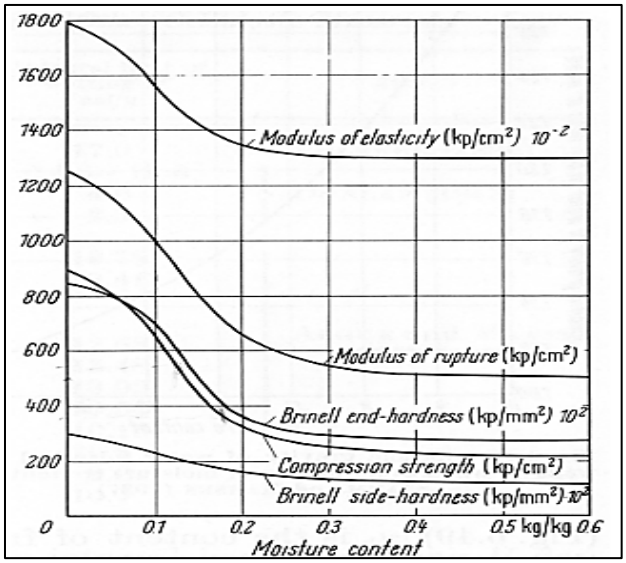

Figure 1. 15 Influence of moisture content on selected wood properties (Dietsch et al., 2015).

Below the fiber saturation point (FSP) (~30%), MOE may initially increase slightly due to water's plasticizing effect on the cellulose matrix, enhancing internal hydrogen bonding and stiffness. However, once MC surpasses FSP, excessive water weakens fiber-to-fiber bonds, leading to a significant decline in MOE. Research by Soares et al. (2021) indicates that increasing MC from 12% to over 30% can reduce MOE by up to 16% in some wood species. Further Kherais et al.(2024) found that moisture saturation reduces MOE by 15–20%, while higher MC levels (12%, 15%, 18%) result in a 10–25% decrease in MOE.

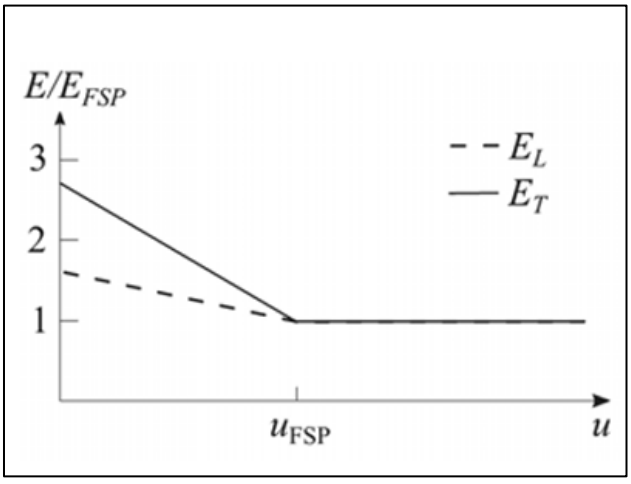

Figure 1. 16 Effect of Moisture Content on Elastic Moduli Parallel, Perpendicular to the Grain, Normalized to FSP (Sabina, 2019).

The impact of MC on elastic and shear moduli is more pronounced perpendicular to the grain than parallel (Sabina, 2019) (Fig. 1.16). Transverse tensile strength, which is lower than longitudinal strength, governs cracking and deformation during drying. Studies on species such as *European Beech*, *Japanese Cedar*, *Poplar*, and *Chinese Fir* document linear declines in transverse tensile

strength and modulus of elasticity with rising MC, especially near the FSP (Jiang et al., 2017; Ozyhar et al., 2012; Yue et al., 2019; Zhan et al., 2019).

Dynamic properties are also MC-dependent. Below the FSP, sound velocity decreases significantly with MC increases, influencing elastic wave propagation relevant to non-destructive evaluation (Ozyhar et al., 2013). Engineered woods like cross-laminated timber experience up to 12% bending stiffness reduction from seasonal MC variations, with moisture gradients fostering cracking and decay; fungal decay notably accelerates beyond FSP, with 40–50% compressive strength loss in affected regions (Zoormand et al., 2024).

Fungal decay requires threshold moisture levels, with Coniophora puteana initiating decay in *Norway Spruce* above 30% MC and optimally between 40% and 70% MC(Benítez et al., 2021). Decay can begin as low as 19% MC under high relative humidity (85%) (Fig. 1.17) (Brischke et al. 2017) Prolonged water submersion maintains high MC and anoxic conditions, inhibiting fungal degradation (Bornemann et al., 2014; Elam, 2022; Malan, 2004).

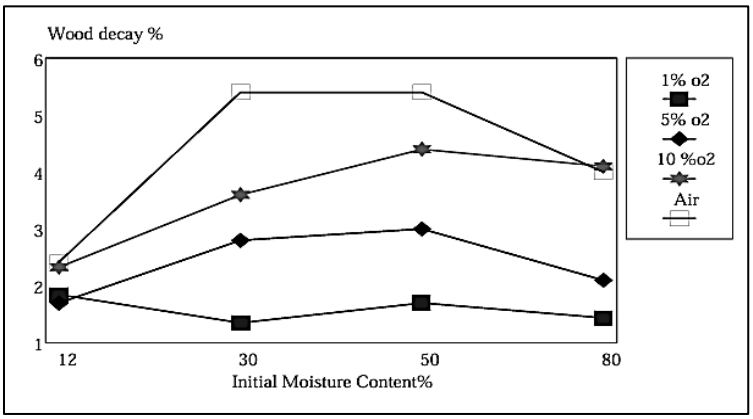

Figure 1. 17 Relationship between moisture content and wood decay in Scots Pine (Kazemi et al., 2001).

Environmental Factors

Temperature variations significantly affect the stability and degradation of wooden piles in aquatic environments. Repeated thermal expansion and contraction cycles induce microcracks and fatigue, gradually weakening the wood structure (Jones et al. 2018; Kubovský et al. 2020; Sedighi Gilani et al. 2013; Stanciu et al. 2020), Although fully submerged conditions mitigate some of these effects, temperature-driven physical and chemical processes generate internal stresses that influence wood integrity.

Prolonged exposure to elevated temperatures causes thermal degradation of wood's primary components, cellulose and lignin, diminishing mechanical strength (Bratasz & Kozłowski, 2005; De Freitas et al., 2015; Godoy et al., 2024; Sik et al., 2010). Moisture content primarily governs dimensional changes, while temperature regulates moisture exchange rates, impacting dimensional stability ((Gerhards, 1982) (Fig. 1.18).

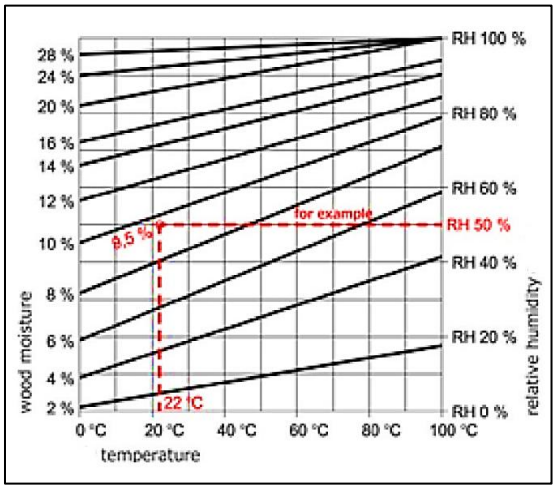

Figure 1. 18 Relationship of temperature and moisture content in wood (Gerhards, 1982).

Water absorption in wood is a temperature-dependent chemical process. Higher temperatures increase molecular mobility, accelerating moisture penetration into cell walls and swelling rates, following Arrhenius kinetics (Dubois et al., 2005; Khazaei, 2008; Sahin, 2010; Thybring et al., 2022; Varnier et al., 2020). Species vary in swelling behavior; for example, fir shows the highest initial swelling, followed by *Pine*, *Chestnut*, And *Cherry* (Sahin & Mantanis, 2011). Mantanis et al. (1994) observed that equilibrium swelling time in aspen declines significantly with temperature increase, illustrating thermal influence.

Temperatures exceeding 100 °C initially accelerate swelling but eventually degrade cellular structures, causing softening and reducing mechanical properties. Bekhta & Niemz, (2003) reported up to 50% reduction in bending strength and notable decreases in the modulus of elasticity (MOE) after 24 hours at 200 °C. Other studies confirmed a decrease in modulus of rupture (MOR) and hardness at elevated temperatures, with some species showing complex responses depending on temperature ranges (Boonstra et al., 2007; Kocaefe et al., 2008; Kubojima et al., 2000; Pavlo & Niemz, 2003)(Fig. 1.19).

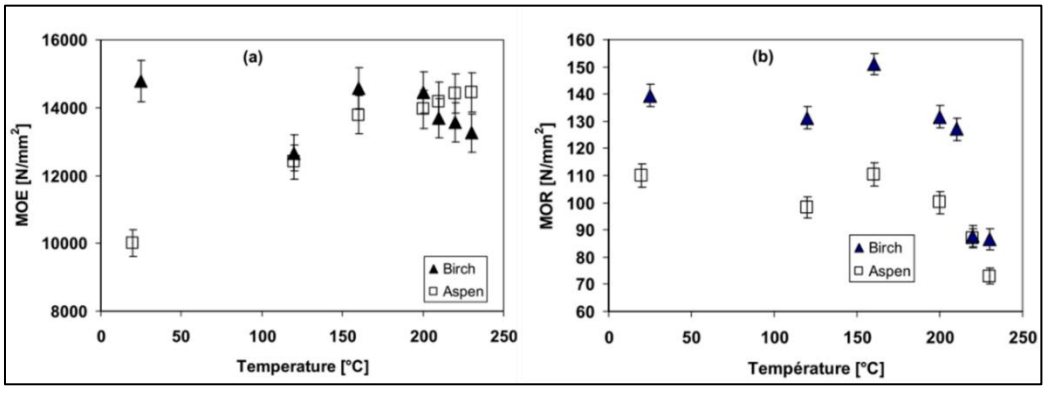

Figure 1. 19 The effect of temperature on the mechanical strength of Birch and Aspen wood (Kocaefe et al., 2008).

At higher levels. Similarly, Pavlo and Niemz, (2003) reported a notable reduction in MOR within the 100–200 °C range for spruce, although they did not investigate higher temperatures. In contrast, the modulus of elasticity (MOE) is generally less sensitive to temperature, showing only slight decreases—or occasional increases—depending on specific conditions. Cold water (< 5 °C) slows moisture absorption by limiting molecular motion, while freezing (< 0 °C) halts swelling

entirely and poses risks of cracking due to ice formation within wood (Bozonnet et al., 2024; Melin, 2019).

Temperature is also a key driver of microbial decay in submerged wood. Elevated temperatures accelerate decay rates by enhancing microbial and enzymatic activity(Fig. 1.20 and 1.21) (Edman et al., 2021; Oberle et al., 2018; Pietsch et al., 2019). Optimal fungal decay occurs between 20 °C and 40 °C, peaking near 35 °C, and microbial decay rates approximately double with each 10 °C temperature increment under adequate moisture (Marais et al., 2020; Zanne et al., 2022). Temperatures below 10 °C inhibit microbial activity and slow decomposition processes (Jones et al., 2018).

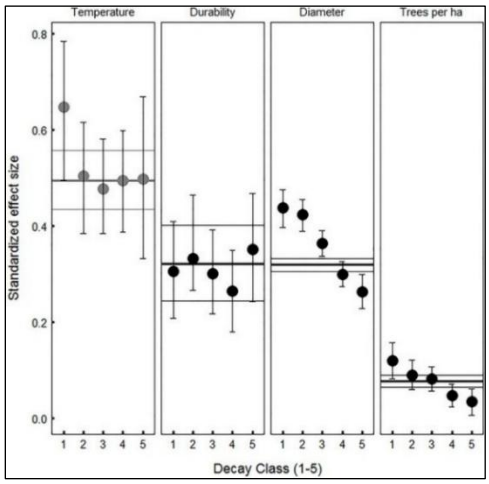

Figure 1. 21 Effect of Temperature on wood decay class (Oberle et al., 2018).

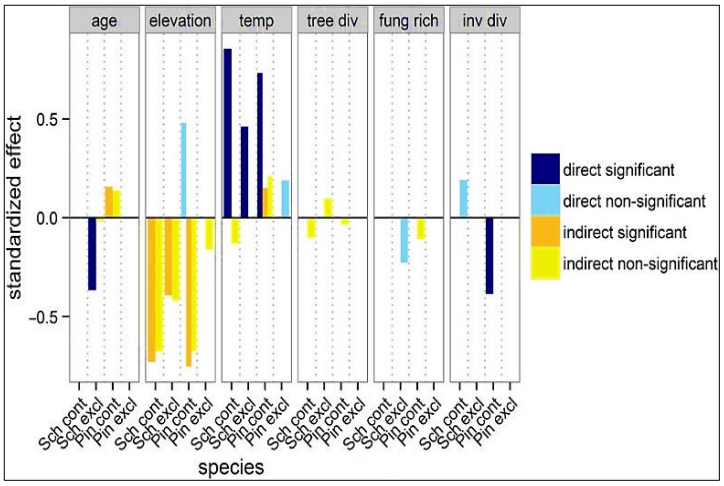

Figure 1. 20 Temperature and Microbial as drivers of wood decomposition (Pietsch et al., 2019).

Furthermore, fluctuating water levels and oxygen availability strongly influence microbial activity and the decay dynamics of submerged wood in aquatic environments (Björdal & Dayton, 2020; Intui et al., 2018; Jones et al., 2018; Y. S. Kim & Singh, 2000). Microbial degradation of wood occurs primarily in the presence of oxygen, with optimal fungal and bacterial growth observed at oxygen concentrations ranging between 5% and 21% (Nofal & Kumaran, 1999; Schroll et al., 2024) (Fig. 1.22).

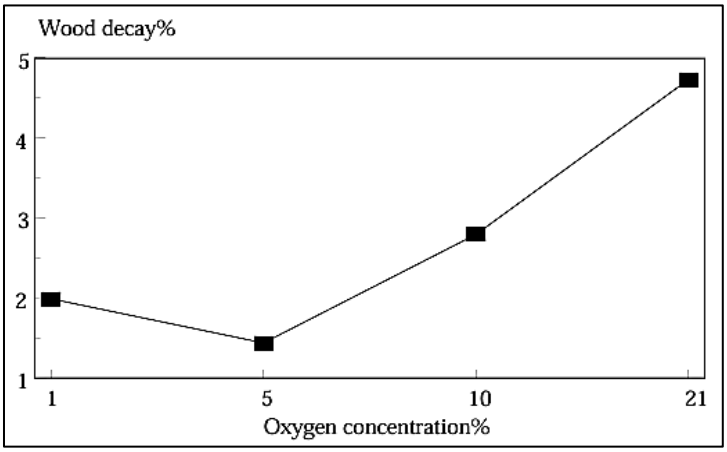

Figure 1. 22 Relationship between oxygen concentrations and wood decay in Scots pine (Kazemi et al., 2001).

Kazemi et al. (2001) reported that some fungi exhibit peak activity within the 5–10% oxygen range. However, submersion often leads to oxygen depletion, limiting aerobic metabolism and favoring anaerobic microorganisms that degrade wood through fermentation and sulfate-reduction processes. Most wood decay fungi cannot survive below 0.2% oxygen concentration, although certain species may persist at around 1% oxygen, albeit with greatly reduced metabolic efficiency.

These oxygen constraints influence decay rates and mechanisms, with aerobic decay dominating in oxygen-rich zones near the water surface or in fluctuating water levels, and anaerobic decay processes prevailing in fully submerged, oxygen-poor regions. The balance between these microbial communities governs the overall rate of wood degradation and the preservation potential of submerged wooden structures.

1.3.3 Non-Destructive Testing Methods in Structural Health Monitoring

Structural Health Monitoring (SHM) is a systematic approach to evaluating the integrity and performance of engineering structures over time. By analyzing periodically sampled response data, SHM enables the early detection of material degradation, geometric changes, fatigue, and other damage modes before critical failure occurs. This proactive methodology enhances the safety, serviceability, and longevity of civil, aerospace, and mechanical systems (Amafabia et al., 2017; Chandrasekaran, 2019; Farrar et al., 2024; Farrar & Worden, 2007). Its importance is underscored in post-event assessments following earthquakes, blasts, or extreme loading conditions (López-Castro et al., 2022).

Nondestructive evaluation

Non-Destructive Evaluation (NDE) is integral to SHM, allowing assessment of material physical and mechanical properties without impairing serviceability. NDE utilizes Non-Destructive Testing (NDT) techniques to deliver accurate and reliable insights into structural performance, facilitating early detection of defects, degradation, and anomalies (Abdallah et al., 2019; Dwivedi et al., 2018; M. Gupta & Khan, 2021; Jolly et al., 2015; Nallar et al., 2023; Schimleck et al., 2019; Umap & Rao, 2023; Zielińska & Rucka, 2021).

NDT encompasses diagnostic tools that evaluate material properties without causing damage, cost-effectively, and in situ, making them invaluable for large-scale infrastructure monitoring. These techniques detect local defects, assess reinforcement integrity, monitor vibration states affecting stability, and map stress concentrations (Baar et al., 2015; Işık et al., 2020; Jamil et al., 2024; Küttenbaum et al., 2018; W. S. Lin & Wu, 2013; Mohammadi, 2004; Park et al., 2015; Puaad et al., 2014; Rainieri et al., 2015; S. K. Sharma & Shukla, 2012; Sklarczyk et al., 2013). By providing real-time structural insights, NDT supports predictive maintenance strategies and enhances long-term reliability.

The choice of NDT methods depends on the targeted property—mechanical strength, corrosion resistance, or hidden defects—with tools ranging from visual inspection to advanced acoustic, magnetic, and radiation-based techniques (Binda & Saisi, 2009; Llana et al., 2020; Mastela et al., 2023; Ottosen et al., 2024). These tailored approaches ensure comprehensive assessment of structural health (Peruń, 2024) (Fig. 1.23).

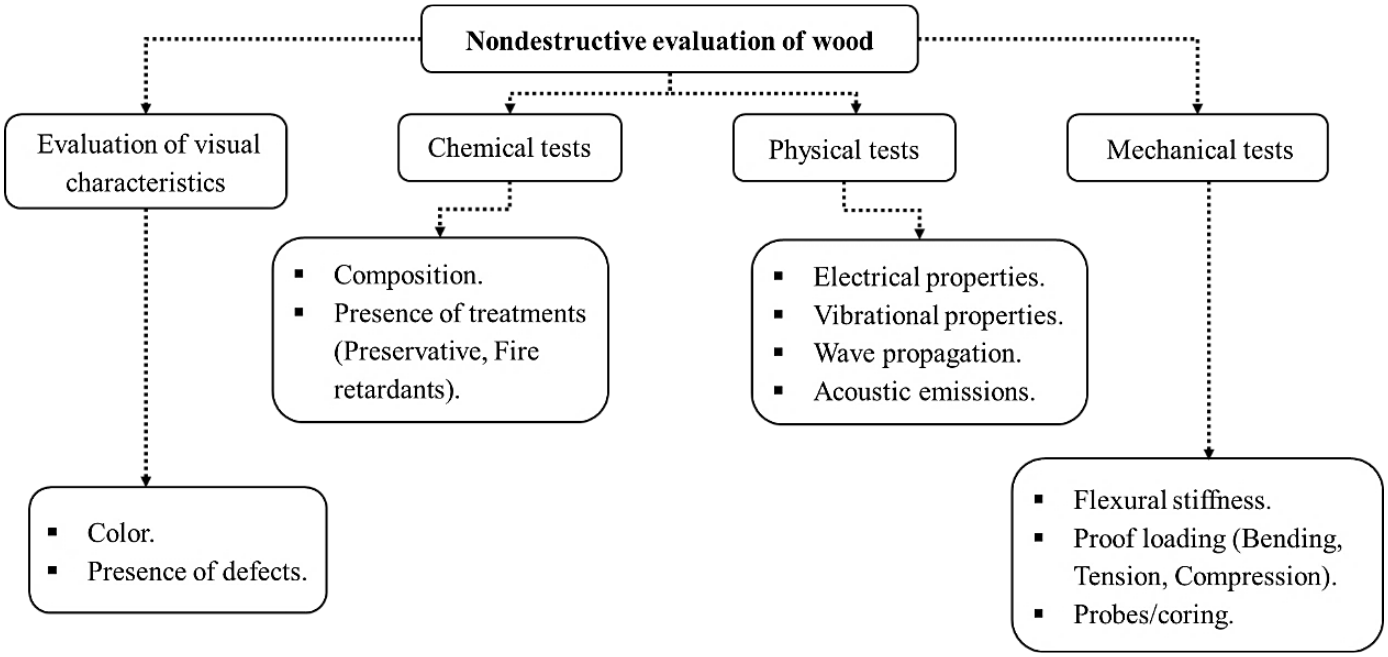

Figure 1. 23 Classification of Nondestructive Testing Techniques (Author).

Non-Destructive Testing methods

Visual inspection is the most traditional and widely used NDT method, primarily for detecting surface defects such as cracks, knots, and discoloration. While effective for quality grading in the forest products industry, it cannot reveal internal flaws or provide quantitative evaluation of mechanical properties (Patel et al., 2022; Sanchez, 2024; Zoidis et al., 2012).

Advanced NDT techniques enable deeper analysis of wood materials, especially for submerged or otherwise inaccessible structures. These include acoustic, radiographic, thermographic, vibrational, and electromagnetic methods, which facilitate non-destructive evaluation of key properties such as modulus of elasticity (MOE), density, and moisture content (Azzi et al., 2025; Dahle et al., 2016; Ettelaei et al., 2019; Kasal & Anthony, 2004; Ross & Pellerin, 1994; Teixeira, 2016).

Ultrasound is particularly effective for measuring MOE and stiffness (Niemz & Mannes, 2012; Reci et al., 2016), while X-ray and microwave technologies are commonly used to assess density and moisture content (Gallardo et al., 2018; Vikberg et al., 2012) (see Table 1.2). By detecting internal defects such as decay and structural inconsistencies at an early stage, these NDT methods enhance the safety, durability, and longevity of wooden elements.

Parameter / Material Property	Non-Destructive Testing Methods
Modulus of Elasticity (MOE)	Ultrasound, Resonance (NMR)
Density	Ultrasound, X-ray, Microwave, Resonance (NMR), Drilling Resistance
Moisture Content (MC)	Electromagnetic Methods, Microwave, Capacitive Sensors
Layer thickness measurement / Wall Thickness	X-ray, Microwave, Resonance (NMR), Electromagnetic Methods
Material Inhomogeneity	Optical Methods, Electromagnetic Methods, X-ray

Cracks / Fractures	Ultrasound, Acoustic Emission, X-ray, Microwave, Resonance (NMR)
Failure / Structural Integrity	Thermography, Microwave, Electromagnetic Methods, Resonance (NMR).
Deformations / Dimensional Changes	Visual Inspection, Laser Scanning.
Stiffness	Ultrasound, Acoustic Emission, X-ray, Thermography, Visual Inspection.

Table 1. 2 Overview of nondestructive testing methods for wood (Niemz & Mannes, 2012; P. Palma & Steiger, 2020).

Optical methods

(Zechel et al. (2020) and Zielińska & Rucka (2021) emphasize that optical NDT techniques employ specialized instruments such as endoscopes, borescopes, videoscopes, and microscopes for the inspection of surfaces and otherwise inaccessible regions. The integration of laser scattering further enhances these methods by generating highly accurate three-dimensional mappings of material geometry, allowing precise assessment of deformations, dimensional variations, and alignment, even under restricted conditions. Numerous studies demonstrate that optical approaches enable non-contact evaluation of displacement, vibrations, and surface deformations, making them particularly effective for structural health monitoring (Andreev et al., 2022; Huke et al., 2013; Kroworz & Katunin, 2018; Sirohi, 2001).

Electromagnetic methods

Electromagnetic NDT techniques, including ground-penetrating radar (GPR) and microwave methods, are effective for evaluating layer thickness, detecting defects, and characterizing material homogeneity (Lachowicz & Rucka, 2016; Rucka et al., 2020). GPR provides rapid large-area inspections, identifying subsurface anomalies via reflected signals that map internal features (David Redman et al., 2016; Jol, 2008; Schajer & Orhan, 2006; Senalik et al., 2022). During GPR surveys, signals collected along a material's surface are compiled into radargrams for reliable defect detection (Baker et al., 2007; Pandharpatte Priyanka et al., 2022) (Fig. 1.24).

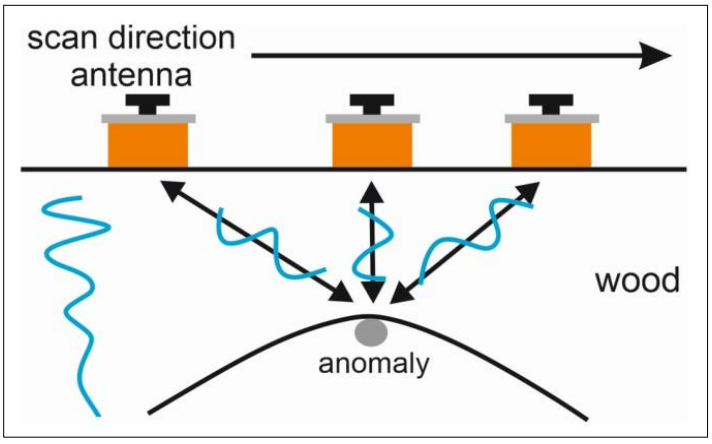

Figure 1. 24 The scheme of surveys using the GPR method (Zielińska & Rucka, 2021).

Thermography

Infrared thermography (IRT) detects surface temperature variations stemming from material property changes or defects, enabling defect localization and density variation mapping (Hatefipour et al., 2014; Ibarra-Castanedo et al., 2013; Qu et al., 2020). Reliability in detecting voids, discontinuities, and material anomalies is supported across various wood types (António & Rui, 2022; López et al., 2013, 2018; Pitarma et al., 2019) (Fig. 1.25).

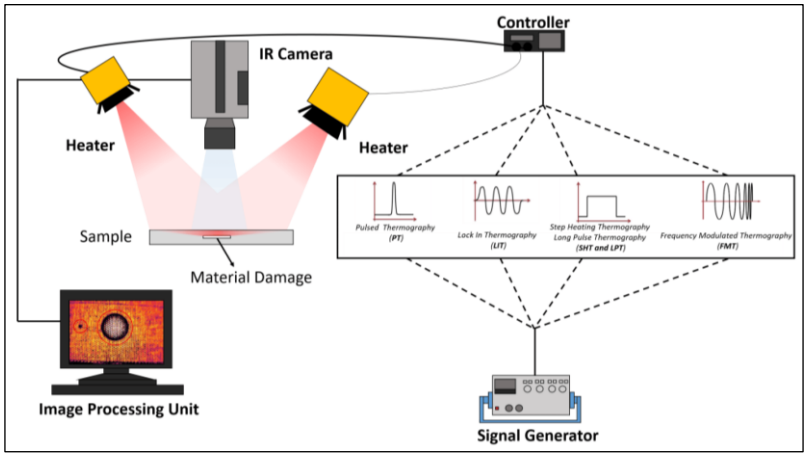

Figure 1. 25 Schematic diagram of infrared thermography method (Ciampa et al., 2018).

X-ray Computed Tomography (X-ray CT)

Zielińska & Rucka (2021) describe X-ray CT as a high-resolution imaging technique that reconstructs internal wood structures based on X-ray attenuation properties. It generates detailed 3D images, enabling the detection of density variations and internal defects such as knots, pith, sapwood, and cracks. Despite high operational costs and safety requirements, it remains an essential tool for detailed timber inspection and quality control (De Ridder et al., 2011; Ge et al., 2018; Jacquin et al., 2017; MacChioni et al., 2007).

Acoustic Methods

Acoustic NDT techniques—including stress wave propagation, ultrasonic testing, guided waves, and acoustic emission (AE)—are widely applied to assess the mechanical performance and internal condition of wood. These techniques analyze elastic wave propagation to evaluate the modulus of elasticity (MOE), stiffness, and detect internal defects.

Guided wave methods: utilize Lamb waves capable of traveling long distances with minimal attenuation, making them particularly suitable for large wooden structures (Ebrahiminejad et al., 2022; Mardanshahi et al., 2020; Yu et al., 2014; Yu & Yan, 2017). These waves effectively evaluate moisture-dependent mechanical properties and weathering effects on wood (Fathi et al., 2020, 2021).

Acoustic Emission (AE) Testing: AE techniques detect stress waves generated by internal microfractures, crack initiation, or fluid movement, enabling real-time monitoring and damage localization during processes such as drying and machining (Barbosh et al., 2022; Ma et al., 2023; Tu et al., 2022). When an AE event occurs, the resulting stress waves propagate through

the material, where they are modified by the wood's microstructure and geometry, altering their amplitude, frequency, and waveform. These signals are then captured and converted into electrical outputs by a transducer for subsequent analysis (Barbosh et al., 2022; Ma et al., 2023; Tu et al., 2022) (Fig. 1.26).

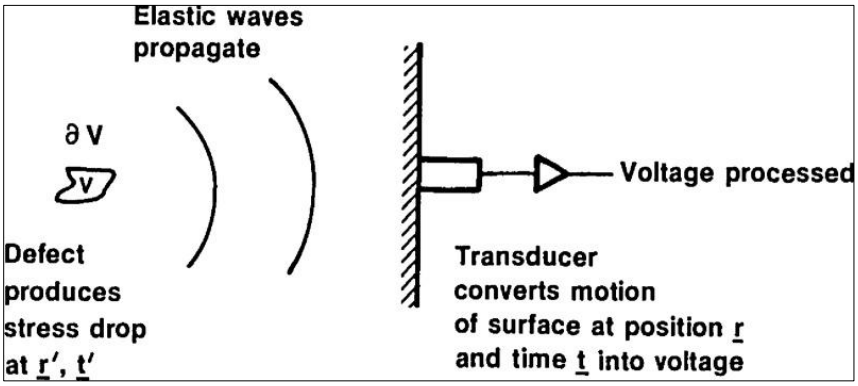

Figure 1. 26 Schematic of AE generation and detection process (Eitzen & Wadley, 1984).

Stress and Ultrasonic Wave Methods: transmits high-frequency waves (1–100 MHz) through wood to detect internal discontinuities and assess mechanical properties (Dackermann et al., 2016; Hirsekorn, 2014; W. S. Lin & Wu, 2013). Wave propagation depends on intrinsic factors like density, moisture content, and species, as well as extrinsic factors such as transducer frequency (Bucur & Böhnke (1994) and H. Yang et al. (2015) (Fig. 1.27).

Ultrasonic testing primarily relies on three key parameters: time of flight (TOF), wave velocity, and attenuation, to assess wood properties.

Time of Flight (TOF) measures the travel time of ultrasonic waves between the transmitter and receiver, offering insights into wood thickness, density, and mechanical performance (Aktharuzzaman et al., 2024; Espinosa, Bacca, et al., 2018).

Wave Velocity is strongly influenced by the internal microstructure of wood, serving as an indicator of stiffness variations and highlighting potential defect zones. It is a highly sensitive measure correlated with wood's modulus of elasticity and overall integrity. Studies, such as those on wooden pillars, have shown wave velocity to be the most reliable ultrasonic parameter for detecting defect severity and structural degradation (Arnold et al., 2023; Espinosa, Brancheriau, et al., 2018).

Attenuation refers to the reduction in wave energy as it propagates through the wood and reflects the presence of voids, cracks, biological decay, or other heterogeneities within the wood matrix. Elevated attenuation correlates with greater material degradation and defect density (Tran et al., 2016).

Figure 1. 27 Ultrasonic test using FAKOPP device (Author).

Together, these parameters provide a robust, non-destructive means for evaluating the wood's elastic modulus, stiffness, and defect distribution with high sensitivity, enabling early diagnosis of structural issues and informed maintenance decisions.

The ultrasonic parameters and their mathematical formulations are summarized in Table1. 3

Ultrasonic parameter	Description	Mathematical expression
Time of flight (TOF)	Measure of the time required for an ultrasonic packet of energy to travel through the material. Usually expressed as per unit length.	$TOF = \frac{t_2 - t_1}{l}$ Where: *t2* - is arrival time, *t1* - initiation time, and *l*- travel distance between source and receiver.
Pulse length (PL)	Measure of spreading of received waveform with respect to a standard waveform. Influenced by differences in path length and sound speed that tend to spread waveform.	$PL = K\Delta t \int v(t)^2 dt$ where: *K*- is a constant, *Δt*- time required for received wave energy integral from 10% to 90% of its final value, *v*- signal voltage as a function of time, and *t*- time.
Insertion loss (IL)	Ratio of energy received, after transmission through material, to energy input.	$IL = 10 \log\left(G \frac{E_r}{E_t}\right)$ Where: *Er*-is received energy, *Et* -transmitted energy, and *G*- receiver gain.
Elastic constants determination	Relate longitudinal and shear wave velocities to Poisson's ratio and dynamic modulus of elasticity.	$C_D = \rho V_L^2$, $G_D = \rho V_\tau^2$ Where: *VL*- longitudinal wave velocity, *Vτ*- shear wave velocity, *ρ*-density, *CD* - dynamic stiffness, and *GD*- dynamic shear elastic modulus.

Table 1. 3 Analysis Techniques for Ultrasonic Measurements (Author).

Ultrasonic wave interactions with internal heterogeneities in wood generate phenomena such as reflection, refraction, diffraction, and scattering, which offer critical insights into subsurface structural irregularities, through detailed signal analysis, it becomes possible to reconstruct the internal structure of the material, facilitating accurate defect characterization and assessment of structural integrity (Cieszko & Kriese, 2008; H. He, 2020; Leiderman & Castello, 2014; Tran et al., 2016).

Jodhani et al (2023) provides a thorough review of primary ultrasonic measurement techniques, which include:

Pulse-Echo Method: This method involves emitting an ultrasonic pulse from a transducer, which reflects off internal boundaries or interfaces and returns to the same transducer (Fig. 1.28). The time interval between pulse emission and reception is used to calculate wave velocity, offering insights into material properties such as density, stiffness, and internal defects.

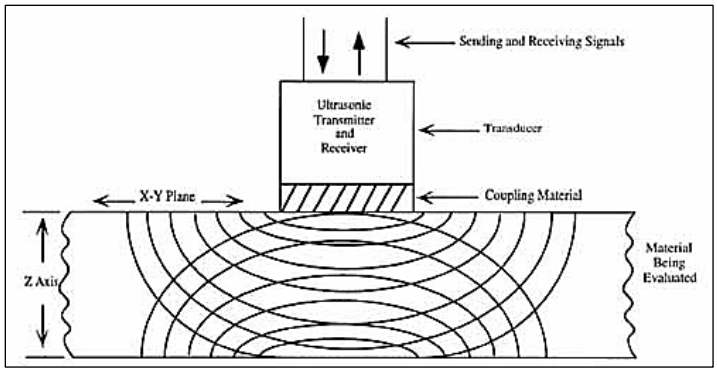

Figure 1. 28 Pulse-Echo Method of ultrasonic testing (NASA MSFC, 1992).

Through-Transmission Method: Utilizing separate transmitting and receiving transducers positioned on opposite sides of the specimen, this method measures the travel time of an ultrasonic pulse traversing the material (Fig. 1.29). The known distance between transducers combined with TOF facilitates accurate calculation of wave velocity, enabling detection of internal discontinuities and evaluation of mechanical properties.

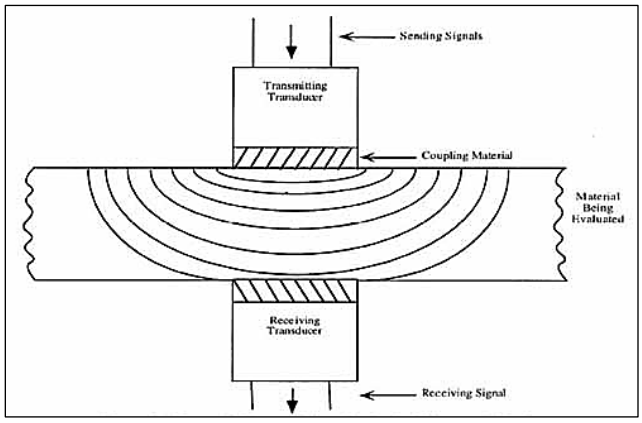

Figure 1. 29 Through-Transmission Method of ultrasonic testing (NASA MSFC, 1992).

The pitch-catch method: In this configuration, ultrasonic waves are transmitted and received at oblique angles relative to the material surface. The receiver detects waves reflected at characteristic angles, permitting effective evaluation of material properties and defect detection, especially suited for curved or cylindrical wood elements (Fig. 1.30).

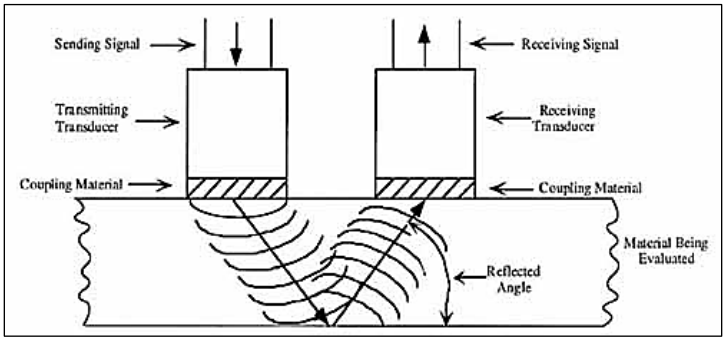

Figure 1. 30 The pitch-catch method of ultrasonic testing (NASA MSFC, 1992).

Key Considerations for Preparing Acoustic Testing

Preparation for acoustic testing requires a thorough assessment of several interrelated parameters, including signal source, power, frequency, receiver type, and coupling mechanism. These factors must be meticulously optimized to ensure accurate and reliable measurements. For example, larger specimens necessitate higher signal power for proper detection, while higher frequencies improve defect resolution but lead to increased signal attenuation.

Signal Source and Power Considerations

Halabe et al (1997) emphasize that the signal source must generate adequate power at the required frequencies to support precise measurements. In configurations like pulse-echo testing, the same transducer often serves as both emitter and receiver.

Acoustic sources are broadly categorized into:

External Excitation Sources: These induce stress waves mechanically or electromechanically, such as with impact hammers or piezoelectric transducers, without harming specimen integrity (Bucur, 2023) (Fig. 1.31).

Figure 1. 31 Schematic of an external excitation source generated with a hammer (Bucur, 2023).

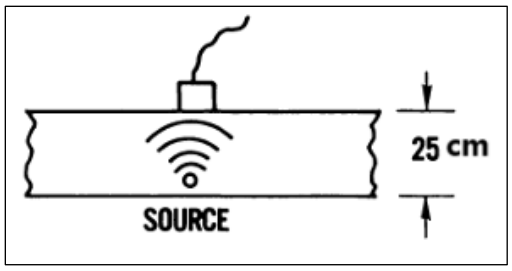

Figure 1. 32 Schematic of Internal excitation source (Eitzen & Wadley, 1984).

Internal Excitation Sources: These rely on naturally occurring stress wave emissions, like microfractures or fluid movements, utilized in acoustic emission (AE) testing for real-time, non-invasive monitoring of structural integrity (Eitzen & Wadley, 1984)(Fig. 1.32).

International standards, including ISO 3741 (reverberant environments) and ISO 3744 (semi-free field), provide formal procedures for measuring sound power emissions, ensuring reproducible and accurate acoustic testing across varied scenarios.

Frequency and Signal Attenuation

Bai et al., (2018); Harris et al., (1991) note that ultrasonic acoustic waves, typically operating above 20 kHz, provide frequency-dependent resolution. A fundamental trade-off exists:

1. Higher frequencies enhance the detection of smaller defects due to improved spatial resolution, as shorter wavelengths are more effective at identifying fine discontinuities.

2. Lower frequencies reduce signal attenuation, allowing deeper penetration into the material, particularly in large specimens.
3. As attenuation increases with frequency, the selection of an optimal frequency range is essential to balancing resolution and signal transmission efficiency.

Receiver Selection and Detection Mechanisms

Receiver choice depends on testing technique and specimen features. **Contact Receivers,** Piezoelectric transducers requiring coupling agents to ensure efficient signal transmission. **Non-Contact Receiver,** Devices like microphones and laser Doppler vibrometers operate without physical contact, suitable for fragile or sensitive samples (Carbol et al., 2015).

Coupling and Transmission Efficiency

Contact-based acoustic testing employs coupling agents such as water, grease, or silicone rubber to minimize interfacial signal loss and optimize wave propagation (Fig. 1.33, 1.34). The coupling medium must not alter specimen properties. Excessive contact pressure, however, can reduce transmission efficiency beyond an optimal point due to nonlinear coupling effects (Mao et al., 2022; Senalik et al., 2014).

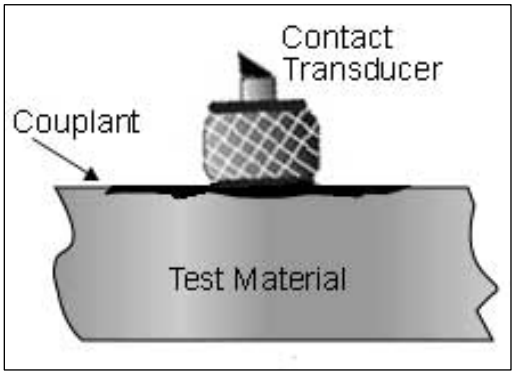

Figure 1. 34 Coupling between the transducer and the test specimen (NDE-Ed.org, n.d.).

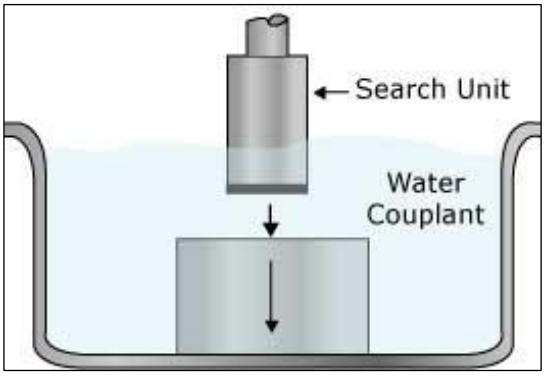

Figure 1. 33 Water-based coupling (NDE-Ed.org, n.d.).

Alternatively, non-contact coupling methods, like air-coupled or immersion transducers, transmit waves through the surrounding medium without direct contact, preserving signal integrity and avoiding mechanical interference. This is especially beneficial for uneven or delicate surfaces (Asokkumar et al., 2021) (Fig. 1.35).

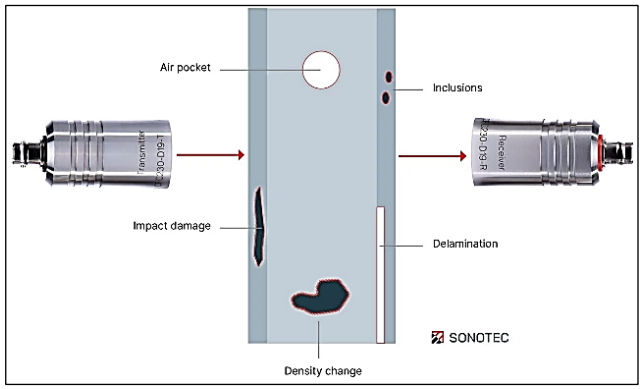

Figure 1. 35 Air-Coupled Ultrasonic test (OneStopNDT, 2020).

Ultrasonic Testing for Wave Velocity and Material Properties

Ultrasonic testing (UT) is a well-established non-destructive technique used to evaluate the mechanical properties and structural integrity of wood-based materials. This method measures the velocity of ultrasonic waves propagating through the material, providing insights into material characteristics such as density, stiffness, and elasticity.

Ultrasonic Wave Propagation in Materials

In isotropic materials, where mechanical properties are uniform across all directions, ultrasonic wave velocity is directly related to elastic constants. Longitudinal waves, which displace particles in the direction of wave propagation, travel faster than shear waves, where displacement is perpendicular to wave travel (Khon et al. 2018; Meeker & Meitzler 1961; Tumšys & Mažeika 2023) (Fig. 1.36).

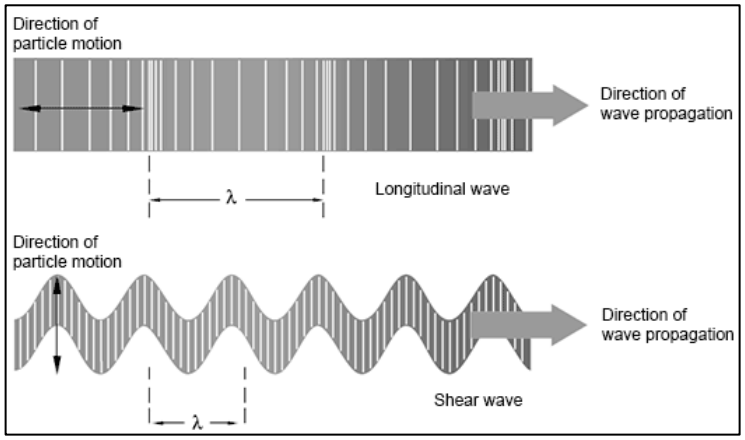

Figure 1. 36 Longitudinal and Shear ultrasonic waves (about-motors.com, n.d.).

Wood, however, exhibits strong anisotropy due to its complex microstructure consisting of aligned fibers and growth rings, making wave propagation highly direction-dependent. Velocity measurements must therefore be conducted along multiple axes to capture the wood's mechanical behavior comprehensively (Bucur, 1988; Espinosa et al., 2019).Waves traveling parallel to the grain encounter lower resistance, resulting in higher velocities, reduced attenuation, and greater stiffness. Conversely, waves propagating across the grain are slowed down by fiber boundaries and microstructural heterogeneities, leading to higher attenuation and lower velocities (El-Hadad et al., 2018; Saadat-Nia et al., 2011).

Research consistently demonstrates that longitudinal wave velocities range from 4,000 to over 6,000 m/s, depending on wood species and environmental (Krauss & Kúdela 2011; Saadat-Nia et al., 2011). Radial and tangential wave velocities are significantly lower; for example, *Radiata Pine* exhibits average tangential and radial velocities of approximately 1,644 m/s and 2,130 m/s, respectively (Hasegawa et al., 2016; Ortiz Mansilla et al., 2009). In *Japanese Cedar*, lateral wave velocities average around 1,450 m/s, contrasted with longitudinal velocities between 3,600 and 4,010 m/s.

Key Factors Influencing Ultrasonic Wave Propagation in Wood

The velocity of ultrasonic waves propagating through wood is affected by a complex interplay of factors, including wood species, anatomical features, moisture content, and the presence of structural defects.

Species-Specific Variability and Wood Anatomy characteristics

Wood species exhibit inherent variability in ultrasonic wave velocity due to differences in cellular structure. Hardwoods and softwoods demonstrate distinct wave propagation behaviors. Studies report coefficients of variation in ultrasonic velocity within species ranging from 3.69% to 7.51%, underscoring significant natural variability (Secco et al., 2012).

In softwoods, tracheid length (TL) and microfibril angle (MFA) are critical determinants of ultrasonic velocity. Longer tracheids provide more continuous pathways for wave transmission, thereby increasing velocity. Hasegawa et al.(2011) observed strong correlations ($p < 0.01$) between ultrasonic velocity and both TL and MFA in *Japanese Cedar* and *Japanese Cypress*. The MFA—the angle between cellulose microfibrils and the tracheid's longitudinal axis—affects wave speed, with smaller MFA values (indicating fibers more aligned with wave direction) resulting in faster propagation (Mason et al., 2017). Consistent with this, Krauss & Kúdela (2011) demonstrated a negative linear relationship ($R^2 = 0.71$) between MFA and ultrasonic velocity along the grain in *Scots Pine*, as MFA increases, ultrasonic velocity decreases.

In hardwoods, fiber length significantly influences ultrasonic wave propagation. Longer fibers tend to facilitate higher velocities by creating more continuous wave propagation paths. Hasegawa et al. (2015) reported strong positive correlations in species such as *Acacia auriculiformis* (R=0.90), *Eucalyptus dunnii* (R=0.92), and *Melia azedarach* (R= 0.68). Similarly, Tippner et al. (2013) confirmed comparable correlations in tropical hardwoods including *Afzelia bipindensis* (0.92), *Intsia bijuga* (0.82), and *Astronium graveolens* (0.81), highlighting the significance of fiber morphology on wave propagation.

Grain alignment also markedly influences ultrasonic velocity. Waves traveling parallel to the grain (grain angle = 0°) encounter minimal impedance, producing maximum wave velocities. Conversely, waves propagating perpendicular to the grain (grain angle = 90°) experience greater resistance, yielding slower transmission speeds (Brémaud et al., 2011; Dickens et al., 1996; Feng et al., 2010; Hu et al., 2005). Quantitatively, Smulski (1991) noted that velocities parallel to the grain are typically two to three times higher than perpendicular velocities. Stress wave velocities along the grain range between approximately 10,000 and 20,000 ft/s, whereas perpendicular velocities reach only 30–50% of these values. This anisotropy crucially affects wood's mechanical properties, including stiffness and efficiency of wave transmission.

Density

Wood density is a fundamental factor affecting ultrasonic wave velocity, with a generally positive correlation observed both between and within species. Denser woods usually exhibit higher wave velocities due to increased stiffness and reduced attenuation during wave propagation.

> Between Species: Comparative studies across different wood species reveal a consistent positive relationship between density and ultrasonic velocity. Denser species, being mechanically stiffer, facilitate faster ultrasonic wave transmission. Fabiana Goia Rosa & Sales

(2006) reported strong correlations for Brazilian tropical woods, with coefficients of determination (R^2) ranging from 0.80 to 0.88 for both hardwoods and softwoods. Similar findings were documented by (Tuğba Yılmaz & Murat, (2018) for species including *Oriental Beech*, *Scots Pine*, *Black Pine*, and *Turkish Red Pine*, where correlation coefficients ranged from 0.83 to 0.98, underscoring the robust association between density and wave velocity.

Within Species: Within individual species, the correlation between density and ultrasonic velocity tends to be positive but often less pronounced than interspecies trends. This variability is influenced by factors such as microscopic anatomical structure, moisture content, and cell arrangement. For instance, Sei Chang (2020 found correlation coefficients of 0.75 in the longitudinal-tangential plane and 0.52 in the longitudinal-radial plane of wood samples. Baar et al.(2012) reported coefficients of determination (R^2) between 0.51 and 0.79 for the heartwood of several tropical hardwoods—including *Doussie*, Merbau, *Panga panga*, *Tigerwood*, and *Zebrano*—highlighting how species-specific anatomical features impact the density-velocity relationship.

Moisture Content (MC)

The effect of moisture content (MC) on ultrasonic wave velocity in wood is well-established and exhibits species-dependent behavior. Generally, increasing MC leads to a decrease in longitudinal ultrasonic wave velocity, reflecting reduced stiffness and increased damping in water-saturated wood ((Kang & Booker, 2002; Ross & Pellerin, 1991; W. T. Simpson & Wang, 2001) (Fig. 1.37). For example, Montero et al. (2015)) reported a strong negative correlation (r = 0.98) between MC and ultrasonic velocity in *Spanish Scots Pine*.

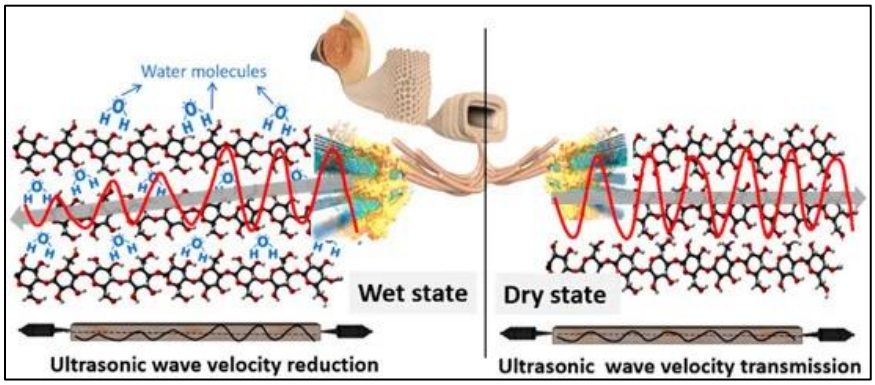

Figure 1. 37 Effect of Moisture Content on Ultrasonic Wave Velocity in Wood (Paniagua et al., 2022).

Research indicates that when wood is dried from moisture content above the fiber saturation point (FSP, approximately 30%) down to the FSP, a slight increase in velocity occurs ((Bucur, 2006; Mishiro, 1995; Sakai et al., 1990; W. T. Simpson & Wang, 2001). A more pronounced increase is observed as MC decreases from the FSP to oven-dry conditions, with velocities rising significantly as the wood loses free water (S. Y. Wang & Chuang, 2000). For *Spruce*, Sandoz, (1989) experimentally determined that longitudinal wave velocity decreases by about 0.8% for each 1% increase in MC between 5% and 30%.

Species-specific studies further illustrate this trend. Goncalves & da Costa, (2008) found that ultrasonic velocity in *Goupia Glabra* decreases by 23.6 m/s for each percentage point increase in MC, whereas *Araucaria Angustifolia* shows a 25.4 m/s increase in velocity as MC reduces from FSP to oven-dry. Increased moisture content not only lowers wave velocity but also amplifies

wave attenuation, with the highest velocities and lowest attenuation consistently recorded under dry conditions (Oliveira et al., 2005).

Structural Defects

Structural defects such as cracks, holes, and notches significantly affect the propagation of ultrasonic waves through wood by altering the wave paths and increasing signal attenuation. Upon encountering defects, ultrasonic waves may be reflected, absorbed, or redirected around the irregularity, effectively lengthening the travel path and reducing the measured wave velocity. (Filgueira et al., 2015; W. Lin & Wu, 2013; Senalik et al., 2014) Additionally, defects cause energy loss through scattering and absorption, weakening the received signal and increasing variability in velocity measurements depending on the defect's size, shape, and location (Berndt & Johnson, 1995; Kabir & Araman, 2003; Van Dyk & Rice, 2005).

Reinprecht & Pánek, (2012) demonstrated that larger notches cause reductions in ultrasonic wave velocity ranging from 35.4% to 70%, highlighting the significant impact of defects on wave propagation. However, the correlation between notch width and velocity reduction was modest (R^2 = 0.473 and 0.214), indicating notable variability between samples.

Similarly, Wang and Wang & Wang (2011) reported a negative correlation between hole size and ultrasonic velocity, with larger holes causing greater velocity decreases due to increased deviation of the wave path, in specific studies on Korean pine, wave velocity and transmission time increased with specimen length in defect-free samples but decreased markedly in defective ones. Additionally, the size of axial holes strongly correlated with ultrasonic velocity, with correlation coefficients of 0.960 and 0.964 for transmission time and velocity, respectively, underscoring the critical influence of defect dimensions on wave propagation parameters.

Propagation Length

The propagation length, or the distance over which ultrasonic waves travel through wood material, significantly influences measured wave velocity. Empirical investigations consistently demonstrate that longer propagation paths correlate with increased ultrasonic wave velocities.

For example, Tuğba Yılmaz and Murat (2018)) studied various wood species—including *Oriental Beech, Scots Pine*, *Black Pine*, and *Turkish Red Pine*—and reported that increasing sample lengths from 20 mm to 40 mm resulted in up to a 25.49% increase in ultrasonic velocity. This substantial rise underscores the importance of considering propagation length in ultrasonic measurements. Similarly, W. Lin & Wu (2013) observed a strong positive correlation (r = 0.883) between wave velocity and sample length in *Korean Pine*, further confirming propagation length as a critical variable in ultrasonic evaluation of wood.

Relationship Between Ultrasonic Velocity and Mechanical Properties

Ultrasonic methods tend to report elastic parameters higher than those from direct mechanical testing, largely due to calculation approaches leading to overestimations of dynamic moduli, especially longitudinally (Bucur, 2006; Ozyhar et al., 2013). Reported discrepancies range from 10% to 40%, often amplified by higher frequencies (Divós & Tanaka, 2005; Keunecke et al., 2007; Kránitz et al., 2014). Wood's natural heterogeneity compounds this effect, as increased frequency heightens sensitivity to localized defects and irregularities (Bucur & Archer, 1984).

Nonetheless, numerous studies demonstrate strong correlations between ultrasonic velocity and MOE, validating ultrasonic methods' reliability. Duong & Hasegawa, (2024) reported a significant

correlation in *Acacia mangium* ($r = 0.83$, $P < 0.001$), with stress wave methods often exhibiting even stronger correlations (r up to 0.94) as consistent with Ishiguri et al. (2008). Comparable results appear in hybrid *Eucalyptus* wood, with correlations of $r = 0.945$ for static MOE and $r = 0.375$ for dynamic MOE (SEIDU et al., 2024).

Species-specific variations are substantial: in *Eucalyptus delegatensis* (Alpine Ash), MOE and dynamic modulus correlation reached 0.95, whereas lower correlations ($r = 0.57$ and 0.45) were recorded in *Cunninghamia Lanceolata* (China Fir) for stress wave and ultrasonic velocity respectively (Duong & Hasegawa, 2024b; Ilic, 2001). These variations highlight the critical influence of wood anatomy on wave propagation and property estimation accuracy.

Studies on large cross-section timber indicate reliable ultrasonic prediction of mechanical properties: *Spruce* reported R^2 values of 0.66 to 0.83 for longitudinal velocity and mechanical properties (Sandoz, 1989, 1993). In Spanish conifers, longitudinal ultrasonic velocity correlated with MOE ($R^2 \approx 0.74$) and strength ($R^2 \approx 0.60$) (Íñiguez et al., 2008). This evidence collectively demonstrates ultrasonic testing's potential and limitations, shaped by species, sample size, and method applied.

Shear waves, traveling perpendicular to the grain, offer additional insights by revealing the shear modulus (G), which measures resistance to shear stress and deformation (Kretschmann, 2010). Understanding G is crucial for predicting wood performance under torsional and bending loads, where shear contributes significantly to structural behavior (Schot, 1999). Experimental research connects higher shear modulus values with stronger resistance to shear deformation and improved structural stability (André Luis et al., 2014; Aydin & Ciritcioğlu 2022; Ukyo et al., 2010).

Sensitivities analyses demonstrate G's importance primarily at grain orientations between 50° and 60°, where maximal wave velocity variations occur (Espinosa, Brancheriau, et al., 2018). Extending this, Espinosa et al. (2019) emphasize the necessity of multi-directional ultrasonic measurements to fully capture and characterize wood's complex anisotropy and mechanical response under variable loading conditions.

1.4 Research rationale and objectives

The submerged timber piles of Hévíz Lake, Hungary, function as both foundational elements and heritage components. These piles are continuously exposed to the lake's aggressive aquatic environment, characterized by geothermal waters with elevated temperatures, high mineral content, and active biological processes. These conditions accelerate the chemical, physical, and biological degradation of timber, resulting in reductions in stiffness, compressive strength, and buckling resistance. Consequently, the stability of lakeside buildings and the preservation of historically significant structures are at risk.

Traditional destructive testing is impractical in this context. Extracting piles would compromise their function and violate heritage protection regulations, while in-situ destructive sampling would further weaken already vulnerable elements. These constraints underscore the necessity of adopting non-destructive evaluation (NDE) techniques that can infer the internal mechanical properties of submerged wood without causing damage.

Among the available NDE methods, ultrasonic testing (UT) is particularly promising, as it allows indirect quantification of wave propagation velocity, from which the dynamic modulus of elasticity (MOE) and critical buckling resistance can be inferred. However, ultrasonic predictions often rely on simplifying assumptions such as material homogeneity and isotropy, limiting their accuracy in field conditions. Finite element modeling (FEM) offers a robust computational approach to

simulate anisotropic timber behavior under submerged and soil-embedded boundary conditions. By integrating UT with FEM validation, this research develops a dual-method framework that enhances reliability, reduces uncertainty, and establishes a scientifically defensible scheme for risk classification of submerged wooden piles.

Research Objectives

The primary aim of this study is to evaluate the structural integrity and buckling behavior of submerged timber piles in Hévíz Lake, using ultrasonic non-destructive testing (NDT) as a diagnostic tool. Specific objectives include:

1. To evaluate the in-situ mechanical condition of submerged timber piles using ultrasonic non-destructive testing (NDT) by quantifying longitudinal wave velocity as an indicator of stiffness degradation and internal defects.
2. To quantify the dynamic modulus of elasticity (MOE) and critical buckling load of the piles from ultrasonic data by applying wave propagation theory and Euler–Bernoulli beam mechanics, establishing correlations between material properties, ultrasonic measurements, and structural performance.
3. To develop a systematic classification framework for structural risk assessment, categorizing submerged piles into stability states (safe, at risk, significant risk) based on velocity thresholds and modulus values, thereby identifying piles at risk of structural failure.
4. To construct three-dimensional finite element models (FEM) of representative pile geometries in COMSOL Multiphysics, explicitly incorporating anisotropic wood properties, lakebed soil–pile interactions, and submerged boundary conditions.
5. To validate the predictive capability of ultrasonic data by comparing it with FEM simulations, emphasizing the accuracy of stress distribution, deformation patterns, and buckling resistance assessments.

1.5 Dissertation Outline

This dissertation is structured into four chapters as follows:

Chapter I – Outlines the problem statement and the research outcomes. It presents a comprehensive review of the structural stability and degradation mechanisms in lake-building construction, emphasizing the interactions among material properties, environmental conditions, and structural factors. The chapter focuses on buckling as a critical failure mode and reviews advanced non-destructive testing (NDT) methods, with special emphasis on ultrasonic testing for evaluating wooden pile integrity via wave propagation.

Chapter II –Details the materials and methods used, divided into two sections. The first section covers non-destructive testing (NDT), specifically ultrasonic testing, to measure material properties—sound velocity, dynamic modulus of elasticity, and buckling load—in wooden piles submerged in the Hévíz Lake environment. To improve the predictive accuracy of these measurements, machine learning techniques were integrated with ultrasonic data analysis using *MATLAB*

R2023a. This approach enabled enhanced interpretation of ultrasonic signals and refined estimation of mechanical parameters beyond traditional methods.

The second section describes the use of finite element modeling (FEM) in *COMSOL Multiphysics 6*. This computational framework was employed to validate ultrasonic test data and simulate the mechanical behavior, stress distributions, and failure modes of timber piles under realistic environmental and loading conditions. The combined experimental-computational methodology strengthens the reliability of timber structural assessments in submerged contexts.

Chapter III – presents and discusses empirical relationships between ultrasonic testing parameters and wooden pile structural stability. It validates ultrasonic findings through FEM simulations, comparing theoretical critical buckling loads derived from ultrasonic data with effective loads from FEM. The chapter identifies failure thresholds for instability and excessive deformation, proposing a risk classification system for submerged piles and evaluating safety margins.

Chapter IV – Presents the conclusions of the research and offers recommendations for future research.

CHAPTER II: METHODOLOGY

2.1 Research Approach

This research employs a comprehensive methodology combining non-destructive testing (NDT) and finite element modeling (FEM) to evaluate the stability of wooden piles submerged in lake environments, focusing on those supporting structures in Hévíz, Hungary.

Ultrasonic testing serves as the primary NDT technique, enabling measurement of key material properties such as sound velocity and dynamic modulus of elasticity (MOE), along with estimation of critical buckling loads. To improve the predictive accuracy of these measurements, machine learning techniques were integrated with ultrasonic data analysis This integration enables enhanced processing and interpretation of ultrasonic signals, allowing more reliable estimation of timber mechanical properties under complex environmental conditions.

A representative subset of 40 wooden piles was selected from an initial population of 400 for detailed analysis. The study aims to establish quantitative relationships between these material properties—sound velocity, MOE, and buckling load—and the piles' structural integrity under the unique environmental conditions of the lakebed.

Complementing the experimental data, FEM simulations model pile behavior under various conditions, validating the ultrasonic testing results and providing detailed insights into internal stresses and potential failure modes, thereby improving predictions of stability and buckling resistance.

The methodology is divided into two main approaches:

1. **Experimental Approach – Non-Destructive Testing and Structural Assessment:** Ultrasonic testing was employed to measure longitudinal sound velocity and derive the dynamic modulus of elasticity (MOE) for each pile. Advanced signal processing and machine learning-assisted analysis in MATLAB R2023a enhanced the accuracy of property estimation under complex environmental conditions. These measurements were used to calculate theoretical critical buckling loads, assess in-situ load-bearing performance, and classify piles into risk categories (low, moderate, high) based on residual structural capacity.

2. **Numerical Approach – Finite Element Modeling (FEM) and Validation:** FEM simulations using COMSOL Multiphysics 6.0 were conducted to replicate the mechanical response of the piles under realistic boundary and loading conditions, including soil-pile interactions and submersion effects. FEM-derived critical buckling loads and deformation patterns were compared with ultrasonic-based estimates to validate experimental results. This comparison also refined the risk classification, offering detailed insights into internal stress distribution, deformation behavior, and potential failure mechanisms.

2.2 Experimental methods

2.2.1 Study Area and Sampling

This experimental investigation was conducted at Hévíz Lake, Hungary, where 40 submerged wooden piles supporting lake-based structures were selected from an initial dataset of 400 piles (Figs. 2.1–2.2). These heritage elements are subject to unique environmental conditions due to prolonged immersion in thermal waters. Piles were selected based on structural significance, accessibility, and visible signs of deterioration or historical damage.

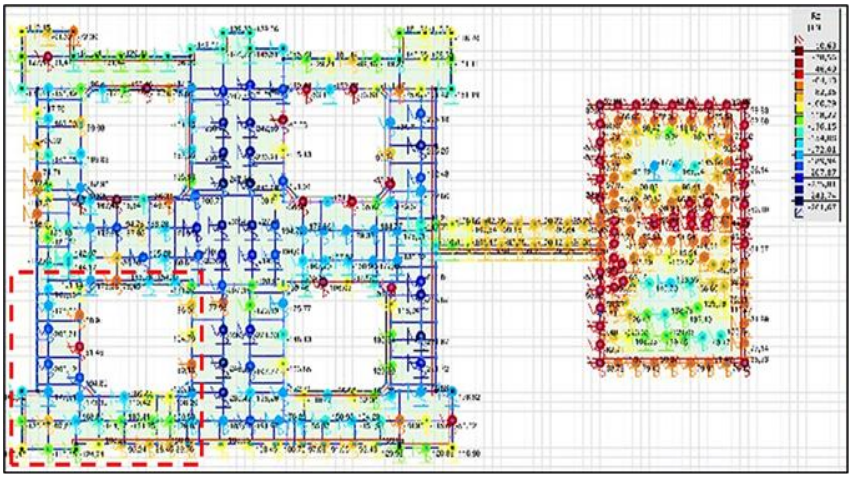

Figure 2.1 Structural modeling of submerged wooden piles in Hévíz Center, emphasizing 40 piles under evaluation (Author).

Figure 2.2 Hévíz Lake Building – Tested Structural Section (Author).

The majority of the piles were composed of timber species such as spruce, larch, and oak. with circular cross-sections between 20–29 cm in diameter. However, the specific research samples analyzed in this study were identified as spruce with a uniform diameter of 20 cm.

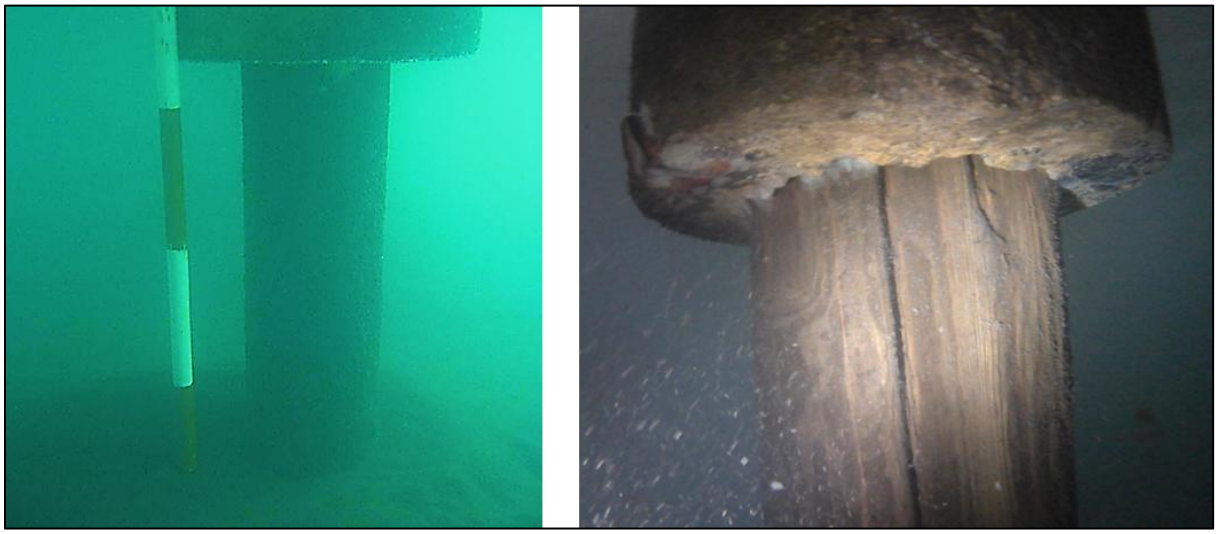

Figure 2.3 A wooden pile submerged in Hévíz lake (Author).

The piles were extracted from the central portions of mature trunks, retaining the presence of the pith. To enhance their structural stability and optimize load distribution, the tops of the piles were

capped with concrete, as shown in Figure 2.3. Over time, these submerged piles have experienced varying degrees of degradation due to prolonged exposure to the lake's thermally enriched and mineral-laden waters (Figure 2.4).

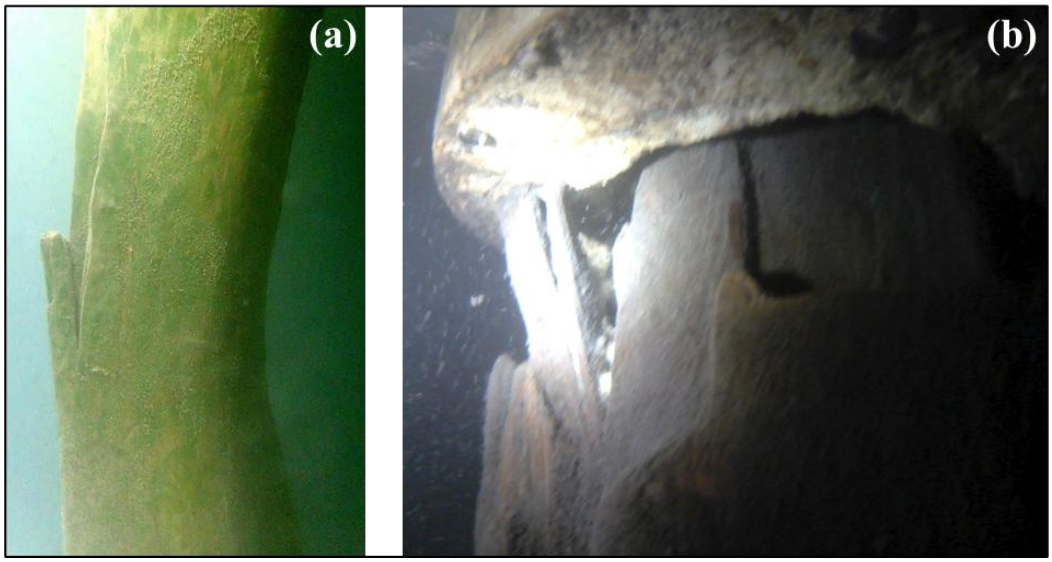

Figure 2.4 (a) Wooden pile exhibiting buckling deformation; (b) Degradation features in a wooden pile (Author).

2.2.2 Site and Environmental Conditions

The piles were driven into the lakebed, consisting of a thin, rocky layer (0.3–1.4 m) above peat, with underlying clay and sand strata. The piles remain fully submerged in geothermal waters with temperatures ranging from 33–36 °C in summer and 23–25 °C in winter. The water, rich in Na, K, Mg, Ca, and SO_4, has a neutral pH (7.14) and plays a significant role in wood degradation.

The piles in this study are modeled as simply supported, with hinged ends, reflecting the boundary conditions observed in the field. This configuration enables free rotation at the pile ends, accurately simulating the natural behavior of the piles under various environmental and loading conditions.

2.2.3 Non-Destructive Testing: Ultrasonic Wave Velocity Measurements

Due to wood's anisotropic nature, ultrasonic wave velocities were measured along multiple axes to assess mechanical behavior. Measurements were obtained using a FAKOPP Microsecond Timer, a non-destructive acoustic time-of-flight instrument consisting of two sensors and a timing unit.

For the longitudinal direction, the sensors were mounted on the lateral surface of each pile with a spacing of 80 cm along the grain. The transmitter and receiver probes were inserted at an angle of approximately 45° into the wood using a rubber mallet to ensure firm coupling. An acoustic pulse was generated by striking the transmitter probe with a metallic hammer, and the travel time was recorded by the receiver in microseconds (μs). Wave propagation in this configuration occurred parallel to the fiber direction.

The procedure was then repeated for the radial–tangential (RT) plane. In this configuration, the system was mounted on the cross-sectional face of each pile, with probes again inserted at approximately 45° within the RT plane. This orientation produced an off-axis path combining radial and

tangential components. The acoustic pulse was generated in the same manner, and wave travel time was recorded in microseconds (μs).

In-situ testing was conducted at Hévíz Lake Spa with assistance from professional divers, who positioned the sensors on the cross-sectional faces of submerged piles. The acoustic signal was triggered by striking the "START" sensor, and the resulting travel times were recorded by a team stationed on a boat (see Figure 2.5). Divers also measured the diameter of each pile and performed visual inspections to identify signs of surface degradation.

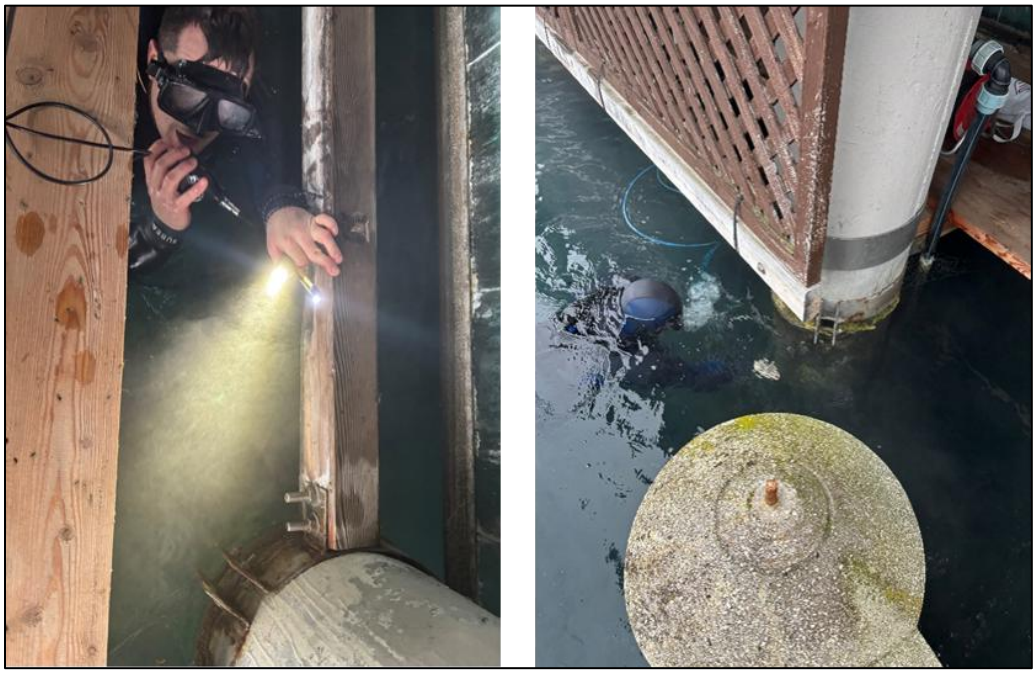

Figure 2.5 In situ diver-assisted sound velocity measurement at Hévíz Lake (Author).

Based on the recorded diameters measured using a folding ruler (see Figure 2.6a), the effective cross-sectional area of each pile was calculated. This approach enabled accurate and repeatable data collection while preserving the structural integrity of the wood. Additionally, the use of an underwater inspection camera system (see Figure 2.6b) provided valuable insights into the condition and degradation of the submerged timber under real-world environmental conditions. The underwater camera system employed was an Endoscope camera featuring a 4.3-inch IPS display, a 7.9 mm triple camera head, and an IP67 waterproof rating, connected via a 10-meter hard cable (model T20).

To ensure measurement reliability, each pile was tested three to five times. Sound velocity was calculated using the known distance between the sensors and the corresponding TOF. This non-destructive testing (NDT) method allowed for internal condition assessment without requiring physical sampling or structural intervention.

All measurements were conducted during the winter season. Ambient air temperature ranged from 5–8 °C, whereas the geothermal lake water remained consistently warmer at 23–25 °C. Relative humidity above the lake surface was recorded at 70–80% using a calibrated Extech SDL500 temperature–humidity meter and data logger, installed 1.2 m above the water. The instrument measures temperature from 0–50 °C with an accuracy of ±1 °C and a resolution of 0.1 °C, and relative humidity from 5–95% RH with an accuracy of ±3% RH and a resolution of 0.1% RH. The

device was mounted on a stable, non-metallic support to ensure unobstructed airflow and minimize interference from water splash.

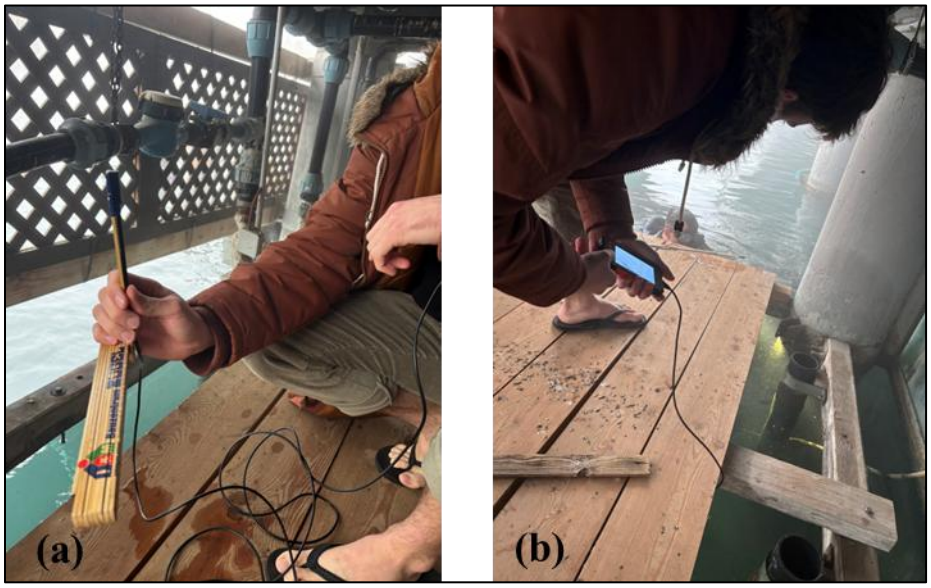

Figure 2.6 (a) Measuring pile diameter using a folding ruler during in-situ inspection, (b) Underwater inspection camera system capturing the condition of submerged timber (Author).

Wave transit time (T) and pile length (L) were used to calculate wave velocity (v), as shown in Equation (1):

$$v = \frac{L}{T} \tag{1}$$

Where: v - is the ultrasonic velocity (m/s) ; L - is the length of the specimen (m) ; T - is the transit time (s).

2.2.4 Dynamic Elastic Modulus of Piles

To evaluate the load-bearing capacity of the submerged wooden piles, it is essential to determine their strength properties, which are assessed through species-specific strength classification. This classification primarily relies on the elastic modulus (MOE), which, in turn, requires knowledge of the wood density and the sound velocity along the grain direction. Since direct density measurements were not feasible due to the submerged conditions, species-specific mean density values were used for estimation. The piles under investigation were predominantly spruce, with a reference mean density of 470 kg/m³(Manuel, 2017; Seim et al., 2022).

To determine the elastic modulus, a methodology developed at the Bódig József Non-Destructive Wood-Testing Laboratory, University of Western Hungary, was employed. This approach allows for the measurement of the dynamic MOE in built-in wood structures and facilitates the estimation of their bending strength. The computed elastic modulus was then used for strength classification according to the MSZ EN 338 standard as illustrated in Table 2.1.

Grade	C14	C16	C18	C20	C22	C24	C27	C30	C35	C40	C45	C50
MOE	7	8	9	10	10	11	12	12	13	14	15	16
MOE 95%	6,650	7,600	8,550	9,025	9,500	10,450	10,925	11,400	12,350	13,300	14,250	15,200

Density	290	310	320	330	340	350	370	380	400	420	440	460
Mean density	350	370	380	390	410	420	450	460	480	500	520	550

Table 2. 1 strength classification according to the MSZ EN 338 standard (European Committee for Standardization (CEN), 2016).

The dynamic modulus of elasticity (Edyn) was calculated based on the relationship between sound propagation velocity and wood density as expressed in Equ.2:

$$E_{\mathrm{dyn}} = \mathrm{v}^2 \cdot \rho \tag{2}$$

where E_{dyn} - represents the dynamic elastic modulus [MPa]; v- is the sound propagation velocity in the wood [m/s]; and ρ- is the density [kg/m³].

It is important to emphasize that MOE calculation was restricted to longitudinal wave velocities. This restriction stems from the underlying assumption of Equation (2) that wave propagation behaves as a one-dimensional longitudinal wave in a homogeneous, elastic medium—conditions most closely approximated along the fiber direction. In the radial–tangential plane, wave propagation is significantly more complex, involving multiple modes such as shear, surface, and mode-converted waves, due to wood's anisotropic and heterogeneous structure across the grain. Consequently, applying this equation to radial–tangential velocities would violate its assumptions and could yield unreliable stiffness estimates. For this reason, radial–tangential velocities were used exclusively to examine anisotropic wave propagation characteristics rather than for direct MOE computation

2.2.5 Critical Buckling Load and Pile Length Determination

To quantify the load-bearing capacity of the piles and determine their susceptibility to buckling failure under axial loads, data on the lengths of the piles were required. The pile lengths were measured using the FNIRSI 1014D digital oscilloscope, which features a 100 MHz bandwidth and a 1 GSa/s sampling rate, enabling high-resolution waveform acquisition. Wave transmission was facilitated by a pair of piezoelectric longitudinal transducers (central frequency: 50 kHz; manufacturer: FNIRSI, Shenzhen, China), which were coupled to the pile surface using beeswax to ensure stable acoustic contact and minimize energy loss.

These transducers primarily generate longitudinal stress waves characterized by particle motion parallel to the direction of wave propagation.

To assess velocity in the grain direction, pile locations were identified from structural blueprints and accessed through the floor above. The transmitter was positioned on the top surface of the pile head, and the receiver was mounted laterally along the vertical axis of the pile, allowing measurement of wave propagation parallel to the wood fibers (i.e., along the grain). Vibrations were induced by impacting the pile head with a blunt steel hammer, generating a stress wave detected by the receiving transducer (Fig. 2.7).

Each pile was tested three to five times, and trials affected by coupling inconsistencies, interface discontinuities, or excessive noise were discarded and repeated.

Figure 2.7 Oscilloscope-Based Measurement and Signal Detection Setup for Pile Vibration Analysis (Author).

The pile length was then calculated by measuring the elapsed time of the sound wave's propagation, which allowed for the determination of the pile's depth. In certain instances, the presence of perturbing factors—such as layers between the flooring and the pile, material defects, or air gaps—impeded the accurate detection of the signal.

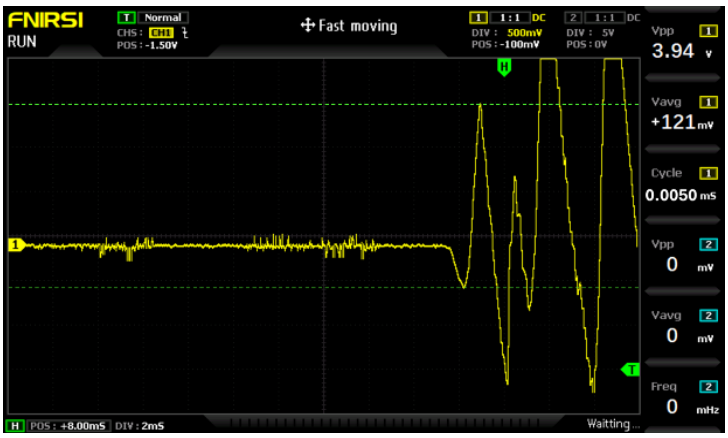

Figure 2.8 Signal acquisition: raw voltage signal recorded from Pile 1 by the FNIRSI oscilloscope during in-situ measurement, showing the unfiltered real-time response prior to any digital processing (Author).

To enhance data accuracy (Fig 2.8), raw ultrasonic signals were post-processed using *MATLAB R2023a* following these steps: (1) bandpass filtering between 30–70 kHz to remove ambient and electronic noise; (2) Hilbert transform-based envelope detection to emphasize wave onset; (3) first arrival time identification using a threshold method, where the first arrival was defined as the time at which the signal envelope exceeded 20% of its maximum amplitude; and (4) outlier rejection and aggregation, with the median of multiple valid trials (3–5 per pile) used to represent the final wave velocity for each direction. Figure 2.9 illustrates a representative raw ultrasonic waveform recorded from Pile 1 alongside the corresponding processed signal, highlighting the identification of the first arrival time using the 20% envelope threshold.

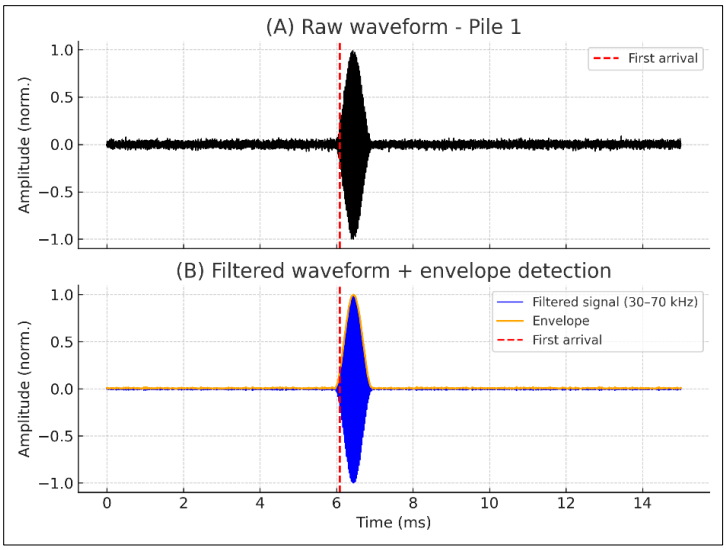

Figure 2.9 (A) Raw ultrasonic waveform from Pile 1. (B) Processed signal after bandpass filtering and envelope detection, with the dashed red line marking the first arrival time at 20% of the envelope's peak. The illustration is based on Pile 1's time (Author).

The time-voltage signal obtained from the oscillator was used to calculate the pile length, with the propagation velocity(c) determined based on the material properties of the pile, using the following equation:

$$\mathrm{L_{pile}} = V_L \cdot \frac{\mathrm{t}}{2} \tag{3}$$

Where L_{pile} – is the length of the pile [m]; v_L– is the longitudinal wave velocity in the wood [m/s]; and t– is the measured round-trip travel time of the acoustic wave[s].

The critical buckling load of submerged timber piles was determined using two complementary analytical methods to rigorously assess structural stability.

Initially, the classical Euler–Bernoulli beam theory was applied to compute the idealized buckling load as expressed by the equation:

$$\mathrm{P_{cr}} = \frac{\mathrm{K}\, E_L\, \mathrm{I}}{\mathrm{L}^2} \tag{4}$$

Where P_{cr} – is critical buckling load [kN]; K– is a constant related to the boundary conditions. In our case, we have a simply Supported Pile (K = 1), E_L– is the longitudinal modulus of elasticity [MPa], I– the moment of inertia of the cross-section [m4], and L– is the pile length [m].

To account for timber's orthotropic material properties and shear deformation effects, the critical load was recalculated using Granholm's correction factor, which modifies the Euler load by

$$P_{\text{cr, Granholm}} = \phi \times P_{\text{cr, Euler}} \tag{5}$$

where the correction factor ϕ is given by:

$$\phi = \frac{1}{1+\frac{P_{cr,\,Euler}}{G_{eff} \times A}} \tag{6}$$

Here, G_{eff} is the effective shear modulus calculated as the average of experimentally derived shear moduli in principal directions (G_{LR}, G_{LT}, G_{RT}), and A is the pile's cross-sectional area.

This dual-method analytical procedure was systematically applied to each of the 40 sampled timber piles. The resulting comparative dataset allows assessment of the influence of shear and anisotropy corrections on buckling load predictions, improving insight beyond the classical Euler model.

2.2.6 Risk classification (data analysis & statistics)

To assess the structural condition of the timber piles, risk classification thresholds were established by integrating ultrasonic wave velocity and dynamic modulus of elasticity (MOE). These thresholds were derived from ASTM D2555 reference design standards and calibrated using both field data and structural performance indicators.

Timber piles were classified into three risk levels—Significant Risk, At Risk, and Safe—based on their mechanical properties. The classification framework is summarized in Table 2.2.

Risk Level	Wave Velocity (v)	Modulus of Elasticity (MOE)	Interpretation
Significant Risk	v < 4500 m/s	MOE < 6 GPa	Pile lacks stiffness; highly susceptible to premature buckling
At Risk	4500 ≤ v ≤ 5000 m/s	6 GPa ≤ MOE ≤ 10 GPa	Moderate stiffness; may buckle under higher loads or in slender configurations
Safe	v > 5000 m/s	MOE > 10 GPa	High stiffness; good resistance to buckling in typical structural conditions

Table 2. 2 Risk classification criteria based on ultrasonic wave velocity and dynamic MOE (ASTM International, 2017).

Risk thresholds were statistically validated using the 33rd and 66th percentiles of the MOE distribution, segmenting the pile dataset into lower, middle, and upper thirds. These thresholds were cross-referenced with historical structural performance records, establishing a reliable, non-destructive basis for maintenance prioritization and assessment of residual load-bearing capacity in submerged timber piles.

2.3 Numerical methods

Finite Element Modeling (FEM) was performed in COMSOL Multiphysics 6.0 to simulate the mechanical behavior of submerged timber piles under realistic boundary and loading conditions. The primary aim was to validate ultrasonic testing results, specifically wave velocities and the derived dynamic modulus of elasticity, by analyzing stress distribution, lateral displacements, and critical buckling loads.

Unlike simplified analytical approaches, the FEM models account for soil embedment and submersion effects, providing a more precise estimation of pile stability, deformation patterns, and

buckling resistance. Detailed models were developed for each of the 40 piles, incorporating measured material properties, boundary conditions, and axial load scenarios. The simulated mechanical responses were then directly compared with experimental ultrasonic-based predictions to evaluate the reliability of non-destructive measurements in assessing in-situ structural performance.

2.3.1 Model Geometry and Material Properties

The FEM models represent each timber pile as a cylinder, with a uniform diameter of 0.2 m and lengths corresponding to experimental measurements (Fig. 2.10). This geometric idealization provides a consistent basis for simulating mechanical response under axial and lateral loads.

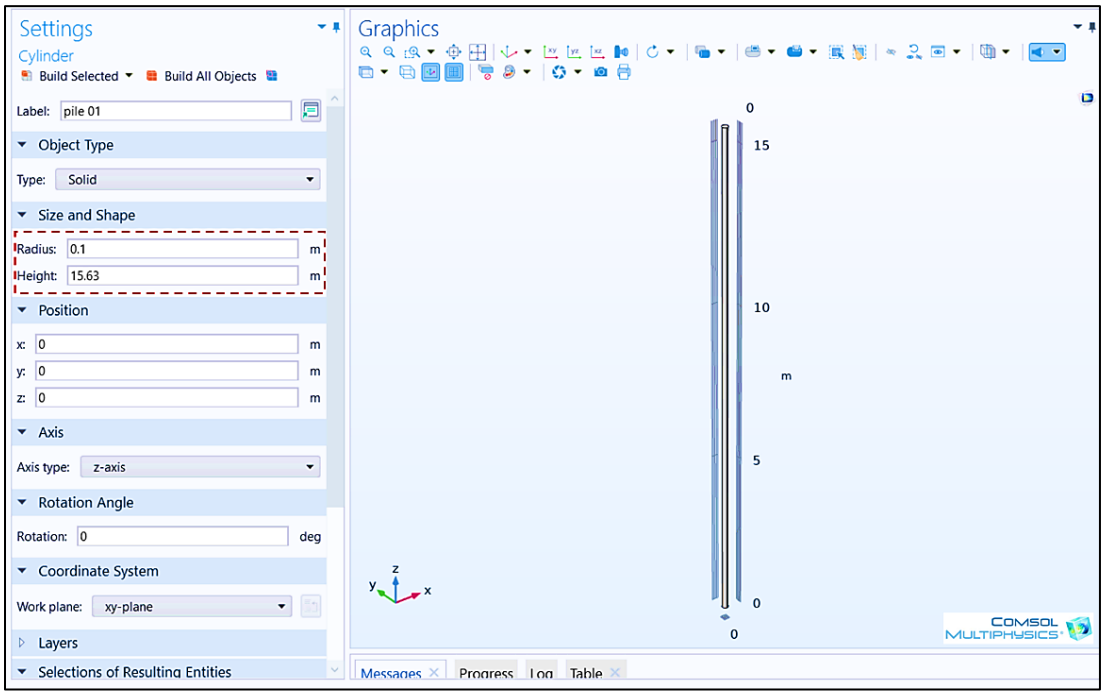

Figure 2.10 Geometric model of wooden pile No. 01 in COMSOL Multiphysics (Author).

Wood was modeled as an orthotropic material to capture directional variations in mechanical behavior. Longitudinal (E_L), radial (E_R), and tangential (E_T) elastic moduli were derived from ultrasonic testing data and calculated using established material property ratios from the literature. These parameters ensure that the FEM accurately reflects anisotropic stiffness characteristics of the submerged timber, enabling reliable prediction of stress distributions, deformations, and critical buckling behavior.

<u>Longitudinal Elastic Modulus (EL)</u>

In each FEM simulation:

$$E_L = MOE_{dynamic}$$

Where E_L- is longitudinal elastic modulus for that pile, $MOE_{dynamic}$ – is dynamic modulus value measured from ultrasonic testing.

Radial and Tangential Modulus

Given that wood exhibits orthotropic mechanical behavior, the Radial Elastic Modulus (E_R) and Tangential Elastic Modulus (E_T) are estimated using standard ratios outlined in ISO 3349 (Determination of Modulus of Elasticity for Wood in Bending).

$$E_R \approx 0.10 \times E_L \tag{7}$$

$$E_T \approx 0.05 \times E_L \tag{8}$$

These calculated values are incorporated into the Finite Element Model (FEM) to accurately simulate the mechanical behavior of the piles under different loading conditions.

Final Material Properties Used in FEM

Property	Symbol	Value
Longitudinal Elastic Modulus	(E_L)	Measured (from ultrasonic testing)
Radial Elastic Modulus	(E_R)	$0.10 \times E_L$
Tangential Elastic Modulus	(E_T)	$0.05 \times E_L$
Density of spruce wood	(ρ)	470 kg/m³

Table 2. 3 Material Properties (Author).

Poisson's Ratios (vLR, vLT, vRT) in Submerged Wooden Piles

As wooden piles are submerged in an aquatic environment, their moisture content increases beyond the Fiber Saturation Point (FSP) (~30%), at which point Poisson's ratios stabilize, showing minimal change. The specific values for Poisson's ratios of spruce wood (ν_{LR}, ν_{LT}, ν_{RT}) in dry conditions are derived from available studies and general trends in wood properties (Arriaga et al., 2023; Bartolucci et al., 2020; Kumpenza et al., 2018).

Poisson's ratio	Dry Wood (0-12% MC)	MC (~FSP, 25-30%)
ν_{LR} (Longitudinal-Radial)	0.37 – 0.42	↑ Increase ~10-15%
ν_{LT} (Longitudinal-Tangential)	0.44 – 0.49	↑ Increase ~10-15%
ν_{RT} (Radial-Tangential)	0.05 – 0.07	↑ Increase ~10-15%

Table 2. 4 General Trend of Poisson's Ratio with Moisture Content (Bartolucci et al., 2020).

Empirical Adjustment Formula for Poisson's Ratio

The following formula is used to adjust Poisson's ratios based on moisture content:

$$\nu_{MC} = \nu_{dry}\left(1 + C_\nu \frac{MC}{30}\right) \tag{9}$$

Where ν_{MC}– is Poisson's ratio at a given moisture content, ν_{dry} – is Poisson's ratio at dry conditions (~12% MC), C_ν – is Moisture correction factor (approx. 0.10 - 0.20 depending on direction), MC

– is Moisture content (%),30% is used as a reference because it represents the fiber saturation point (FSP).

Poisson's ratio	Dry Wood (0-12% MC)	Adjusted for Submersion (~30%MC)	Average Value
ν_{LR} (Longitudinal-Radial)	0.37 – 0.42	0.41 – 0.48	0.445
ν_{LT} (Longitudinal Tangential)	0.44 – 0.49	0.48 – 0.56	0.52
ν_{RT} (Radial-Tangential)	0.05 – 0.07	0.06 – 0.085	0.0725

Table 2. 5 Adjusted Poisson's Ratios for Submersion (~30% MC) (Author).

These properties are input into *COMSOL Multiphysics 6.0* to define the material's mechanical response. Furthermore, the material is modeled as orthotropic to accurately represent the directional dependence of wood's mechanical behavior (Fig 2.11).

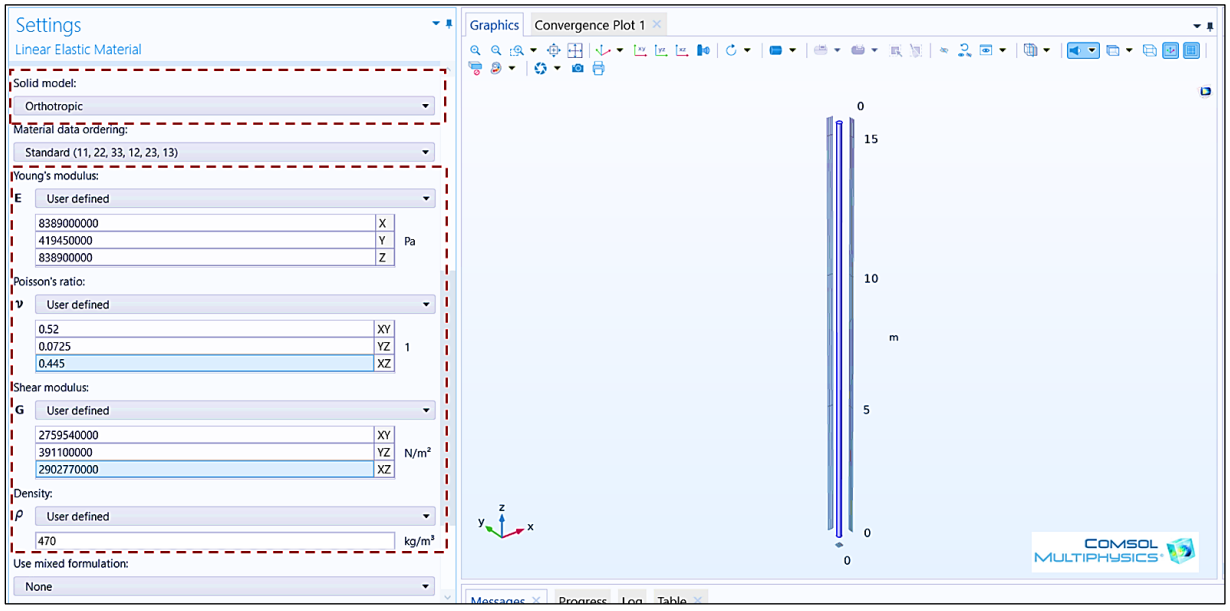

*F*igure 2.11 Orthotropic material properties of wooden pile No. 01 in COMSOL, showing anisotropic elastic behavior with moduli, Poisson's ratios, and density for finite element modeling (Author).

2.3.2 Boundary Conditions

Boundary conditions were established to realistically simulate pile–soil interaction and structural response under axial loading. Piles were modeled as simply supported with hinged ends, reflecting typical field conditions. Vertical displacements at the top and base were restrained (uy = 0), while horizontal displacements and rotations were left unconstrained to allow realistic bending.

In COMSOL Multiphysics 6.0, these conditions were implemented within the Solid Mechanics interface using *Prescribed Displacement boundary conditions*. At both ends, vertical displacement (uy = 0) was applied, while horizontal motion and rotation remained free, reproducing the hinge-like support observed in situ (Figure 2.12).

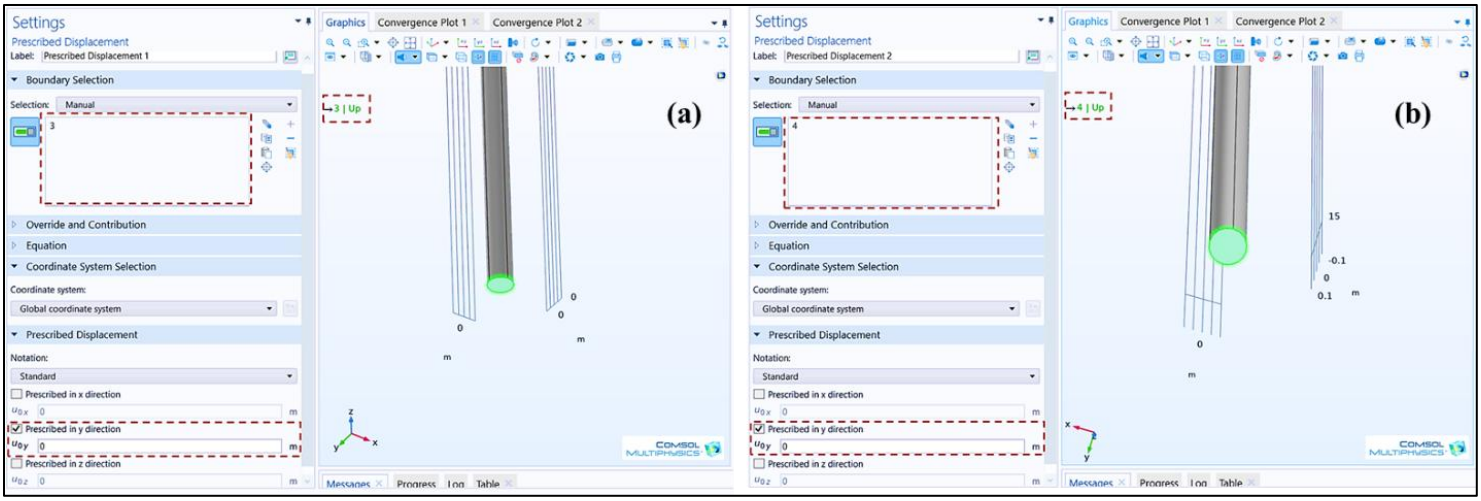

Figure 2.13 COMSOL boundary conditions for a simply supported pile No. 1 with hinged ends: (a) top, uy=0, rotation free; (b) base, uy=0, rotation free (Author).

Axial loading was applied incrementally to the pile head to simulate compressive forces from overlying structures or environmental loads. Two representative load steps were considered: 1,000 N to represent initial service conditions and 10,000 N approaching the critical buckling threshold. These loading increments allowed assessment of stress distribution, deformation patterns, and buckling response under realistic operational scenarios (Figure 2.13).

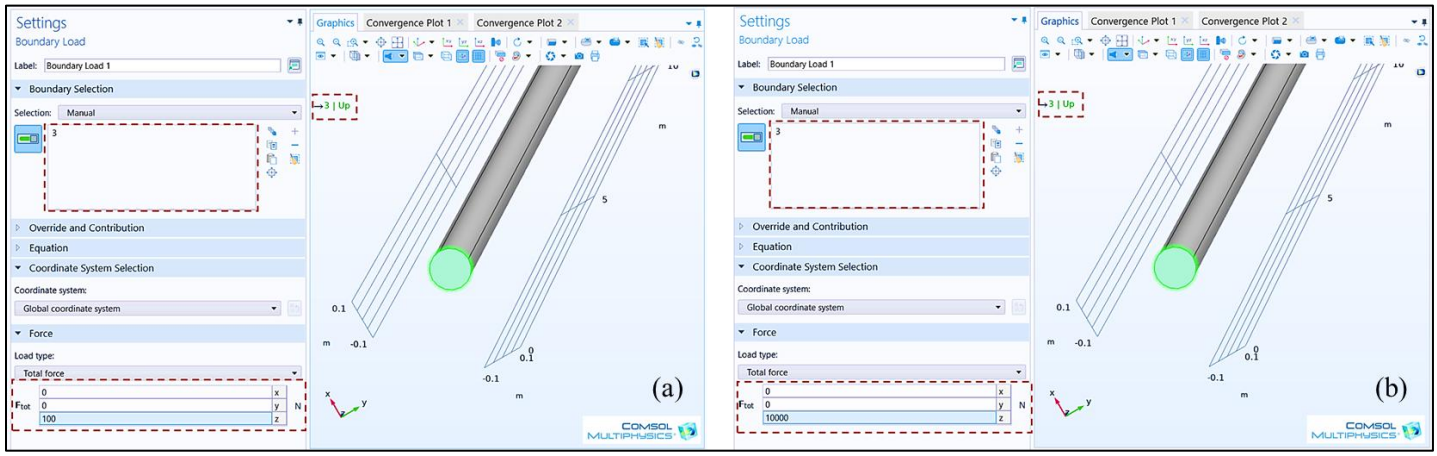

Figure 2.12 COMSOL loading conditions for pile No. 1: (a) vertical compressive load of 1000 N applied at the top; (b) vertical compressive load of 10000 N applied at the top (Author).

2.3.3 Modeling Assumptions and Limitations

Soil–pile interaction was modeled using elastic spring supports located at the pile base, with a stiffness value of 1.4×10^6 N/m^3 derived from site-specific geotechnical assessments (Figure 2.14). The surrounding soil was assumed to behave as a linear-elastic medium, omitting nonlinear behaviors including plastic deformation, hysteresis, and pore water pressure effects. This simplification was necessitated by the limited availability of detailed geotechnical data and aims to balance model fidelity with computational feasibility.

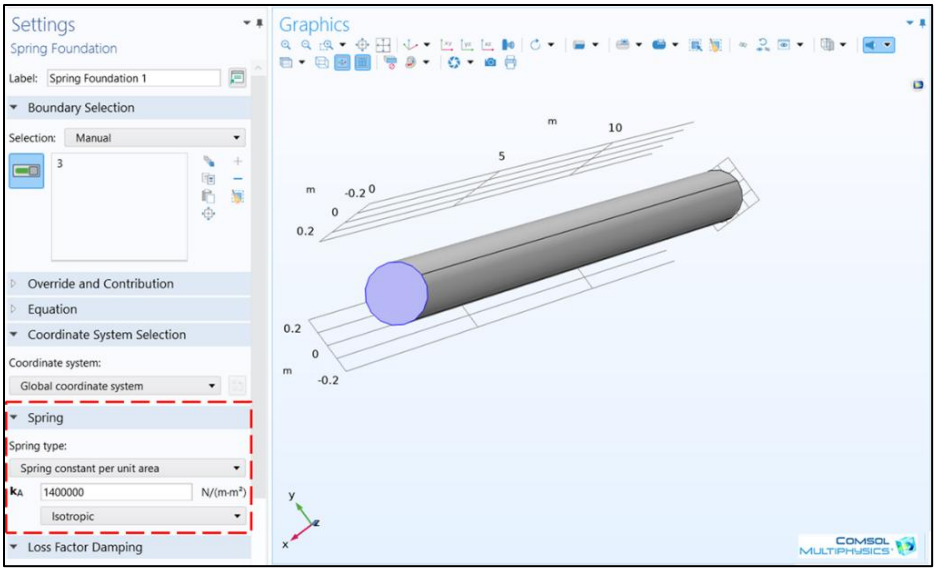

Figure 2.14 COMSOL model of Pile 01 with elastic spring supports to simulate soil–pile interaction (Author).

The geotechnical report for the Hevis Lake site indicates a shallow rocky stratum approximately 0.3–1.4 m thick overlaying peat, clay, and sand layers. However, detailed information regarding the thickness and lateral extent of these soil layers, as well as the precise embedment depth of piles, was unavailable. Consequently, advanced modeling of complex layered soil constitutive behaviors, such as nonlinear, elastoplastic, or coupled hydro-mechanical interactions, was not feasible without making unverified assumptions that would compromise model reliability.

Therefore, this approach employs a pragmatic linear-elastic spring model to represent soil–pile interaction, effectively capturing the essential soil stiffness contributing to pile behavior, while clearly acknowledging limitations related to ignored nonlinear and spatially variable soil responses. Future work may consider incorporation of more detailed soil constitutive models as field and laboratory data availability improves.

2.3.4 Mesh Generation and Convergence Study

Following the definition of pile geometry and material properties, the finite element model was discretized into tetrahedral elements to enable numerical analysis. Mesh refinement was applied strategically near the pile ends—both base and top—where stress concentrations and potential buckling initiation are expected. In regions with lower stress gradients, a coarser mesh was adopted to improve computational efficiency.

Element sizes were defined between 0.056 m (minimum) and 0.77 m (maximum), with a growth rate of 1.4 and a curvature factor of 0.4, ensuring adequate resolution of geometric features and capturing the structural response of the piles (Figure 2.15a). The resulting mesh comprised 30,069 tetrahedral elements, 7,186 vertices, and 7,978 triangular faces, with a mesh volume of 1.933 m^3. Edge elements were limited to 8, reflecting minimal contributions from linear edges.

Quadratic (second-order) tetrahedral elements with mid-edge nodes were employed to further enhance the accuracy of bending and stress predictions, particularly in capturing critical buckling behavior (Figure 2.15b).

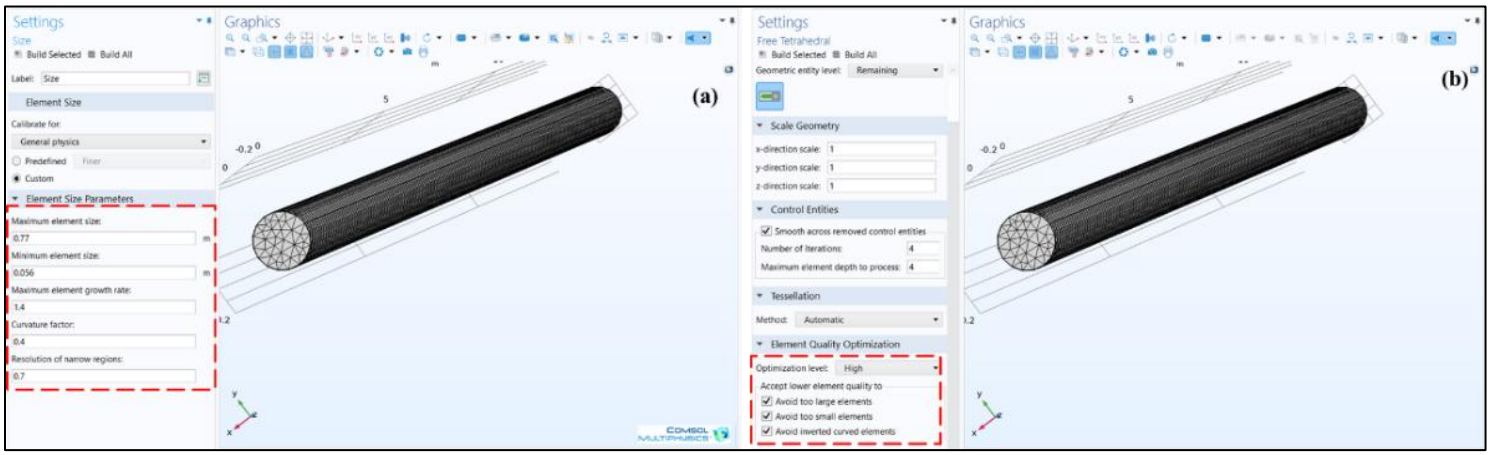

Figure 2.15 FEM mesh of Pile 01 in COMSOL Multiphysics: (a) general mesh; (b) quadratic (second-order) elements with mid-edge nodes. (Author).

Mesh convergence was verified by incrementally refining the mesh until variations in critical buckling load and maximum displacement were within 1%, ensuring that the numerical results are independent of mesh size and represent a stable solution. This approach balances computational efficiency with solution accuracy, providing reliable FEM predictions of stress distribution, deformation, and buckling response in submerged timber piles.

2.3.5 Validation Strategy for FEM Results Using Ultrasonic Data

The FEM simulations aim to validate the ultrasonic testing results by comparing predicted mechanical responses under axial loads with the ultrasonic-derived dynamic modulus of elasticity and critical buckling loads.

Validation will be performed by:

1. Comparing the critical buckling load predicted by FEM with the buckling load estimated using ultrasonic-based dynamic MOE and analytical formulas.
2. Assessing the correlation between FEM-predicted lateral displacements and expected pile deflections under known loads.
3. Quantifying error margins by calculating percentage differences between FEM results and ultrasonic predictions, targeting an acceptable deviation range.
4. Using regression analysis or correlation coefficients to measure the strength of agreement between methods.

This approach ensures that the ultrasonic test data are not only theoretically sound but also practically reliable in reflecting the actual structural performance of the timber piles.

CHAPTER III: RESULTS AND DISCUSSION

3.1 Experimental Results

This section presents the outcomes of the experimental investigation into ultrasonic wave velocity, dynamic modulus of elasticity (MOE), and buckling stability in wooden lake piles. The objective is to evaluate whether ultrasonic wave velocity can serve as a reliable predictor of pile deterioration and structural performance.

3.1.1 Ultrasonic Measurements

Non-destructive ultrasonic testing (NDT) revealed time-of-flight (TOF) values ranging from 0.00195 to 0.00847 s in the radial–tangential direction (see Figure 3.1a) and from 0.000152 to 0.000234 s in the longitudinal direction (Figure 3.1b). Shorter TOF values in the radial–tangential plane—particularly in Piles 25, 21, and 34—indicate superior internal integrity, while longer TOF readings in Piles 35 and 39 suggest internal defects or degradation.

The pronounced directional disparity in TOF reflects wood's inherent anisotropy. Longitudinal TOF values were consistently shorter due to the alignment of cellulose microfibrils and tracheids along the grain, facilitating faster wave propagation (Espinosa et al., 2019; Senalik et al., 2014; Yaitskova & van de Kuilen, 2014) . In contrast, wave transmission in the radial–tangential direction is impeded by the heterogeneous cellular structure, leading to greater scattering and attenuation (Ban et al., 2018; Palma et al., 2018; Sugimoto et al., 2018) . These findings confirm TOF's sensitivity to fiber orientation and material condition, supporting its use in NDT applications for timber.

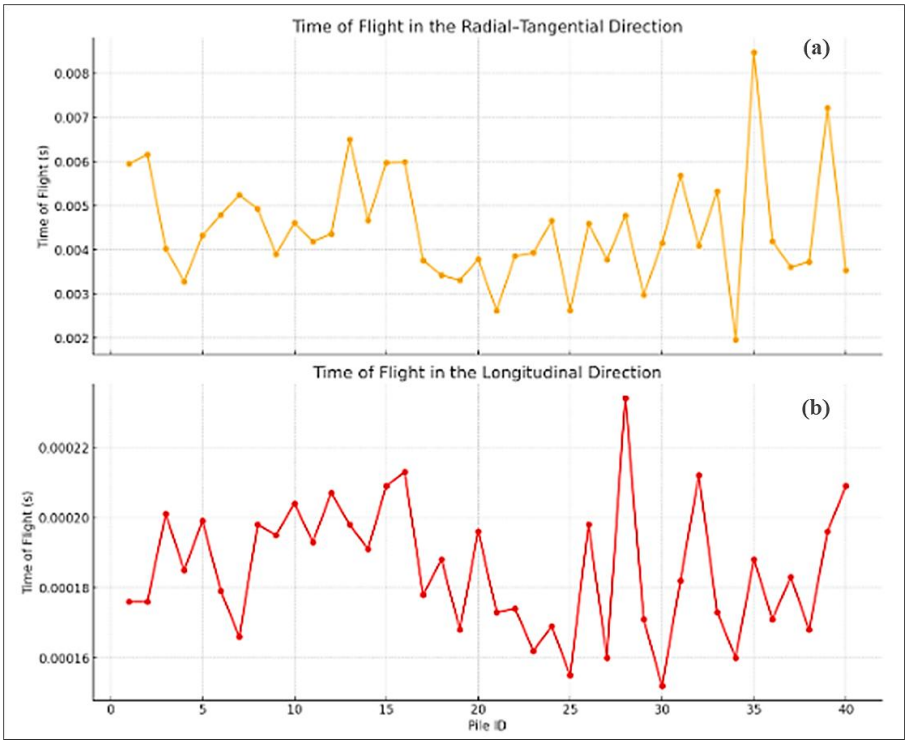

Figure 3. 1 Time-of-flight (TOF) measurements in wooden piles: (a) radial–tangential direction; (b) longitudinal direction (Author).

As shown in Equation 1, TOF differences directly affect wave velocity. The mean longitudinal velocity which propagates along the grain was 4360 m/s (σ = 426 m/s), ranging from 3416 m/s to 5255 m/s (Figure 3.2). reflecting significant variation in material properties and internal integrity. Due to their sensitivity to changes in stiffness and density, a key determinant of mechanical performance (Emms et al., 2013; Fang et al., 2022; Gongalves et al., 2011; Hasegawa et al., 2011; Montero et al., 2015).

Approximately 60% of samples fell within 4000–4800 m/s, typical for sound timber with uniform density and minimal defects. The observed mean wave velocity of 4360 m/s suggests that the majority of the tested spruce piles possess relatively good structural integrity, with a significant proportion displaying values consistent with defect-free material. Around 15% exceeded 4800 m/s, indicating high-density wood with well-aligned fibers , while about 10% fell below 3800 m/s, suggesting degradation or internal flaws as established in many studies (Ajabshir et al., 2023; L. Chang et al., 2021; Krause et al., 2015; Mahalil et al., 2024; Pahnabi et al., 2024; Shaji et al., 2000). The observed variability highlights the importance of structural health monitoring in assessing the long-term performance of wooden piles.

The coefficient of variation (CV) for longitudinal velocities was approximately 9.8%, reflecting heterogeneity in wood density, moisture content, fiber alignment, and internal anomalies.

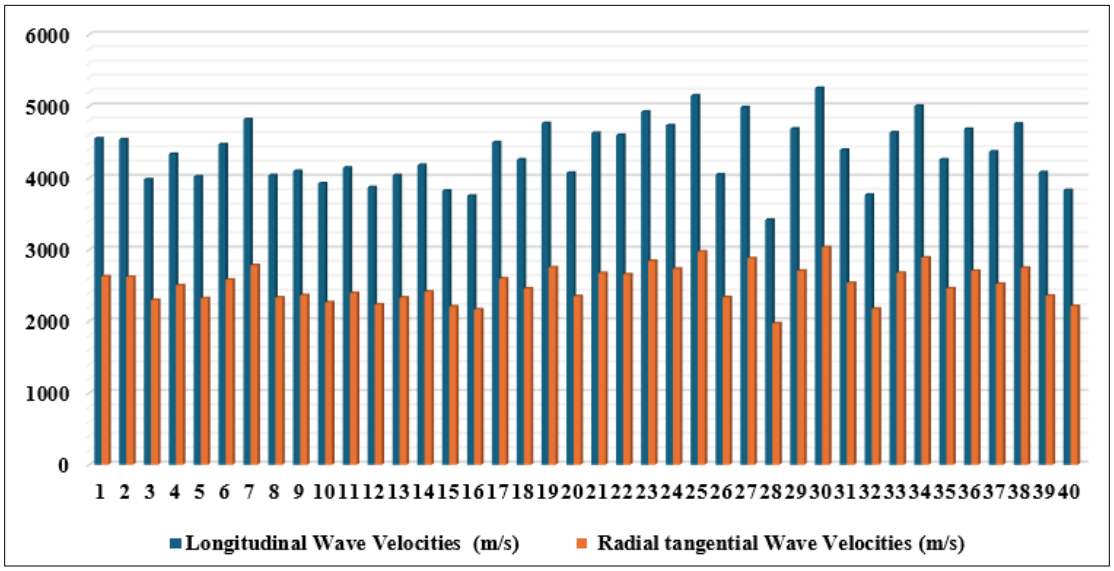

Figure 3. 2 Distribution of longitudinal and radial-tangential wave velocities across various wooden pile samples (Author).

In the radial–tangential direction, which propagates perpendicular to the grain, serves as a valuable indicator for assessing defect severity, material heterogeneity, and overall structural integrity in anisotropic materials like wood (Espinosa et al., 2018; Hasegawa et al., 2015; Sasaki & Hasegawa, 2007). The mean wave velocity was 2527.6 m/s (σ = 264.9 m/s), ranging from 1972.23 to 3033.98 m/s, as depicted in Figure 3.2. This variability suggests substantial heterogeneity, likely influenced by differential water absorption, moisture content, microbial degradation, or fatigue due to prolonged submersion (Hasegawa et al., 2011; Huan et al., 2018; Montero et al., 2015a).

Wood's anisotropic structure leads to characteristic wave velocity patterns in orthotropic directions, typically observed as longitudinal > radial > tangential. The expected wave velocity ratio

typically ranges from 2.2–2.8 (Bucur & Declercq, 2006; Espinosa et al., 2019; Hasegawa et al., 2015, 2016), but the observed ratio of 1.73 suggests deviation from ideal anisotropy—likely due to the presence of internal anomalies, such as micro-cracks, decay, or irregular grain alignment, all of which disrupt wave propagation. This could signal reduced mechanical performance, especially under axial loads where buckling is critical.

Figure 3.2 also highlights the pronounced directional dependency of ultrasonic wave velocities in wood. The highest velocities are observed along the longitudinal axis, while significantly lower values are recorded in the radial and tangential directions. This directional disparity reflects the inherent anisotropy of wood, primarily driven by the orientation of cellulose fibers and structural density variations—an observation widely supported in literature (Hasegawa et al., 2016; Krauss & Kúdela, 2011b; Ortiz Mansilla et al., 2009; Saadat-Nia et al., 2011).

3.1.2 Dynamic Modulus of Elasticity (MOE)

The dynamic Modulus of Elasticity (MOE) values, derived from ultrasonic velocity and wood density, ranged from 4727 MPa to 11186 MPa, with an average of 7777 MPa (Figure 3.3). Higher MOE values correspond to improved structural performance and reduced susceptibility to buckling under compressive forces. These values reflect the inherent variability in the material properties of wood , influenced by species, strength class, moisture content, and structural defects (e.g., knots, grain orientation).

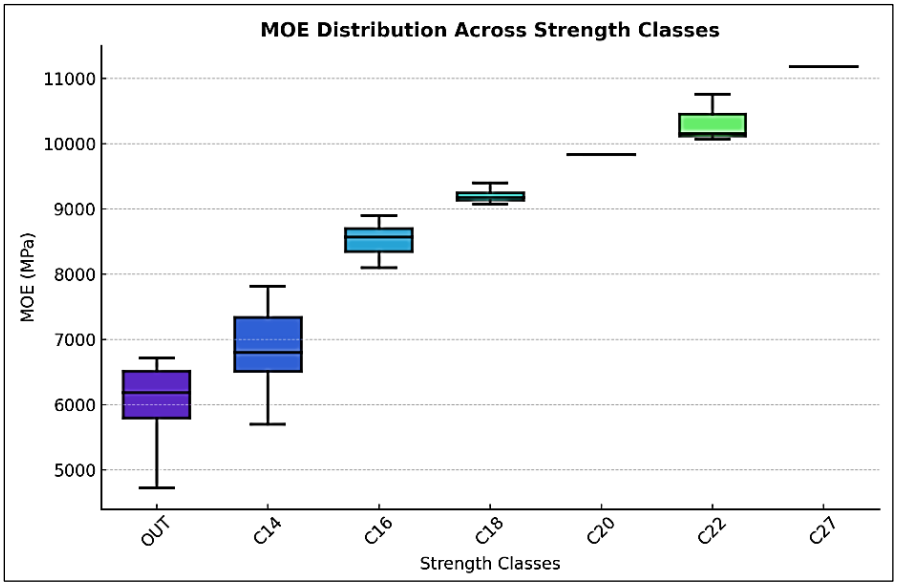

Figure 3. 3 Dynamic modulus of elasticity (MOE) distribution among evaluated timber piles (Author).

As reported by Gil-Moreno et al. (2016) and Karampour et al. (2020), piles with a modulus of elasticity (MOE) above 9000 MPa are considered to exhibit high stiffness or fall within the upper range of structural timber. In this study, piles 19, 23, 24, 25, 27, 30, and 38 met that criterion. The dynamic MOE varied significantly by strength class: C14 piles averaged 6580 MPa, while C22 and C27 reached 10,620 MPa and 11,186 MPa, respectively. These differences reflect the influence of wood density and anatomical structure, as denser species generally possess thicker cell walls and higher lignin content, leading to increased stiffness. This trend is consistent with

findings by Li et al. (2021), Wang et al. (2018), Rais et al. (2020) and Sharapov et al. (2019), who reported that hardwoods like oak and beech exhibit higher MOE values than lighter softwoods due to their denser cellular morphology.

Relationships between ultrasonic wave velocity and modulus of elasticity

A strong linear relationship was established between ultrasonic wave velocity and the dynamic modulus of elasticity (MOE) in Hevis wooden piles (Figure 3.4), yielding a Pearson correlation coefficient of r = 0.998 and a p-value = 1.45×10^{-48} (n = 40), confirming high statistical significance.

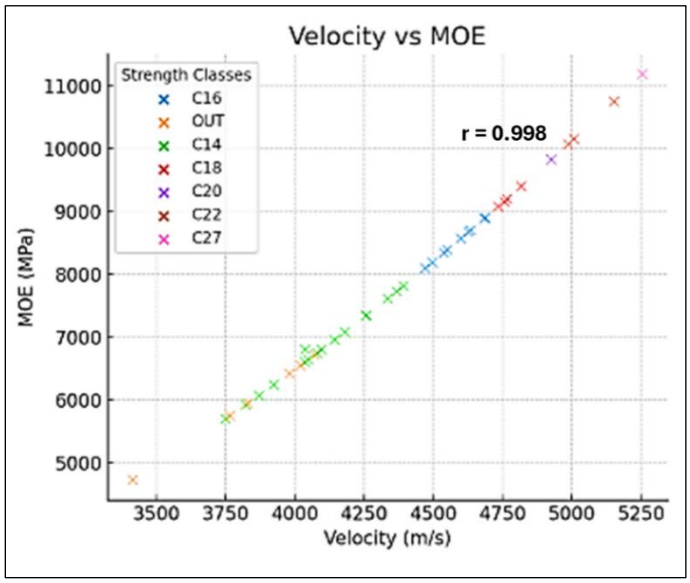

Figure 3. 4 Correlation between ultrasonic wave velocity and dynamic MOE in submerged timber piles (Author).

This indicates that as wave velocity increases, MOE rises proportionally, owing to the intrinsic dependence of wave propagation on material stiffness and density. Stiffer materials transmit waves more efficiently, with less energy loss, resulting in increased propagation speeds.

The near-perfect correlation reflects the direct influence of elastic modulus and density on wave transmission efficiency. As MOE increases, the material resists deformation more effectively, enabling faster wave to travel due to reduced attenuation and enhanced energy transfer.

Given the strong interdependence between these parameters, ultrasonic testing offers a robust non-destructive method for estimating stiffness and inferring mechanical capacity in submerged or otherwise inaccessible wooden structures. These findings are consistent with existing literature, although correlation strength may vary depending on species and experimental conditions (Duong & Hasegawa, 2024b; Giaccu et al., 2017; Ishiguri et al., 2008; Madhoushi & Boskabadi, 2019; Madhoushi & Daneshvar, 2016).

3.1.3 Pile Length and Critical Buckling Load

Based on Equations (3) and (4), pile lengths ranged from 5.65 meters to 20.83 meters, with an average length of 10.2 meters. Pile length significantly influences buckling behavior, as longer piles are more vulnerable to lateral instability under compressive forces. The calculated critical buckling loads (Pcr) ranged from 13.12 kN to a peak value of 246.65 kN, as shown in Figure 3.5. The lower end of this range corresponds to severely deteriorated timber elements with minimal resistance to axial loading, while the upper end reflects moderately preserved structural integrity.

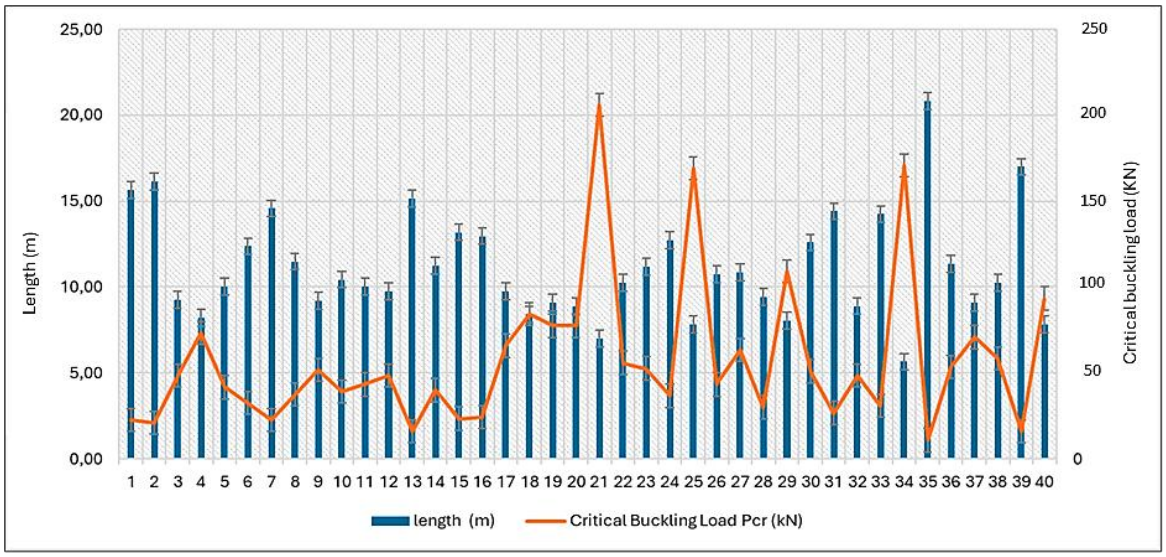

Figure 3. 5 Pile length vs. critical buckling load across different pile samples (Author).

Shorter piles (e.g., 5.65 m and 6.99 m) demonstrate significantly higher critical buckling loads, with values of 246.65 kN and 138.35 kN, respectively (Fig 3.5), indicating enhanced stability and resistance to lateral deflections under compressive forces and buckling resistance. Shorter piles improve structural stability by reducing their effective length, which limits lateral deflection under compression. According to Euler's Buckling Theory, even minor reductions in pile length lead to disproportionately higher critical buckling loads, significantly enhancing stability. These shorter piles also exhibit increased stiffness, providing greater resistance to lateral deformations (Karampour et al., 2020; Tabarestani & Naghipour, 2022). Additionally, with lower slenderness ratios, shorter piles are less susceptible to higher-order buckling modes and instead experience simpler, lower-order buckling, improving axial stability as supported by Euler–Bernoulli beam theory and confirmed by recent studies (e.g., (Fernández-Escobar et al., 2023; Giese et al., 2023; L. He et al., 2023; Jais et al., 2024).

In contrast, longer piles (e.g., 20.83 m and 17.00 m) have significantly lower critical buckling loads (13.12 kN and 18.01 kN, respectively), as demonstrated in Figure 3.5. This reduction is due to increased flexibility and deflection potential, as longer piles are more prone to lateral displacements under axial loads, reducing their load-bearing capacity and buckling resistance (Hasan, 2019). Additionally, extending the length from 5.65 m to 10.25 m reduces the critical buckling load by approximately 74.2%.

The slenderness ratio (effective length divided by average diameter) ranged from 113 to 416.60, with a mean value of 222.92 (*Appendix A*). Based on this parameter, most piles fall within the "*Slender*" category (slenderness ratio > 150), with only Piles 21 and 34 classified within the "*Intermediate*" range (50–150). This classification provides an additional parameter for evaluating buckling susceptibility and complements the interpretation of critical load capacities.

Comparative Analysis of Analytical Buckling Predictions: Euler vs. Granholm Approaches

To quantitatively assess the influence of advanced analytical models on the critical buckling load prediction for submerged timber piles, both the classical Euler–Bernoulli approach and the Granholm-corrected method were systematically applied across the dataset. The complete dataset is available in *Appendix A*.

Pile ID	length (m)	Slenderness Ratio (λ)	Longitudinal Elastic Modulus (MPa)	effective shear modulus (MPa)	Granholm correction factor (Φ)	$P_{cr,\ Euler}$ (kN)	$P_{cr,Granholm}$ (kN)
01	15,63	312,60	8389	6053,40	0,99986	26,59	26,586
02	16,13	322,60	8345	6021,65	0,999861	24,88	24,877
03	9,25	185,00	6420	4632,60	0,999746	58,17	58,155
04	8,20	164,00	7612	5492,73	0,999484	87,71	87,665
05	10,30	200,60	6548	4724,96	0,999663	50,42	50,403
06	12,37	247,40	8096	5841,98	0,999777	41,02	41,011
07	14,57	291,40	9400	6782,93	0,999832	34,280	34,275
08	11,48	229,60	6602	4763,93	0,999677	38,81	38,797
09	9,21	184,20	6799	4906,08	0,99959	62,1	62,075
10	10,43	208,60	6241	4503,43	0,999684	44,48	44,447
……..	……..	……..	……..	……..	……..	……..	……..
40	7,81	156,20	5943	4288,40	0,999569	75,33	75,294

Table 3. 1 Summary of pile geometric and material properties alongside classical and Granholm-corrected buckling load predictions (Author).

Systematic inspection of Table 3.1 reveals a remarkable convergence in predicted buckling capacities, with the Granholm factor ϕ approaching unity uniformly. The discrepancy between the classical Euler critical load and the Granholm-corrected load remains consistently below 0.05%, evidencing the negligible contribution of shear deformation and orthotropic effects under the observed pile geometries.

This convergence is directly attributable to the high slenderness ratios of the piles ($L/r \approx 113–417$), a geometric regime in which the governing assumptions of Euler–Bernoulli beam theory—namely, the dominance of flexural rigidity and the negligible influence of shear deformation and rotary inertia—are satisfied to a high degree of accuracy. A broad body of theoretical and experimental literature confirms that, advanced corrections introduce minimal changes to classical predictions (Fernández-Escobar et al., 2023; B. K. Gupta & Basu, 2018; S.-W. Liu et al., 2020; Soffietti et al., 2024).

Therefore, while the application of Granholm's orthotropic correction provides a comprehensive physical validation, these results empirically reinforce the sufficiency of the Euler–Bernoulli approach for slender timber piles in submerged conditions. The rigor of the dual-model approach

documents, with quantified evidence, that the neglect of shear effects in classical practice is justified for geometrically slender elements.

Relationship between pile length and critical buckling load

The analysis reveals a general inverse relationship between pile length and critical buckling load, with a correlation coefficient of -0.73, as shown in Figure 3.6.

Longer piles tend to experience lower critical buckling loads, indicating a higher susceptibility to lateral instability under compressive forces. This trend aligns with classical buckling theory, which predicts that longer, more slender structures are more prone to buckling, consistent with structural stability principles.

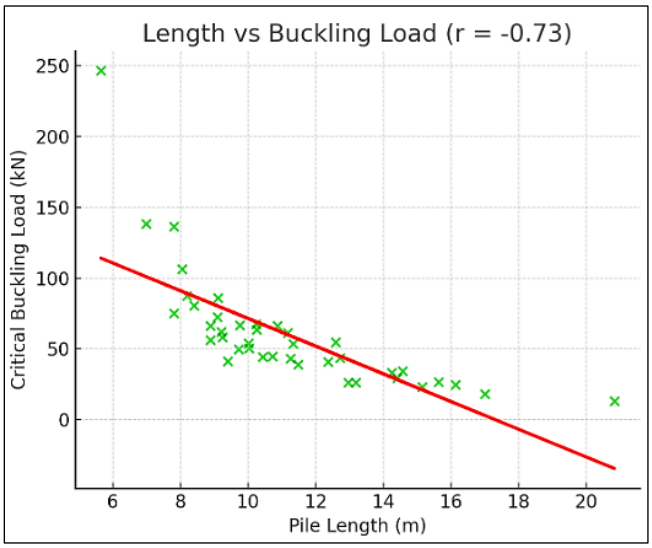

Figure 3. 6 The relationship between pile length and critical buckling load (Author).

Despite the overall trend, significant variability in the data was observed. For example, piles with lengths between 8 and 9 meters exhibited critical buckling loads ranging from 41.33 kN to 87.71 kN, suggesting that factors other than length, such as material properties or pile diameter, may also influence buckling behavior. Pile geometry, particularly diameter and shape, affects resistance. Larger diameters increase stiffness and critical buckling load (Liu et al., 2020; R. Zhang et al., 2021).

Piles with larger cross-sectional areas or circular shapes exhibit higher loads due to increased stiffness, with circular sections offering optimal resistance (Fenu et al., 2021; Shatri et al., 2013). Additionally, outliers in the dataset, such as the 5.65-meter pile with a critical buckling load of 246.65 kN and the 20.83-meter pile with a critical buckling load of 13.12 kN, deviate from the general trend, indicating that these piles may have unique structural characteristics that influence their buckling resistance.

Interrelation of Wave Velocity, Dynamic Modulus of Elasticity, and Buckling Resistance in Timber Piles

The data indicates a general trend where higher dynamic Modulus of Elasticity (MOE) values correlate with increased resistance to buckling, reflected by higher critical buckling loads. Figure 3.7 illustrates that piles with higher MOE typically demonstrate greater stiffness, enhancing their capacity to resist deformation under applied loads. For example, piles with MOE values of 10751 MPa and 11186 MPa exhibit relatively higher critical buckling loads of 136.63 kN and 54.70 kN, respectively (Hasan, 2019; Moita et al., 2020), compared to those with lower MOE values of 4727 MPa and 5919 MPa, which correspond to critical buckling loads of 41.33 kN and 26.33 kN. This implies that lower material stiffness increases flexibility, potentially reducing buckling resistance at specific pile lengths, as described in the literature (Jawad & Albusoda, 2024; Sabaliauskaite et al., 2024; R. Zhang et al., 2021).

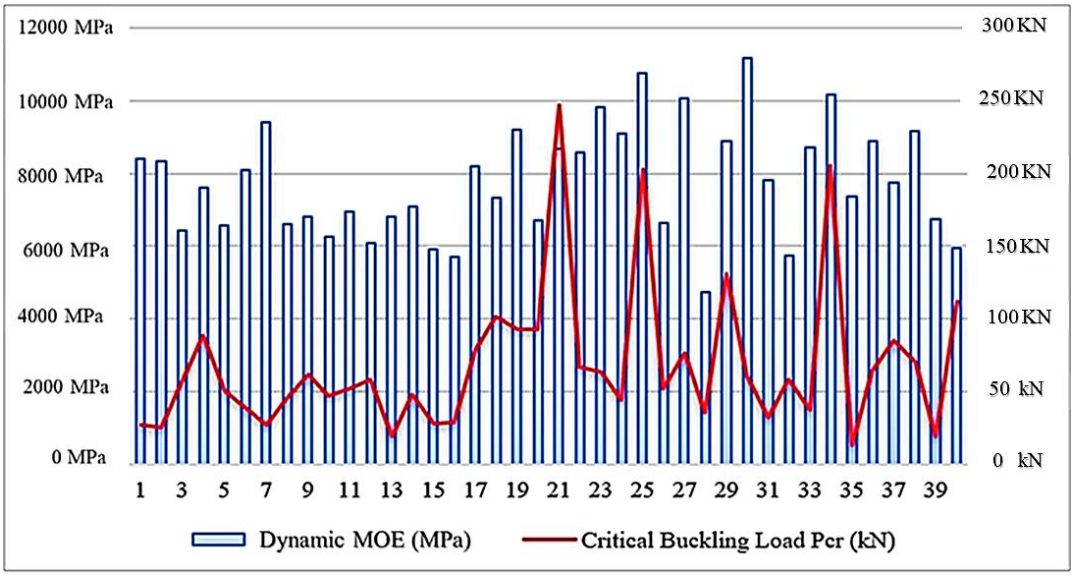

Figure 3. 7 Relationship between dynamic MOE and estimated critical buckling load for timber piles (Author).

However, the relationship between MOE and buckling load is not perfectly linear, as shown in Figure 3.8, which presents a moderate positive correlation (r = 0.43). Some piles with intermediate MOE values exhibit varying buckling loads, indicating the influence of additional factors such as pile length, material properties, and loading conditions.

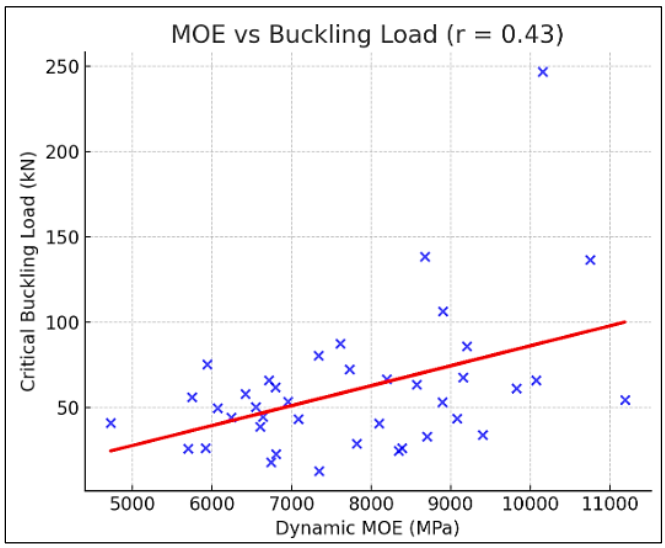

Figure 3. 8 The relationship between Dynamic MOE and critical buckling load (Author).

For example, despite having an MOE of 8389 MPa, one pile has a buckling load of 26.59 kN. Conversely, piles with lower MOE values, such as 4727 MPa, still demonstrate a notable buckling load of 41.33 kN. This variability suggests that while higher MOE generally corresponds to increased buckling resistance, buckling behavior depends on a complex interplay of factors beyond material stiffness alone.

In addition, the pile with a dynamic MOE of 10751 MPa and a length of 7.81 m has a critical buckling load of 136.63 kN, while the pile with a dynamic MOE of 11186 MPa and a length of 12.59 m shows a critical buckling load of 54.70 kN. This suggests that pile length may influence buckling behavior more significantly than stiffness alone, aligning with findings by Hasan, (2019) and Moita et al. (2020). While higher dynamic MOE is generally associated with greater bearing capacity and theoretically increased buckling resistance, the relationship between MOE and buckling load is complex. Furthermore, the pile with a length of 9.41 m and a dynamic MOE of

4727 MPa has a critical buckling load of 41.33 kN, implying that lower material stiffness increases flexibility, potentially reducing buckling resistance at specific pile lengths, as described in the literature (Dyka & Klempka, 2023; Jawad & Albusoda, 2024).

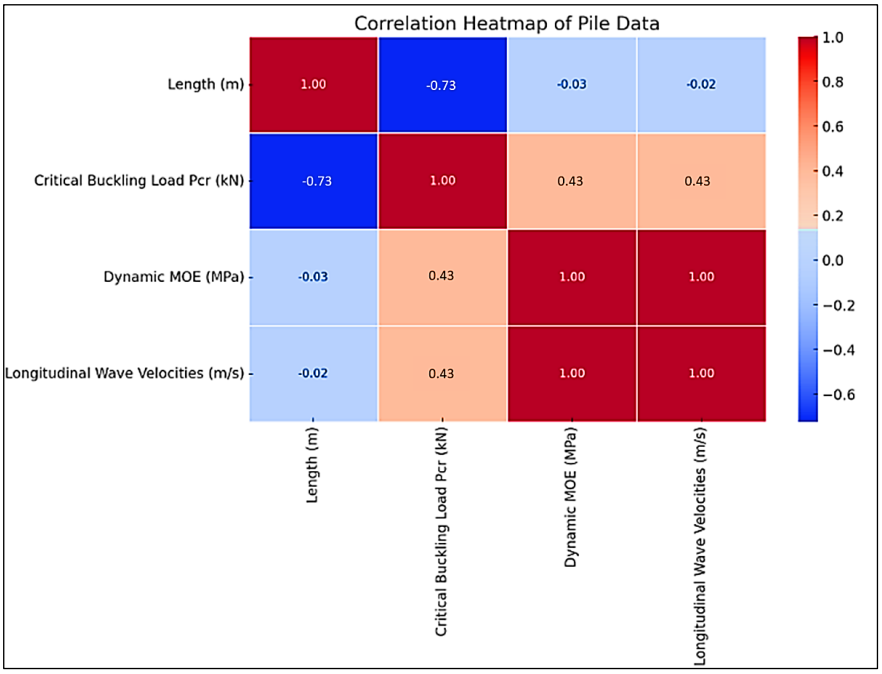

Figure 3. 9 Correlation Heatmap of Structural and Material Parameters for Wooden Piles (Author).

Accordingly, correlation heatmap illustrated in figure 3.10 provides a quantitative overview of the interrelationships between key structural parameters of wooden piles, specifically pile length, critical buckling load (Pcr), dynamic modulus of elasticity (MOE), and longitudinal wave velocities. A strong negative correlation (-0.73) is observed between pile length and Pcr, which is consistent with Euler's buckling theory, where longer columns exhibit reduced buckling resistance. In contrast, a very strong positive correlation (1.00) between dynamic MOE and longitudinal wave velocities confirms the theoretical relationship governed by wave propagation mechanics, where wave speed increases with material stiffness.

Moderate positive correlations (~0.43) between both dynamic MOE and longitudinal wave velocity with critical buckling load suggest that stiffer materials and faster wave propagation are associated with enhanced buckling resistance. Finally, the negligible correlations between pile length and both dynamic MOE (-0.03) and wave velocity (-0.02) imply that geometrical length has minimal influence on inherent material properties. Collectively, the heatmap illustrates how ultrasonic wave velocity and dynamic stiffness metrics can serve as reliable indicators for evaluating structural stability and predicting buckling behavior in wooden piles.

3.1.4 Predictive Modeling of Buckling Failure

To assess the predictive capability of ultrasonic data for estimating the buckling resistance of wooden piles, a second-degree polynomial regression model was developed. The model demonstrated a strong fit, with a coefficient of determination of $R^2 = 0.943$ (Figure 3.10), indicating that 94% of the variance in critical buckling loads was explained by ultrasonic velocity, MOE, and pile length.

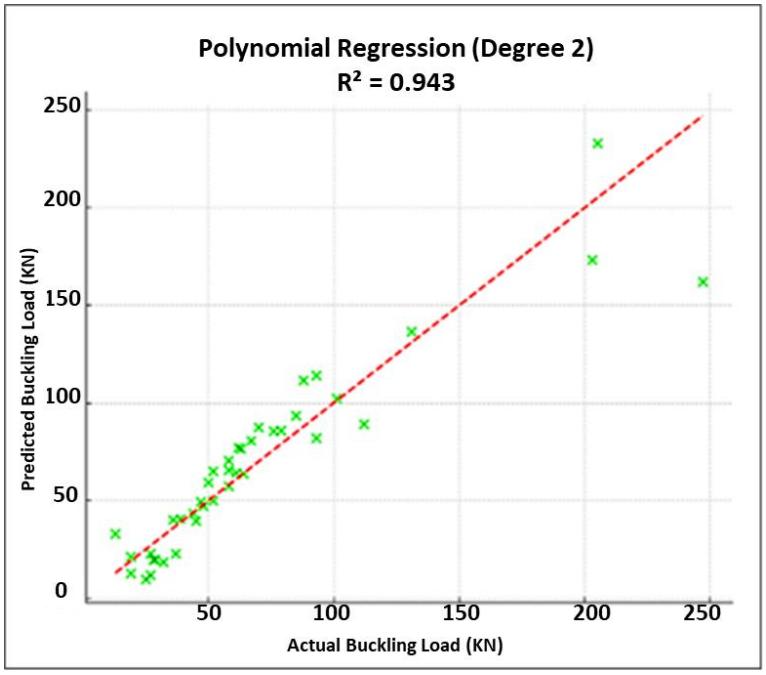

Figure 3. 10 Polynomial regression model predicting critical buckling load from ultrasonic velocity and MOE (Author).

Incorporating ultrasonic wave velocity significantly enhanced model accuracy due to its strong association with internal stiffness and material integrity. As a non-destructive parameter, ultrasonic velocity reflects structural soundness, with higher values typically indicating well-aligned cellulose fibers and minimal internal deterioration—critical factors for resisting compressive buckling as reported by (Espinosa et al., 2019; Lee et al., 2015; Teder et al., 2012; Verbist et al., 2020).

The polynomial model effectively captured the non-linear relationship between mechanical and geometric parameters. While higher MOE generally contributes to greater buckling resistance, its influence is modulated by pile length, which affects the slenderness ratio and critical load capacity, as confirmed by recent studies (e.g., (Hajdo et al., 2024; Hasan, 2019; L. He et al., 2023; Kotzamanis & Kalliontzis, 2023). By accounting for these interactions, the model outperforms linear alternatives, highlighting the suitability of non-linear approaches for evaluating stability in anisotropic, heterogeneous materials such as wood.

However, despite its strong predictive performance, the polynomial regression model exhibits certain limitations. It is based on submerged timber piles of a single species under specific environmental conditions, which constrains its generalizability to other wood species, moisture levels, or environmental exposures. These factors should be considered when applying the model beyond the tested conditions.

3.1.5 Failure Thresholds

Three classification schemes were compared for pile condition assessment:

Velocity-Based Risk Assessment

Longitudinal ultrasonic wave velocities were measured to evaluate the mechanical integrity of timber piles, given their sensitivity to defects perpendicular to the grain and their established use

in estimating in-situ stiffness and strength. Figure 3.11 presents the correlation between wave velocity and dynamic modulus of elasticity (MOE), with risk levels indicated by color coding.

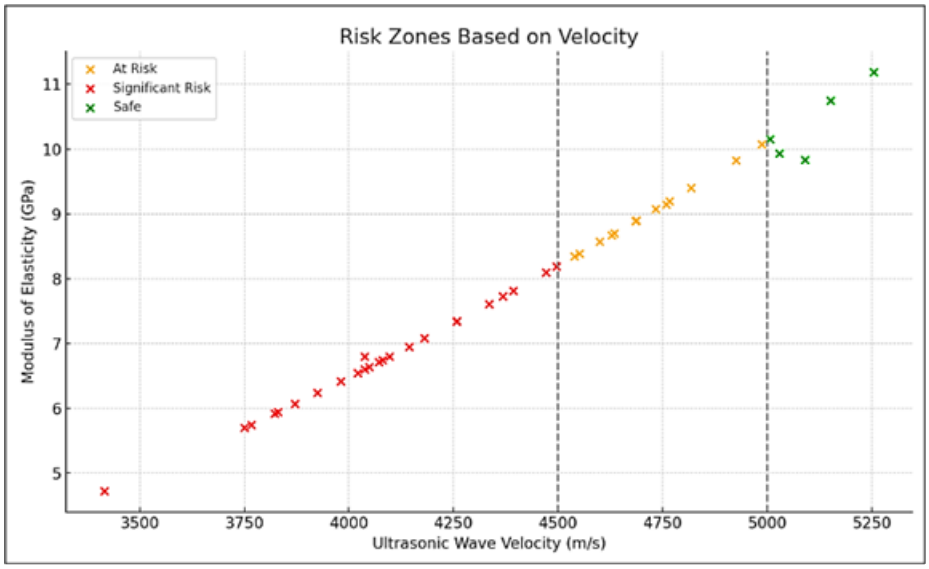

Figure 3. 11 Ultrasonic wave velocity–MOE scatter plot with velocity-based risk classifications (Author).

Following ASTM D2555 and corroborated by previous studies (Holt et al., 1994; Huang & Floyd, 2009; Sherif, 1989, 1991; Sotomayor-Castellanos & Villaseñor-Aguilar, 2014), piles were classified according to velocity thresholds. Piles with velocities below 4500 m/s (e.g., Piles 3–6, 8–18, 20, 26, 28, 31–32, 35, 37, 39, 40) were deemed to present *significant risk* of internal defects. Those with velocities between 4500 and 5000 m/s (e.g., Piles 1–2, 7, 21–25, 27, 29, 33, 36, 38) were considered at *moderate risk*, while piles exceeding 5000 m/s (e.g., Piles 19, 30, 34) were categorized as *safe*.

Although this velocity-based approach effectively detects material degradation, a critical limitation was observed: several piles classified as "*safe*" ($v > 5000$ m/s) exhibited relatively low dynamic MOE values (< 10 GPa, e.g., Piles 19, 34; Fig. 26), indicating reduced stiffness and increased susceptibility to buckling under axial load. This discrepancy demonstrates that elevated wave velocities can conceal internal decay or localized defects not captured by surface measurements, potentially leading to overestimation of structural integrity. Consequently, while ASTM D2555 provides a standardized framework for preliminary risk assessment, reliance on ultrasonic velocity alone may not fully reflect the load-bearing performance of timber piles, particularly in heterogeneous or anisotropic materials.

MOE-Based Risk Assessment

Figure 3.12 presents the velocity–MOE scatter plot, color-coded according to MOE-based risk levels. Piles with MOE below 6 GPa, including Piles 15–16, 28, 32, and 40, were classified as significant risk due to critically low stiffness. Piles with MOE between 6 and 10 GPa (e.g., Piles 1–14, 17–23, 26–27, 29, 31, 33, 34–39) were considered at moderate risk, whereas piles exceeding

10 GPa (e.g., Piles 24–25, 30, 38) were deemed structurally adequate in terms of axial load resistance.

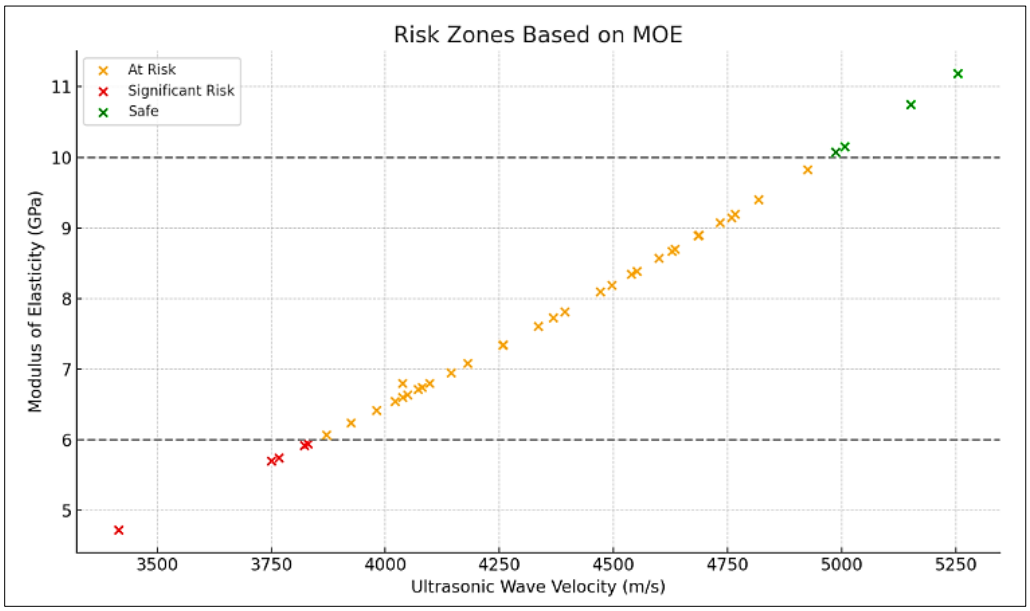

Figure 3. 12 Ultrasonic velocity–MOE scatter plot with MOE-based risk classifications (Author).

MOE, as a stiffness-dependent parameter, quantitatively reflects a pile's resistance to axial deformation and susceptibility to buckling. The scatter plot indicates that MOE-based assessment captures a wider spectrum of structural risk than velocity alone. Nevertheless, a subset of piles with high MOE (>10 GPa), including Pile 24 and Pile 25 (Fig. 3.12), exhibited subcritical ultrasonic velocities (<5000 m/s). This discrepancy implies the presence of internal discontinuities, early decay, or localized defects that do not immediately reduce static stiffness but can compromise dynamic load transfer and the integrity of the pile under operational conditions.

These observations underscore a fundamental limitation of MOE-based evaluation: while it accurately represents load-bearing capacity, it is insensitive to incipient decay or internal flaws that disrupt stress wave propagation. Such defects may remain latent under static loading yet progressively undermine long-term structural performance (Bhattacharyya et al., 2024). Therefore, integrating MOE with ultrasonic velocity measurements enables a more rigorous assessment, combining mechanical performance indicators with diagnostics of internal condition, and thereby improving predictive reliability for heterogeneous and anisotropic timber piles.

Integrated Risk Classification

To overcome the limitations of single-parameter evaluation, a dual-criteria framework combining longitudinal ultrasonic wave velocity and dynamic MOE was applied (Figure 3.13). Piles exhibiting both low velocity (<4500 m/s) and low MOE (<6 GPa), such as Piles 35 and 39, were classified as *Significant Risk*, indicative of advanced material degradation and compromised load-bearing capacity. Piles with intermediate values (4500–5000 m/s and 6–10 GPa), including Piles 01, 02, 07, 21 and 27, were categorized *At Risk*, representing transitional conditions where internal defects or reductions in stiffness may be incipient. Piles exceeding 5000 m/s and 10 GPa

(e.g., Piles 23, 24, 25, 30, 38) were classified as *Safe*, reflecting well-preserved internal structure and mechanical robustness.

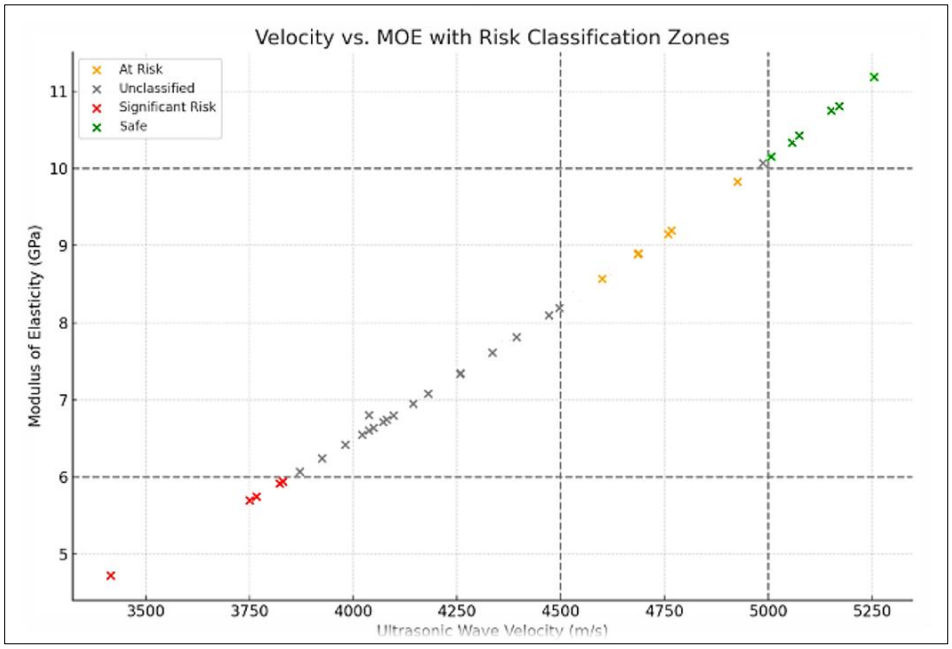

Figure 3. 13 Integrated Risk Classification of Timber Piles Based on Ultrasonic Velocity and Dynamic MOE (Author).

This integrated assessment simultaneously considers mechanical stiffness and internal material integrity, providing a more comprehensive evaluation of pile structural performance. *Significant Risk* piles exhibit dual deficiencies that compromise both stress-wave transmission and axial stiffness, increasing susceptibility to buckling under service loads. Some *At Risk* piles, such as Pile 25, display adequate MOE but subcritical velocities, signaling internal flaws, early decay, or voids not yet affecting static stiffness. Conversely, piles with high velocity but lower MOE may reflect microstructural heterogeneity or localized geometric irregularities affecting elasticity. These intermediate cases underscore the limitations of single-parameter assessments and highlight the necessity of integrated evaluation.

By combining ultrasonic velocity and dynamic MOE, this dual-criteria approach captures complex interactions between material condition and mechanical performance. It enhances diagnostic accuracy and predictive reliability, particularly in anisotropic and heterogeneous timber, where degradation may manifest unevenly across different physical properties. This framework supports targeted monitoring and early detection of incipient failure mechanisms that could be overlooked by conventional evaluation methods, providing a robust basis for risk classification and structural assessment.

3.1.6 Buckling Resistance Consideration

Pile length was incorporated as a proxy for slenderness, a key factor influencing compressive instability in columns. Assuming relatively uniform cross-sections, longer piles are inherently more susceptible to buckling under axial loads.

Analysis of dynamic MOE versus pile length (Figure 3.14) indicates that many *Significant Risk* piles also have greater lengths, demonstrating compounded vulnerability due to reduced stiffness and increased slenderness. This observation aligns with classical beam theory, confirming that

low-stiffness, slender piles are structurally more susceptible to instability (L. Chen et al., 2017; Vogt et al., 2009). The *At Risk* and *Safe* groups generally conform to these theoretical expectations, supporting the integrated risk assessment framework.

Notably, some shorter piles, such as Pile 40 (7.89 m) and Pile 17 (9.76 m), were classified as *Significant Risk*, indicating that internal decay or material defects can dominate structural vulnerability even when geometric slenderness is low. These cases underscore the importance of assessing both mechanical integrity and internal condition, not relying solely on geometry.

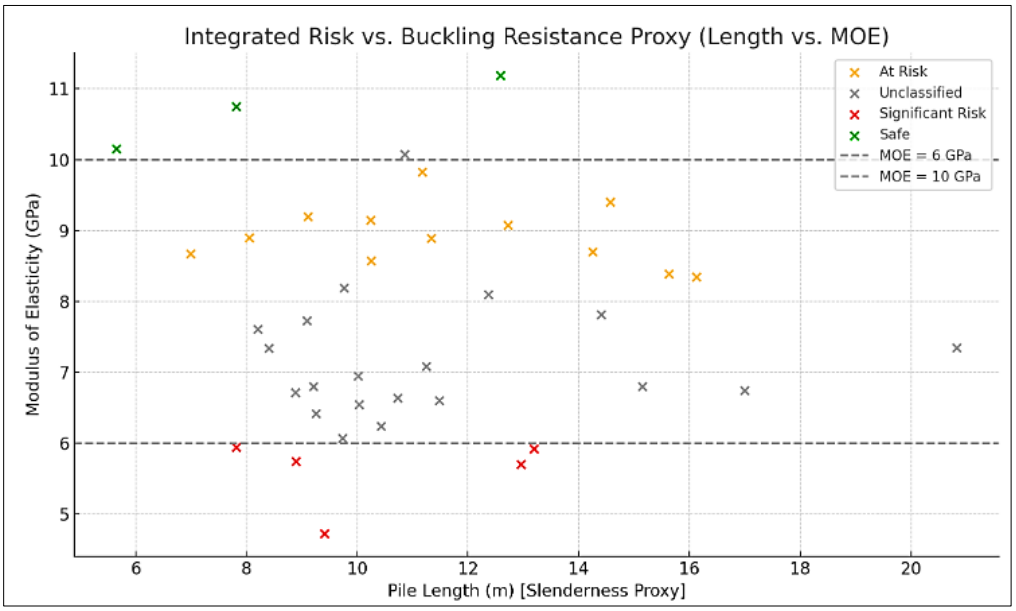

Figure 3. 14 Correlation Between Dynamic MOE and Pile Length to Assess Buckling Vulnerability (Author).

Field observations—including tilting, localized softness, and deformation—corroborated the MOE–length classification, with most visibly compromised piles falling within the *Significant Risk* zone. This evidence validates the combined influence of stiffness, internal integrity, and slenderness in predicting pile performance and failure susceptibility.

3.2 Numerical Results

In this section, the mechanical behavior of the 40 submerged wooden piles was analyzed using Finite Element Modeling (FEM) in *COMSOL Multiphysics*. The simulations were designed to replicate the real conditions experienced by the piles, including their geometry, material anisotropy derived from ultrasonic data, boundary conditions, and loading scenarios. The primary goal was to validate the ultrasonic test findings and provide a detailed understanding of stress distributions, deformation patterns, and buckling resistance.

3.2.1 Critical Buckling Load: FEM vs Ultrasonic Data

The critical buckling load (P_{cr}) of 40 piles was evaluated using both FEM simulations and ultrasonic-derived predictions combined with classical Euler-Bernoulli beam theory. This comparative framework enables validation of ultrasonic testing as a reliable non-destructive technique while

highlighting the limitations of analytical models when applied to submerged wooden piles. Summary statistics are presented in Table 3.2, with full results for all individual piles provided in *Appendix B*.

Parameter	Mean	Std. Dev	Min	Max	Count
Length (m)	11.14	3.03	5.65	20.83	40
MOE (MPa)	7776.725	1509.23	4727	11186	40
Ultrasonic Buckling (KN)	60.32	40.69	13.12	246.65	40
FEM Buckling (KN)	57.40	38.99	12.62	236.29	40
Difference (%)	5.26	1.50	2.98	8.46	40

Table 3. 2 Summary statistics of pile properties and critical buckling loads predicted by FEM and ultrasonic methods (Author).

FEM predictions of Pcr ranged from 12.62 kN to 236.29 kN, (mean 57.4 ± 38.99 kN). Ultrasonic-based estimates exhibited a slightly broader range of 13.12–246.65 kN, (mean 60.32 ± 40.69 kN). An overview of these critical buckling loads is illustrated in Figure 3.15, which shows both FEM and ultrasonic-based estimates for all 40 piles. Both methods capture the same order of magnitude and general distribution of Pcr, demonstrating that ultrasonic-derived estimates reliably reflect FEM predictions, with an overall mean difference of 5.26% and a bound range of 2.98–8.46%, This validates ultrasonic NDT as a reliable predictor of pile buckling capacity under submerged conditions, in agreement with Kim et al. (2022) and Z. Wang et al. (2021). Similarly, Chen et al. (2019) demonstrated comparable accuracy in finite element simulations integrated with ultrasonic phased-array data, reporting errors within -1.37% to 4.11%, thereby further suggesting that ultrasonic-derived estimates reliably reflect FEM predictions in terms of sound pressure amplitude distribution and structural response.

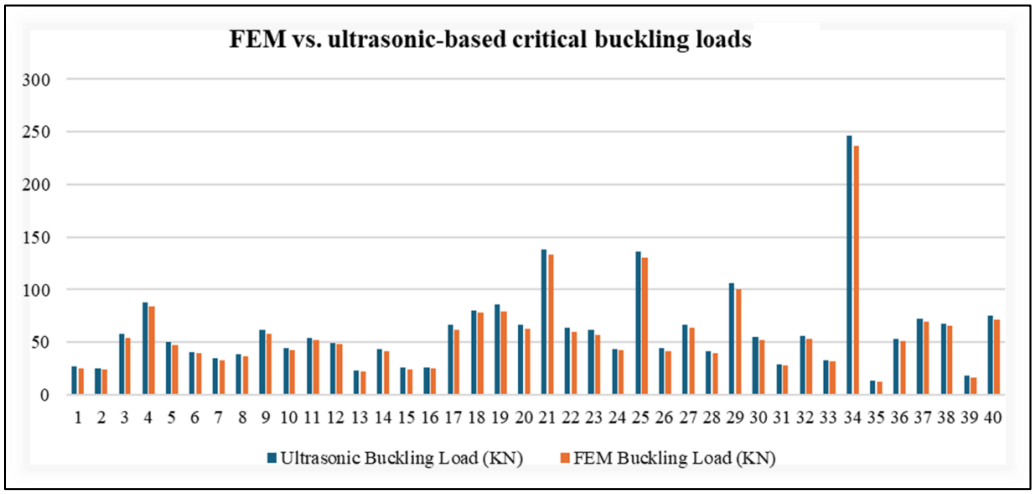

Figure 3. 15 Overview of critical buckling loads for 40 piles FEM predictions and ultrasonic-based estimates (Author).

The Pearson correlation coefficient between the two methods was calculated as 0.9998 ($p = 4.38 \times 10^{-65}$), confirming an extremely strong and statistically significant correlation (see Figure 3.16).

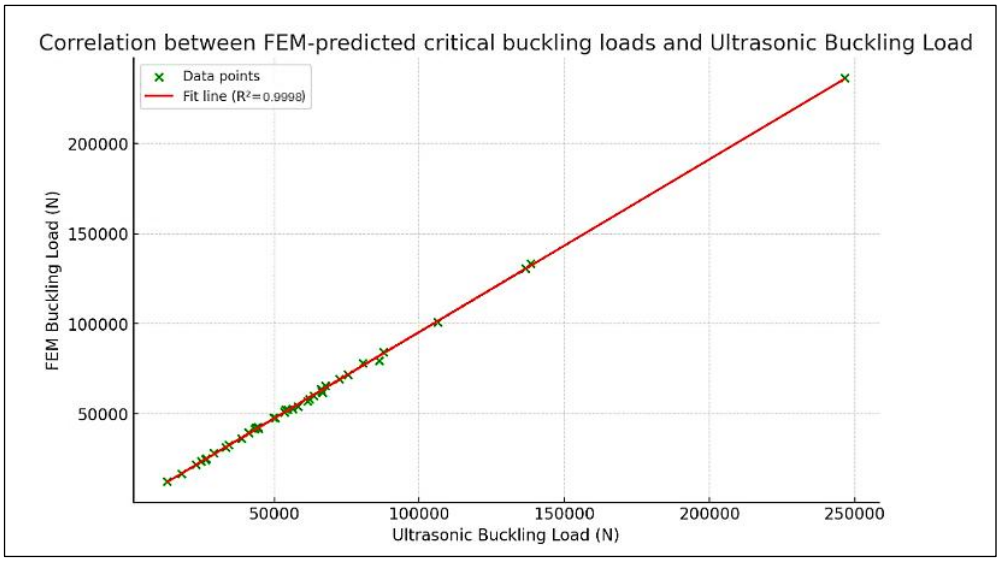

Figure 3. 16 Correlation between ultrasonic-predicted and FEM buckling loads for 40 piles (Author).

Despite this near-perfect correlation, ultrasonic predictions show a slight tendency to overestimate buckling capacity. This deviation can be attributed to several factors:

Material Anisotropy and Moisture Effects: Wood is an orthotropic material, with mechanical properties varying along the longitudinal, radial, and tangential directions. Ultrasonic testing primarily measures wave propagation along the longitudinal axis, corresponding to the highest stiffness, which may overestimate the effective MOE relevant for global buckling. Submerged piles in Hévíz Lake exceed the fiber saturation point (FSP ≈ 30%), where residual swelling and internal stress redistribution reduce the effective stiffness relative to ultrasonic-derived values. Moisture affects ultrasonic wave propagation, decreasing phase velocity by ~7% as moisture rises from 0% to 27% (Yassine et al., 2024).

Boundary Condition Effects: Ultrasonic-based predictions rely on the Euler–Bernoulli beam theory, which assumes idealized simply-supported boundary conditions. In practice, the piles are partially embedded and submerged, producing complex pile–soil–water interactions. FEM incorporates lateral restraint from soil stiffness, providing more conservative and realistic buckling estimates This trend aligns with previous (Halimi & Kouloughli, 2021; Kareem, 2024),while (Ike, 2024) quantified that Euler–Bernoulli beams on elastic foundations can exhibit critical load deviations of ~4–7% relative to FEM predictions depending on boundary conditions.

Simplification of Analytical Assumptions: The analytical formulation used with ultrasonic MOE assumes homogeneous material and ignores imperfections (e.g., knots, grain deviations, decay). FEM captures boundary effects and interactions more accurately, explaining why ultrasonic predictions are slightly optimistic while still exhibiting strong trend alignment.

These factors explain the small systematic difference between methods, aligning with literature reporting <5% deviations between ultrasonic/simulation results (Lee et al., 2020; Tallavo et al., 2022), and <10% differences between simulated and measured (X. Wang et al., 2024). Larger deviations in other studies (–45.9% to +35.2%) were mainly due to uncertainties in material properties (Murat & Yasin, 2024).

3.2.2 Stress Distribution and Buckling Behavior

The stress results for Cases 01 and 02 were obtained directly from finite element simulations performed in *COMSOL Multiphysics*. In these models, the piles were represented as orthotropic materials with boundary conditions reflecting partial embedding in soil and submersion in water. The analysis captured both axial and bending stresses under incremental axial loads of 1000 N (initial service load) and 10 000 N (high load approaching buckling).

Case 01: Initial Load (1000 N)

At 1000 N, axial stress across all piles remained approximately uniform at ~0.0318 MPa, consistent with the proportionality between applied load and cross-sectional area, as reported in previous studies (Cheikh et al., 2024; C. Chen et al., 2013; L. He et al., 2022; Kog, 2016). Bending stresses were minimal (0.008–0.029 MPa), with localized amplification observed at a pile length of 9.21 m (~0.115 MPa), indicative of initial geometric or stiffness imperfections such as slight curvature, localized degradation, or boundary eccentricity. These stress concentrations correspond to reduced load-carrying capacity at specific points, as supported by prior investigations (Gérard et al., 2018; W. Liu et al., 2023; Nadeem et al., 2015; Quan et al., 2024; Shen & Wadee, 2019).

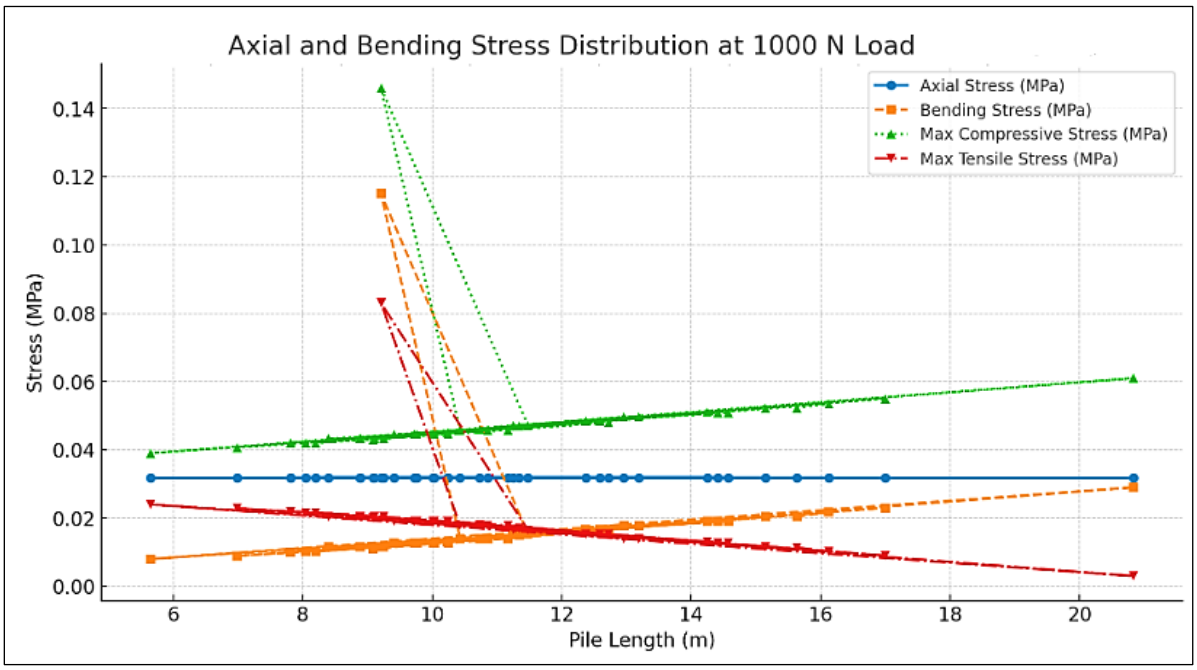

Figure 3. 17 Stress distribution in representative piles under an initial 1000N load (COMSOL FEM) (Author).

Maximum compressive stresses reached ~0.146 MPa, while tensile stresses remained below 0.022 MPa, confirming that, under low loads, the piles behave elastically with negligible bending (Bourne-Webb et al., 2007; Masoumi et al., 2009; Randolph, 1981). Stress contours in Figure 3.17

indicate a stable elastic regime, consistent with Euler–Bernoulli beam theory predictions for linear response prior to lateral displacement development.

Case 02: High Load (10000 N, Approaching Buckling)

Under 10000 N, piles exhibited a pronounced pre-buckling response dominated by flexural amplification. Axial stresses increased linearly to ~0.318 MPa, consistent with elastic behavior, while bending stresses escalated nonlinearly—from ~2–13 MPa for typical pile lengths to ~30.7 MPa for the longest pile (20.83 m).

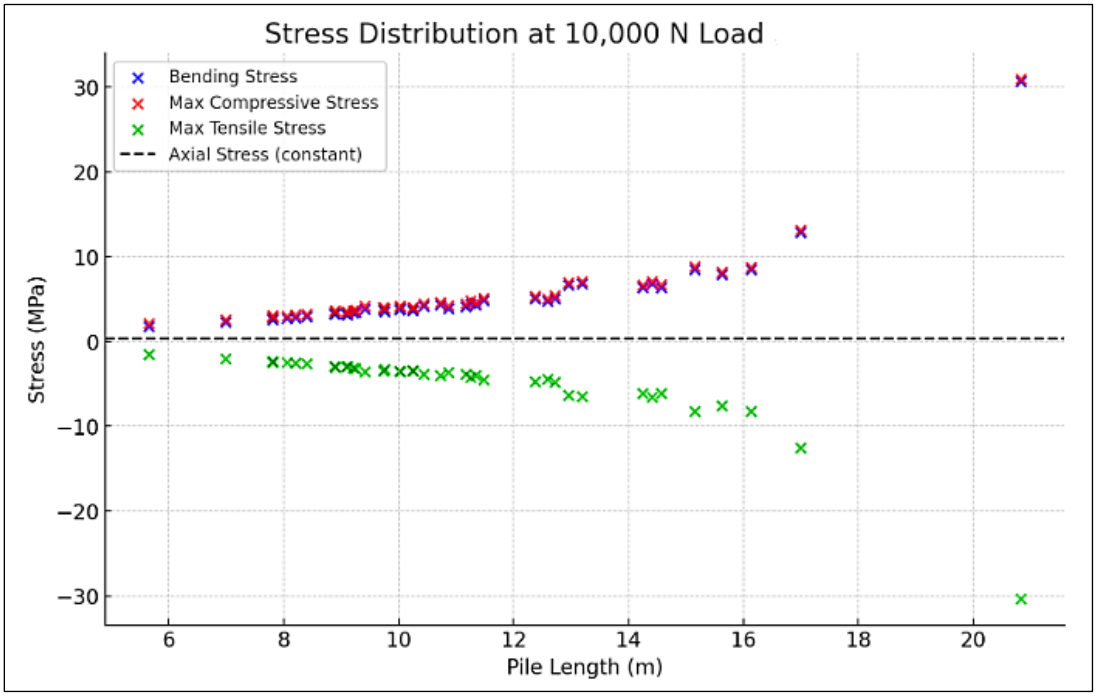

Figure 3. 18 Stress distribution in representative piles under an initial 1000N load (COMSOL FEM) (Author).

This disproportionate growth reflects second-order (P–Δ) effects, in which small lateral deflections interact with internal forces to generate additional bending moments, accelerating instability as the load approaches the critical state (Figure 3.18). Such behavior aligns with previous nonlinear buckling analyses of slender structural elements (Bondre & Gaikwad, 2016; De Francesco & Sullivan, 2023; Pourali et al., 2019; Pouya, 2019; Siddig Ibrahim & Rahman Elzubair Mohamed, 2016).

Extreme-fiber compressive and tensile stresses were nearly symmetric, with maximum compressive stresses of 30.97 MPa and tensile stresses of −30.34 MPa, approaching the compressive strength of water-saturated softwoods. For comparison, Aicher & Stapf (2016) report that saturated spruce typically exhibits compressive strengths of 16–20 MPa, with some specimens exceeding 30 MPa, consistent with the present observations.

Longer, and more slender piles demonstrated heightened sensitivity, with bending stresses approaching material capacity, highlighting the dominant influence of geometric nonlinearity in pre-buckling behavior. The resulting asymmetric distribution of tensile and compressive zones confirms that buckling onset is governed primarily by flexural instability rather than axial stress (Bhattacharya et al., 2005; Nadeem et al., 2015; Ravi Prakash & Prashant, 2016).

Pre-buckling Transition and FEM Validation

Under incremental loading, submerged wooden piles transition from uniform axial compression at low loads to bending-dominated behavior near the critical load, in agreement with classical buckling theory. Slender piles (>14–15 m) exhibited disproportionately large lateral deflections and amplified bending stresses, reflecting reduced buckling resistance and heightened sensitivity to geometric imperfections. Outliers, such as the 9.21 m pile at 1000 N and the 20.83 m pile at 10000 N (Figures 3.19 and 3.20), illustrate localized bending spikes of approximately 0.145 MPa and 30.66 MPa, respectively, due to minor imperfections or boundary compliance, providing diagnostic insight into low stability margins.

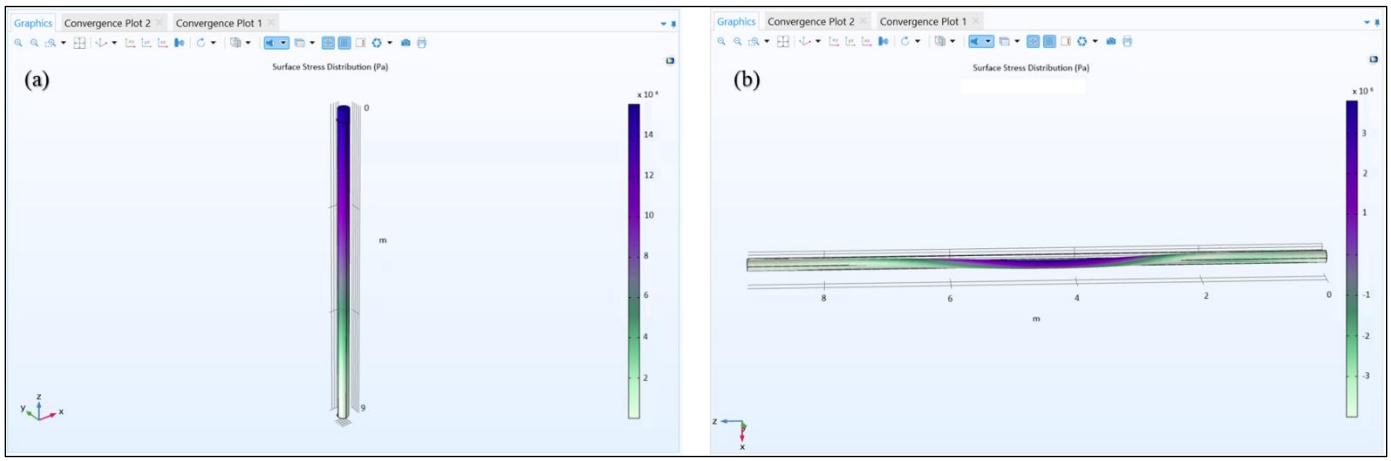

Figure 3. 19 Surface plots of stress distribution in Pile 9 (length: 9.21 m), generated in COMSOL Multiphysics (a) Response under an applied load of 1 000 N; (b) pre-buckling response under an applied load of 10 000 N (Author).

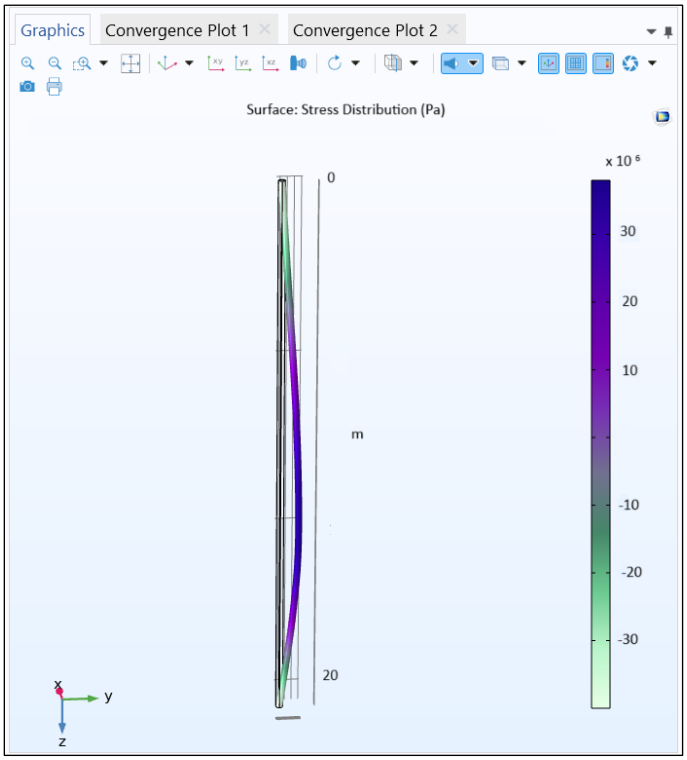

Figure 3. 20 Surface plots of stress distribution in Pile 35 (length: 20.83 m), generated in COMSOL Multiphysics. showing pre-buckling response under an applied load of 10 000 N (Author).

FEM simulations incorporating soil restraint and geometric nonlinearity accurately reproduce both stress distributions and critical loads, validating ultrasonic-based material property estimates and capturing pre-buckling instability mechanisms. Full results for all individual piles are provided in *Appendix C*.

3.2.3 Displacement and Deformation Analysis

The displacement and deformation behavior of the piles under incremental axial loading was assessed using FEM simulations in *COMSOL Multiphysics*. While stresses determine internal force distribution, displacement analysis provides direct insight into structural stability, serviceability, and pre-buckling response. Results were compared against theoretical Euler buckling predictions to evaluate the influence of geometric imperfections, slenderness, and soil restraint.

Axial and Lateral Displacements at Service Load (1000 N)

At the service load of 1000 N (case 01), the piles primarily experienced axial shortening, with lateral displacements uniformly small across all lengths, ranging from 0.006 m to 0.09 m, confirming that the piles remained in the elastic compression regime (see Figure 3.21). The minimum lateral displacement was observed for the shortest pile, Pile 34 (5.65 m; see Figure 3.22a), reaching only ~0.006 m, indicating high bending stiffness and very limited pre-buckling deformation.

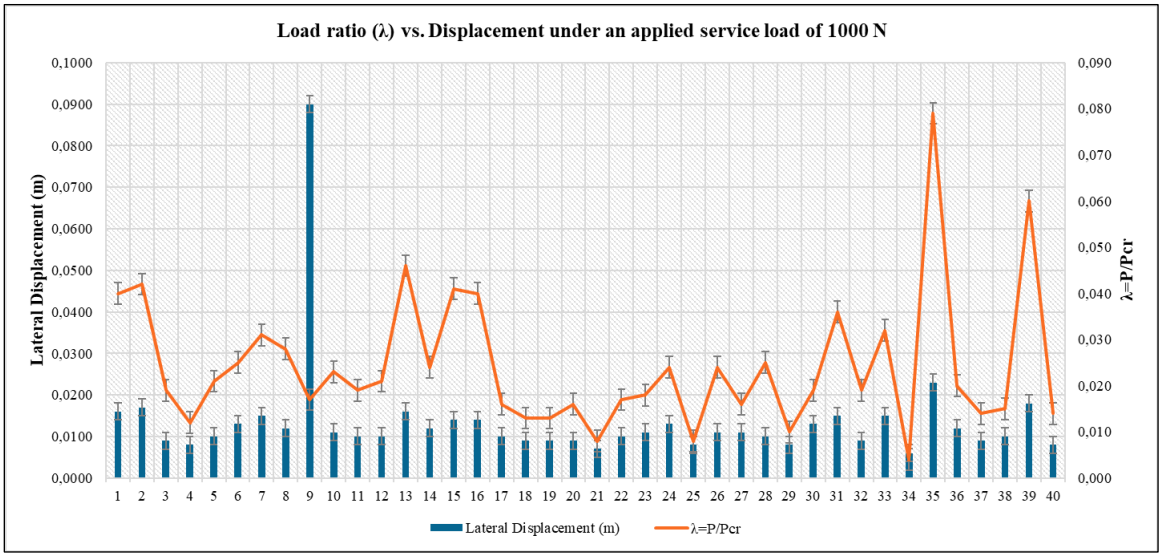

Figure 3. 21 Load ratio (λ) versus axial and lateral displacement of piles under an applied service load of 1000 N (Author).

Piles of intermediate lengths (8–12 m) exhibited slightly larger lateral displacements, ranging from ~0.008 to 0.013 m, while longer piles, such as the 15.63 m and 20.83 m specimens, showed displacements of 0.016 m and 0.023 m, reflecting the expected reduction in bending stiffness with increased slenderness. In contrast, Pile 09 (9.21 m; see Figure 3.22b) displayed the maximum lateral displacement, exceeding 0.09 m, despite its moderate length. This anomalously high response is likely due to localized geometric imperfections or boundary compliance, which can trigger early flexural deformation even under relatively low loads, consistent with the observations of Hariswaran & Premalatha (2021).

These findings demonstrate that, although pile length and slenderness are primary factors controlling lateral displacement, minor geometric irregularities or soil heterogeneities can substantially amplify lateral response in specific cases, in agreement with Gatto & Montrasio (2021). Overall, the behavior at service load is consistent with linear Euler–Bernoulli predictions, with lateral displacement proportional to axial load and geometric stiffness.

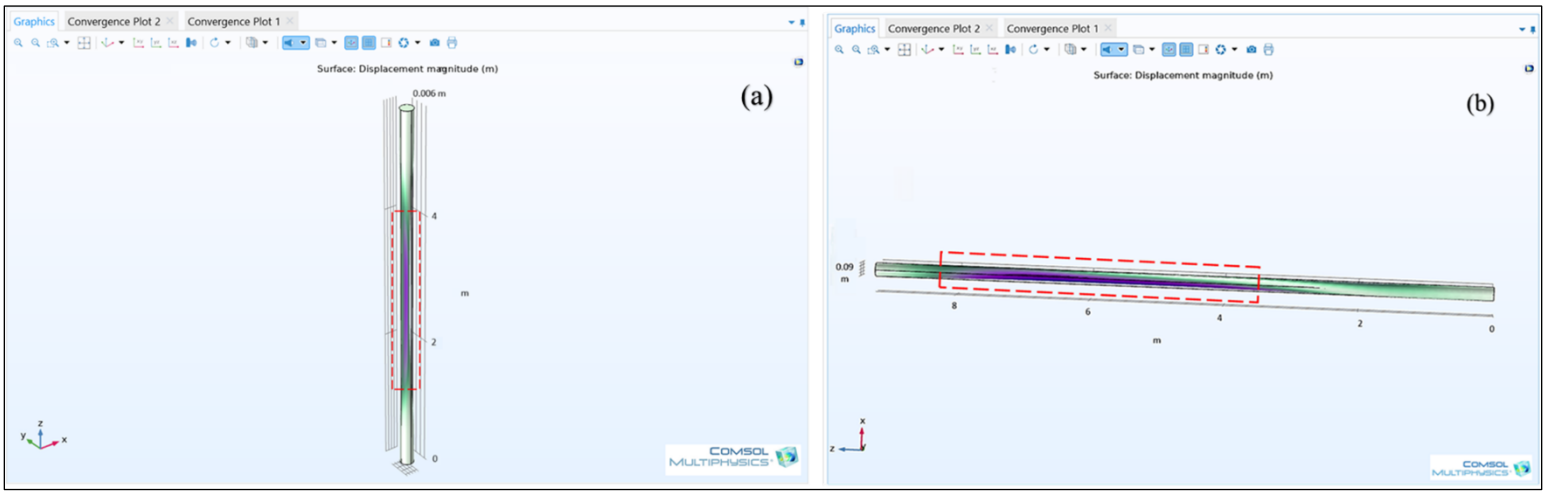

Figure 3. 22 Displacement magnitude surface plots generated in COMSOL Multiphysics under an applied load of 1000 N, showing (a) Pile 34 (5.65 m) and (b) Pile 09 (9.21 m) (Author).

Pre-Buckling Response at High Load (10 000 N)

As the axial load increased to 10 000 N, deformation patterns shifted from primarily axial compression to a bending-dominated response, indicating entry into the pre-buckling regime. Lateral displacements scaled strongly with pile length, ranging from 0.14 m to 2.41 m, revealing the dominant influence of slenderness on structural stability. Short piles (<10 m) exhibited modest lateral deflections (<0.3 m), while intermediate lengths (12–15 m) experienced amplified deflections of 0.4–0.67 m. slender piles (>20 m) displayed extreme lateral deflections, exemplified by the 20.83 m pile, which reached 2.41 m, as shown in Figure 3.23.

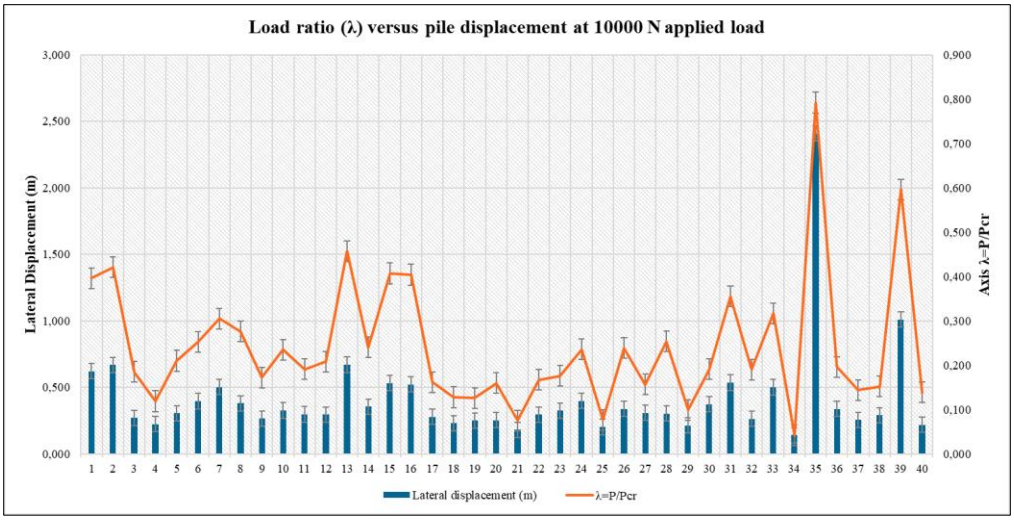

Figure 3. 23 Load ratio (λ) versus lateral displacement of piles under a high axial load of 10 000 N, showing pre-buckling behavior (Author).

These results demonstrate that lateral displacements grow nonlinearly with pile length, with long, slender piles experiencing disproportionately large deflections. Pre-buckling deflections in slender piles become significant before reaching the theoretical critical buckling load, primarily due to imperfection sensitivity and geometric effects, consistent with previous (Chi Wai, 2013; Hasan, 2019; Nadeem et al., 2015).

Comparison with Euler Buckling Theory

According to Euler's classical buckling theory, an ideal, perfectly straight column should exhibit negligible lateral displacement until reaching the critical buckling load (λ=1), at which point displacement theoretically grows without bound. However, FEM results diverge significantly from this idealization, showing that lateral displacements begin to develop well before the Euler limit, typically around λ ≈ 0.2–0.3.

Figure 3.23 shows that, at the higher load case of 10,000 N, medium-length piles (12–15 m) exhibit λ values ranging from 0.21 to 0.46. In particular, the 15.63 m pile (Pile 01) already displays substantial lateral deflections of approximately 0.67 m at a load ratio of λ = 0.46, well below the theoretical Euler limit (see Figure 3.24). Similarly, the 12.96 m pile (Pile 16) records a lateral displacement of 0.522 m at λ = 0.404, while the 12.72 m pile (Pile 24) shows a displacement of 0.399 m at λ = 0.236 (see Figures 3.25 and 3.26).

These results confirm that even medium-length piles undergo significant pre-buckling displacements before reaching the critical load, highlighting the sensitivity of slenderness and imperfections in this regime. For the complete set of displacement and deformation outcomes for all individual piles across the loading spectrum, refer to *Appendix D.*

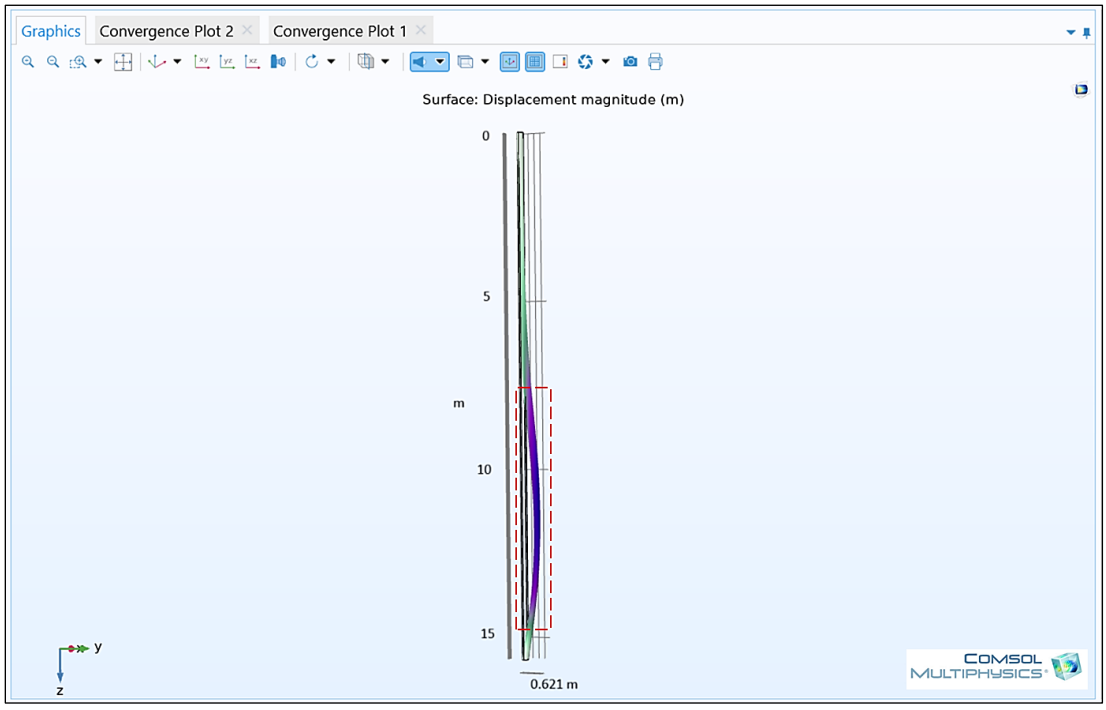

Figure 3. 24 Displacement magnitude surface plots of Pile 01 (15.63m), generated in COMSOL Multiphysics: showing the pre-buckling response under an applied load of 10 000 N (Author).

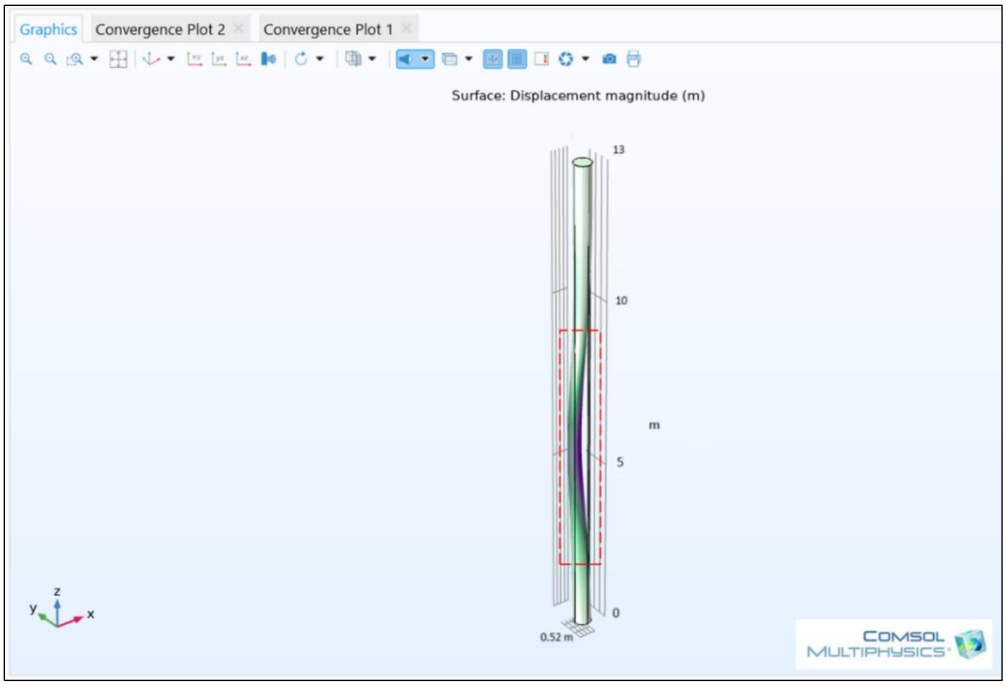

Figure 3. 25 Displacement magnitude surface plots of Pile 16 (12.96 m), generated in COMSOL Multiphysics, showing the pre-buckling response under an applied load of 10 000 N (Author).

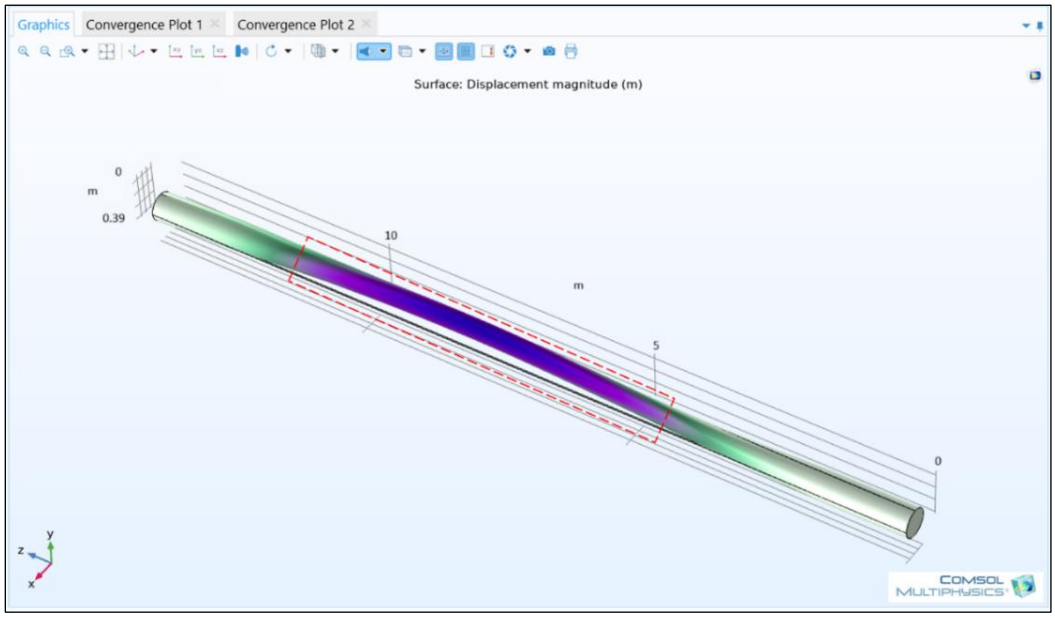

Figure 3. 26 Displacement magnitude surface plots of Pile 24 (12.72 m), generated in COMSOL Multiphysics: showing the pre-buckling response under an applied load of 10 000 N (Author).

The longest piles exhibited pronounced lateral displacements, indicative of a near-critical structural state. Specifically, Pile 39 (17 m) reached a lateral displacement of approximately 1 m at a load ratio of $\lambda = 0.596$ (see Figure 3.27), whereas Pile 35 (20.83 m) experienced an even larger deflection of 2.41 m at $\lambda = 0.79$ (see Figure 3.28). These observations suggest that, despite the applied loads remaining below the theoretical buckling capacities (18 kN for Pile 39 and 13.1 kN for Pile 35), the piles approach critical instability due to their increased slenderness. The results

highlight the pronounced influence of pile length on lateral stiffness and pre-buckling behavior, confirming that longer, slender piles are more susceptible to significant lateral deflections under sub-critical loads (Abbas et al., 2008; L. Y. Chang et al., 2010; Han & Frost, 2000; X. Zhang et al., 2024).

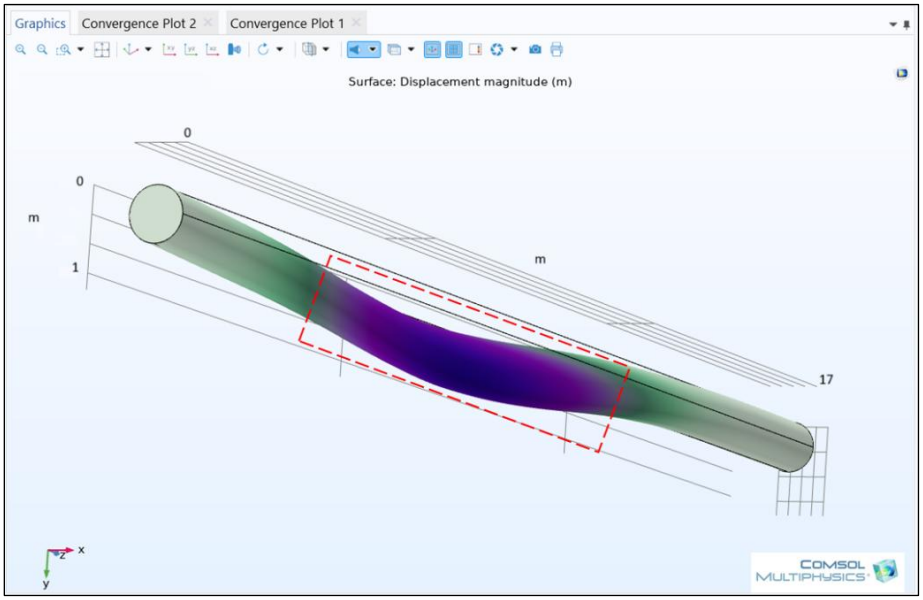

Figure 3. 28 Displacement magnitude surface plot of Pile 39 (length: 17 m), generated in COMSOL Multiphysics, showing the pre-buckling response under an applied load of 10 000 N (Author).

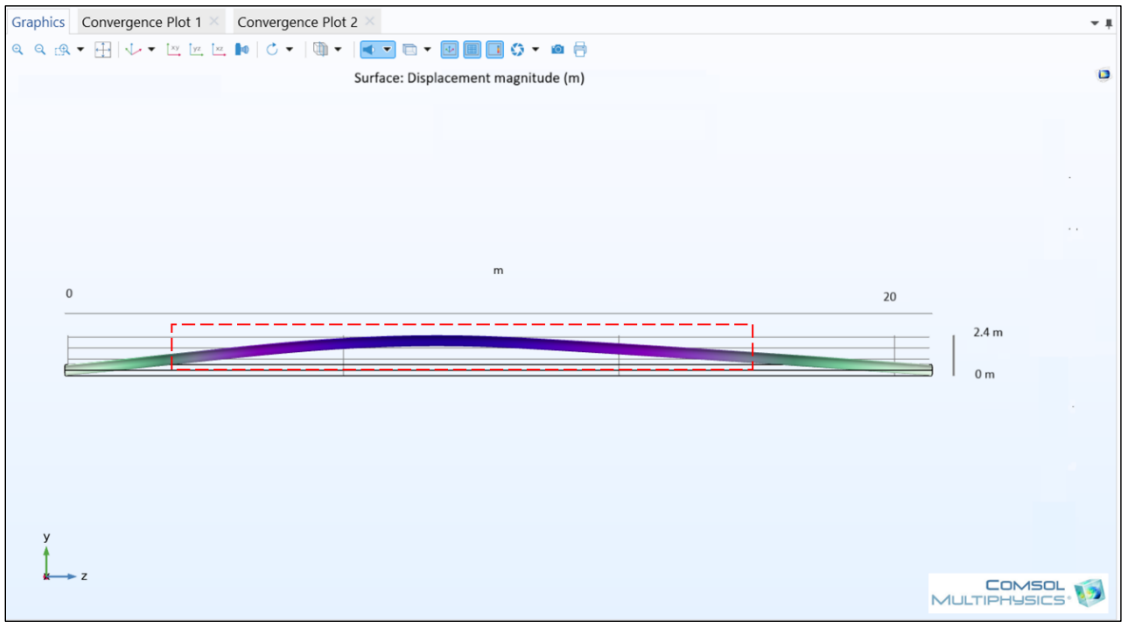

Figure 3. 27 Displacement magnitude surface plot of Pile 34 (length: 20.83 m), generated in COMSOL Multiphysics, showing the pre-buckling response under an applied load of 10 000 N (Author).

In contrast, short piles (~10 m) show comparatively minimal lateral deflections, around 0.3 m even at lower load ratios ($\lambda = 0.208$) (see Figure 3.29), reflecting higher buckling resistance, stiffer response, and less pronounced geometric nonlinearity as reported by (Darvishi Alamouti et al., 2017; Uncuoğlu & Laman, 2012).

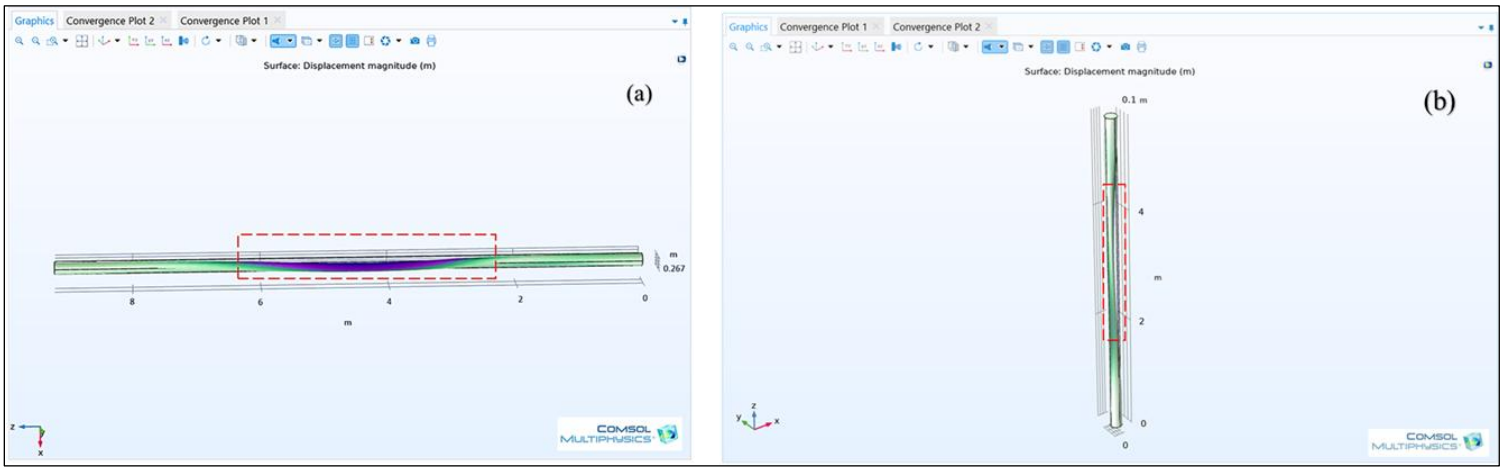

Figure 3. 29 Displacement magnitude surface plots generated in COMSOL Multiphysics under an applied load of 1000 N, showing (a) Pile 09 (9.21 m) and (b) Pile 35 (5.65 m) (Author).

In addition, Lateral displacement versus λ exhibits a pronounced S-shaped nonlinear trend, marking the transition from elastic compression to pre-buckling instability. In the initial phase ($\lambda < 0.2$), displacements grow slowly and nearly linearly, reflecting elastic axial behavior. Beyond $\lambda \approx 0.2$–0.6, deflections accelerate sharply, forming the steep middle segment of the S-curve (see Figure 3.30). This corresponds to stiffness degradation driven by geometric imperfections, initial curvature, and soil interactions, signaling the onset of pre-buckling instability, as supported by (Kerr & Soifer, 1964; J. Li et al., 2024; Szymczak & Kujawa, 2017). Near the Euler limit, lateral displacement increases sharply depending on boundary conditions, representing near-critical instability (Doaré & de Langre, 2006; Klarbring, 2002).

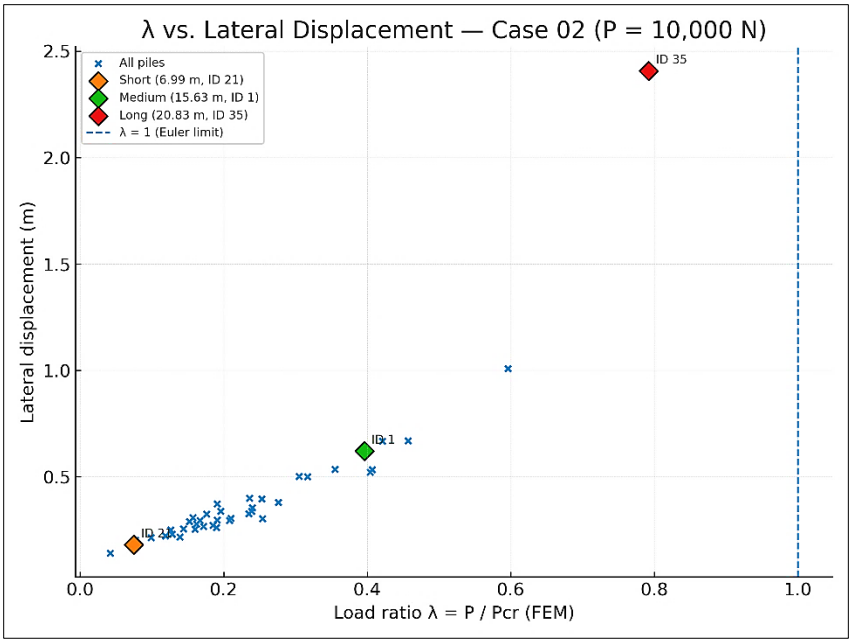

Figure 3. 30 Relationship between load ratio (λ = P/Pcr) and lateral displacement for piles subjected to 10 000 N axial load approaching Buckling (Author).

This S-shaped trend shows that λ is not merely a measure of axial load relative to critical capacity but also a sensitive indicator of pre-buckling susceptibility, particularly in slender piles. The inflection points around $\lambda \approx 0.2$ mark the load at which imperfections and soil effects begin to dominate, highlighting the importance of realistic FEM analysis in capturing lateral displacements absent in Euler's idealized model.

3.2.4 Risk Classification and Validation

Risk thresholds were established based on the design-to-capacity ratio ($\lambda = P_{design}/Pcr$) consistent with the methodology derived from MOE and velocity results. Four categories were established to characterize the likelihood of buckling under the applied operational load:

Safe ($\lambda \leq 0.30$), *At Risk* ($0.30 < \lambda \leq 0.60$), *Significant Risk* ($0.60 < \lambda \leq 1.0$), and *Critical* ($\lambda \geq 1.0$). The design load, $P_{design} = 10{,}000$ N, was selected to represent a conservative high-load condition approaching the onset of buckling.

For each pile, the design-to-capacity ratio (λ) was computed using two distinct approaches: the finite element method (FEM), which provides a numerically derived critical load, and the ultrasonic-informed Euler buckling prediction, which is based on analytical formulations incorporating ultrasonic data. The resulting classifications from these methodologies were systematically compared, as depicted in Figure 3.31.

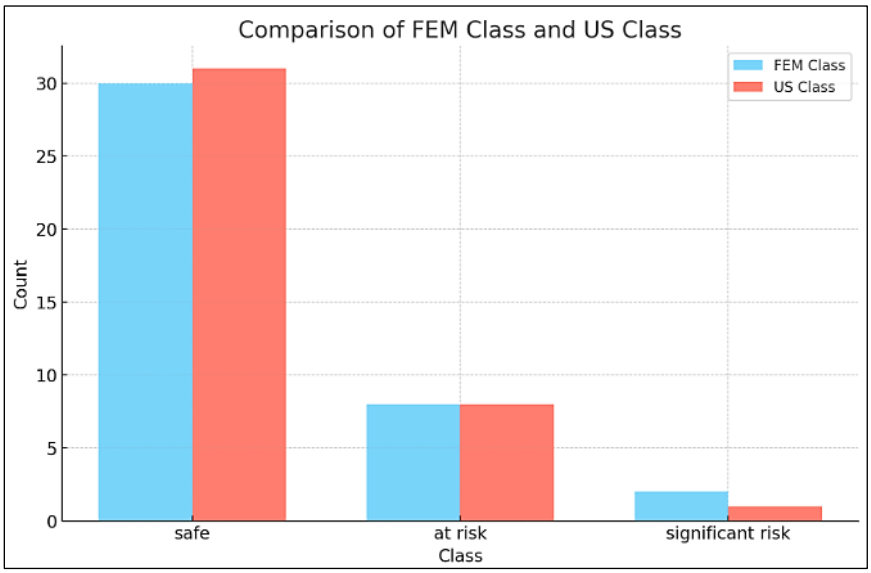

Figure 3. 31 Comparison of pile risk classifications using FEM and ultrasonic-informed Euler methods (Author).

Figure 3.31 shows the number of piles assigned to each risk category according to the FEM and ultrasonic (US) methods. Both methods agreed closely in categorizing the majority of piles as *Safe*—30 piles according to FEM and 31 piles according to the US method. This reflects the substantial margin between design loads and critical buckling loads for these cases. Eight piles were classified as *At Risk* by both methods, demonstrating consistent recognition of piles with intermediate vulnerability and relative insensitivity to geometric imperfections and boundary flexibility. Notably, only a few piles fell into the *Significant Risk* category—2 according to FEM

and 1 according to the US method. No pile was classified as *Critical*. This graphical comparison reinforces the reported high overall agreement rate of 95% and a Cohen's κ value of 0.92, corresponding to an "almost perfect" classification concordance.

Table 3.3 summarizes the discrepancies between the two methods, which mostly occur near category boundaries, particularly for long, slender piles sensitive to geometric imperfections. For example, Pile 39 (L = 17.0 m) was classified as *Significant Risk* by FEM ($\lambda_{FEM} = 0.60$) but only *At Risk* by the US method ($\lambda_{US} = 0.56$). Similarly, Pile 7 (L = 14.57 m), located near the *Safe*-to-*At Risk* threshold, was classified as *At Risk* by FEM ($\lambda_{FEM} = 0.31$) and *Safe* by the US method ($\lambda_{US} = 0.29$). Pile 35 (L = 20.83 m) reached the *Significant Risk* category. Both FEM ($\lambda_{FEM} = 0.79$) and the ultrasonic-informed Euler method ($\lambda_{US} = 0.76$) classified it as *Significant Risk*. The slightly higher λ predicted by FEM reflects its greater sensitivity and precision in capturing pre-buckling effects, as evidenced by substantial lateral displacements (2.41 m) at the design load that were not captured by the Euler-based estimate.

Pile ID	Length (m)	λ_{FEM}	FEM Class	λ_{US}	US Class	Cause of Disagreement
7	14.57	0.31	risk	0.29	safe	Near threshold, FEM captures imperfection sensitivity earlier
35	20.83	0.79	Significant risk	0.76	Significant risk	Slender pile; large pre-buckling displacement captured in FEM
39	17.00	0.60	Significant risk	0.56	risk	Near threshold, FEM captures imperfection sensitivity earlier

Table 3. 3 Summary of classification disagreements between FEM and ultrasonic/Euler methods (Author).

These patterns highlight a key distinction: the ultrasonic/Euler method, based on idealized analytical solutions, does not account for geometric imperfections, second-order effects, or soil boundary compliance. FEM, in contrast, incorporates these nonlinear mechanisms, capturing displacement amplification earlier ($\lambda \approx 0.3–0.8$). Consequently, FEM classifications are more conservative for slender piles and better reflect realistic instability phenomena.

Overall, ultrasonic-informed Euler analysis provides a reliable, efficient tool for large-scale screening of clearly Safe or Critical piles, whereas FEM is essential for accurate classification of piles in intermediate risk ranges.

CHAPTER IV: CONCLUSIONS, LIMITATIONS, AND RECOMMENDATIONS

This research comprehensively examined the structural integrity and buckling behavior of submerged timber piles in lake building constructions, focusing on the heritage timber piles in Hévíz Lake, Hungary. Employing an integrated methodological framework combining non-destructive ultrasonic testing, analytical buckling analysis, and finite element modeling, the study aimed to address critical gaps in the evaluation of submerged timber piles under realistic environmental and boundary conditions.

Key Findings

1. **Ultrasonic Velocity and Buckling Resistance Prediction:** Ultrasonic wave velocity demonstrated a high linear correlation ($r = 0.998$) with the dynamic modulus of elasticity (MOE), affirming its validity as a rapid, non-destructive indicator of internal stiffness and structural integrity of submerged timber piles. Extending this correlation, a predictive model was developed that integrates ultrasonic velocity with geometric parameters, enabling accurate estimation of critical buckling loads ($R^2 = 0.943$). This represents a significant, field-validated correlation that links ultrasonic nondestructive testing data directly to buckling stability assessments in full-scale, long-term submerged heritage piles. The findings underscore the capacity of ultrasonic testing not only for detecting internal degradation but also as a robust predictor for buckling failure, facilitating early intervention and improved management of timber pile stability in environmentally challenging aquatic environments.

2. **Geometry–Material Interaction in the Buckling Resistance of Submerged Timber Piles**: This research confirms that pile length is the principal factor determining the critical buckling load of submerged timber piles, exhibiting a strong inverse correlation ($r = -0.73$). Dynamic modulus of elasticity (MOE) derived from ultrasonic measurements exerts a significant secondary influence ($r = 0.43$), particularly impacting intermediate-length piles where stiffness variability critically modulates stability. The negligible difference between classical Euler–Bernoulli and Granholm-corrected beam models (0.05%) validates the adequacy of classical theory for slender submerged piles. Integrating ultrasonic-derived material properties with geometric parameters yields reliable predictions of structural stability, advancing precise structural health monitoring methods for heritage aquatic timber infrastructure.

3. **Dual-Criteria Risk Classification for Submerged Timber Piles:** This research identifies critical limitations in the ASTM D2555 ultrasonic classification, where elevated ultrasonic velocities can conceal subsurface defects and early decay stages. The proposed dual-parameter framework, integrating ultrasonic velocity and dynamic modulus of elasticity (MOE), improves detection of complex degradation

patterns missed by single-parameter methods. Incorporating pile length further refines risk categories, reliably distinguishing vulnerable piles consistent with observed damage. This framework significantly enhances the precision of non-destructive evaluation for submerged timber structures.

4. **Finite Element Model Validation:** The FEM simulations validated the analytical findings while also highlighting important differences. Although Euler's approach provides theoretical simplicity, the FEM models developed in *COMSOL Multiphysics*—incorporating orthotropic wood properties, submerged and soil-embedded boundary conditions, and axial loading—closely aligned with ultrasonic-derived predictions. FEM-predicted critical buckling loads correlated strongly with ultrasonic estimates ($r = 0.9998$), with mean discrepancies below 5%, thereby confirming the reliability of ultrasonic NDT for preliminary structural assessment.

5. **Pre-buckling and Deformation Behavior:** Nonlinear finite element modeling demonstrates that submerged timber piles initiate lateral instability at a load factor of approximately $\lambda \approx 0.8$, significantly preceding classical ultrasonic-based buckling predictions at $\lambda = 1$. This early onset is driven by nonlinear escalation of bending stresses and lateral displacements, influenced by geometric imperfections, heterogeneous stiffness distribution, and soil–structure interactions. These insights highlight the limitations of linear elastic theories and ultrasonic testing alone, underscoring the necessity for advanced FE simulations to accurately capture complex pre-buckling behavior for improved structural health monitoring and failure prediction of submerged timber infrastructure.

6. **Environmental Degradation Considerations:** Prolonged exposure to the geothermal, mineral-rich lake environment accelerates decay processes affecting wood density and stiffness. The anisotropic, heterogeneous nature of timber and environmental factors such as moisture content, temperature, and microbial activity complicate direct mechanical evaluation, reinforcing the necessity of non-destructive testing methods validated by computational simulation.

Scientific and Practical Contributions

This study contributes academically by bridging timber material mechanics and structural health monitoring through a rigorously validated hybrid methodology that combines field-based ultrasonic measurements with high-fidelity numerical modeling to provide reliable, quantitative assessments of submerged timber pile stability. The approach addresses key challenges associated with the anisotropic nature of wood, the effects of submerged environmental conditions, and the practical limitations of invasive testing in heritage and operational settings.

The proposed classification framework and predictive models offer practical guidance for maintenance prioritization, safety assessment, and service-life optimization of wooden lake structures. Furthermore, the study establishes a methodological template for integrating field testing with finite element analysis in wood engineering research.

Limitations

The study's scope was restricted to spruce piles submerged in a geothermal lake characterized by unique water chemistry and thermal conditions. Assumptions including uniform density and static moisture content introduce inherent uncertainties. Ultrasonic testing focused predominantly on longitudinal wave measurements, limiting comprehensive evaluation of anisotropic stiffness variations. Soil–pile interaction was modeled through elastic spring supports at the pile base, with stiffness values derived from geotechnical assessments. The soil was assumed to behave as a linear-elastic medium, thus neglecting plastic deformation, hysteresis, and pore water pressure effects—simplifications necessitated by limited site-specific data. The geotechnical report for Hevis Lake indicates a thin, rocky stratum (0.3–1.4 m) overlying peat, clay, and sand layers, yet lacks detailed characterization of soil layer thickness and pile embedment extent. Consequently, modeling more complex soil constitutive behaviors or layered soil interactions was not feasible without introducing unverified assumptions, potentially limiting the accuracy of lateral soil restraint and buckling behavior predictions.

Recommendations for Future Work

Future research should broaden the scope to diverse timber species, environmental conditions, and degradation stages. Incorporating complementary non-destructive methods such as resistograph drilling, acoustic emission, and ground-penetrating radar can enhance damage detection accuracy. Moreover, machine learning models trained on expansive ultrasonic and imaging datasets may improve predictive mechanical property estimation. Advancing FEM to integrate nonlinear soil behavior, hydrodynamic forces, and time-dependent degradation will yield more precise simulations. Long-term monitoring through periodic ultrasonic assessments can offer valuable insights into deterioration progression and maintenance scheduling. An important application lies in heritage preservation and rehabilitation of submerged timber structures worldwide.

CHAPTER V: NOVEL FINDINGS OF THE RESEARCH

Thesis 1: Integrated Non-Destructive Evaluation Framework for Submerged Timber Piles

This research presents a novel, validated framework that integrates ultrasonic non-destructive testing (NDT), machine learning techniques for enhanced predictive accuracy, analytical buckling analysis using Euler–Bernoulli beam theory, and high-fidelity finite element modeling (FEM) to quantitatively assess the structural integrity and buckling behavior of submerged timber piles. This methodological approach addresses a critical gap in underwater timber infrastructure evaluation by enabling reliable in-situ diagnostics that holistically account for anisotropic wood properties, soil–pile interactions, and submerged boundary conditions under realistic environmental influences.

Related Publications:

Brougui, M., Andor, K., & Szabó, P. (2025). Finite Element Modeling of Submerged Timber Piles: Validation of Ultrasonic Non-Destructive Testing for Buckling Resistance. *Structural Health Monitoring Journal*, 19 p. https://m2.mtmt.hu/api/publication/ 36450184

Brougui, M., Andor, K., & Szabó, P. (2025). Evaluation of Timber Mechanical Properties Through Non-Destructive Testing: A Bibliometric Analysis. *Buildings*, 15(13), 2192.

https://doi.org/10.3390/buildings15132192

Thesis 2: Ultrasonic-Based Prediction of Buckling Failure in Submerged Timber Piles

This thesis extends the well-established correlation between longitudinal ultrasonic wave velocity and the dynamic modulus of elasticity (MOE) by applying and validating it specifically in submerged timber piles exposed to thermal, mineral-rich aquatic environments—a context not previously examined in the literature ($r = 0.998$). To assess the capability of ultrasonic measurements in predicting the buckling resistance of timber piles, ultrasonic velocity is integrated with geometric parameters to develop a predictive buckling-failure model, which accurately estimates critical buckling loads ($R^2 = 0.943$). This work provides the first field-validated link between ultrasonic measurements and buckling stability in full-scale, long-term submerged heritage piles, enabling early, non-destructive detection of stiffness loss and structural degradation.

Related Publications:

Brougui, M., Andor, K., & Szabó, P**.** (2025). Sensitivity of Buckling Resistance to Pile Length and Structural Imperfections in Submerged Timber Piles. *International Wood Products Journal*, 24 p. https://m2.mtmt.hu/api/publication/ 36450180

Thesis 3: Quantitative Analysis of Geometry and Material Property Interactions Governing Buckling Resistance in Submerged Timber Piles

This thesis quantitatively assesses the critical buckling load (P_{cr}) of submerged timber piles by integrating dynamic modulus of elasticity (MOE), derived from ultrasonic velocity measurements, within the classical Euler–Bernoulli beam framework. While the inverse correlation between pile length and buckling capacity ($r = -0.73$) is well-documented in classical column stability theory,

this study provides the first comprehensive investigation—combining ultrasonic non-destructive testing, analytical modeling, and field validation—of heritage timber piles submerged in thermally and chemically complex aquatic environments. Notably, it demonstrates that environmentally driven variations in dynamic MOE critically modulate buckling resistance in intermediate-length piles (approximately 10–15 meters), where stiffness fluctuations significantly influence structural stability.

Related Publications:

Brougui, M., & Andor, K. (2024). Investigating the stability of wooden lake piles: The influence of dynamic MOE and pile length on buckling behavior. In *Wood 4 Sustainability: Processing, Construction, Products and Design* (pp. 161–174). Sopron University Press. ISBN 978-963-334-5412. https://doi.org/10.35511/978-963-334-541-2-16

Thesis 4: Dual-Parameter Risk Classification Framework Enhancing Degradation Assessment of Submerged Timber Piles

This thesis identifies a critical limitation in the ASTM D2555 (2017) ultrasonic-based risk classification: elevated ultrasonic wave velocities can obscure subsurface defects and incipient decay that are not adequately reflected in stiffness reduction measurements alone. To overcome this challenge, a novel dual-parameter framework integrating ultrasonic wave velocity and dynamic modulus of elasticity (MOE) is proposed and validated.

The integrated approach reveals that transitional degradation states in submerged timber piles, characterized by asynchronous evolution of mechanical stiffness and internal defects, cannot be reliably identified by any single diagnostic parameter. By combining wave velocity and dynamic MOE indicators, the framework substantially enhances the sensitivity and accuracy of material degradation detection in submerged timber environments, where anisotropy, heterogeneity, and complex moisture dynamics affect degradation pathways.

Related Publications:

Brougui, M., Andor, K., & Szabó, P. (2025). Integrated Risk Classification and Buckling Resistance Prediction in Timber Piles Using Ultrasonic Wave Velocity and Dynamic Modulus of Elasticity, Journal of Nondestructive Evaluation, 11 p.
https://doi.org/10.21203/rs.3.rs-6813815/v1

Thesis 5: Validation of Ultrasonic-Based Assessment through Finite Element Modeling Incorporating Anisotropy and Environmental Boundary Conditions

This thesis validates ultrasonic-derived pile stiffness and buckling capacity estimates using orthotropic finite element models in COMSOL Multiphysics, incorporating submerged and soil-embedded boundary conditions with realistic loading. The FEM simulations correlate strongly with ultrasonic predictions (correlation coefficient 0.9998; mean difference ~5%), confirming ultrasonic NDT reliability. FEM further reveals nonlinear buckling behaviors and pre-buckling displacements absent in analytical models, emphasizing the importance of integrating computational and experimental approaches for structural health monitoring of submerged timber piles.

Related Publications:

Brougui, M., Andor, K., & Szabó, P. (2025). Finite Element Modeling of Submerged Timber Piles: Validation of Ultrasonic Non-Destructive Testing for Buckling Resistance. *Structural Health Monitoring Journal*, 19 p. https://m2.mtmt.hu/api/publication/ 36450184

Thesis 6: Nonlinear Finite Element Analysis of Pre-Buckling Lateral Instability in Submerged Timber Piles

This dissertation quantitatively demonstrates through nonlinear finite element modeling that submerged timber piles exhibit lateral instability initiation at a load factor of approximately $\lambda \approx 0.8$, significantly preceding classical ultrasonic-based buckling predictions ($\lambda = 1$). The onset of instability arises from nonlinear escalation in bending stresses and lateral displacements, driven by geometric imperfections, heterogeneous stiffness, and soil–structure interaction effects. These findings underscore the limitations of classical linear elastic theories and ultrasonic testing alone, highlighting the necessity of realistic FE simulations to capture complex pre-buckling behavior for accurate structural health assessment and failure prediction in marine timber infrastructure.

Related Publications:

Brougui, M., Andor, K., & Szabó, P. (2025). Finite Element Modeling of Submerged Timber Piles: Validation of Ultrasonic Non-Destructive Testing for Buckling Resistance. *Structural Health Monitoring Journal*, 19 p. https://m2.mtmt.hu/api/publication/ 36450184

References

Abbas, J. M., Mohammed, Q. S., Mohd, S., Taha, R., & Malaysia, K. (2008). Effect of Shape and Slenderness Ratio on the Behavior of Laterally Loaded Piles. *Al-Nahrain Journal for Engineering Sciences*, *11*(1).

Abdallah, W., Saliba, J., Sbartaï, Z.-M., Sadek, M., Chehade, F. H., & ElAchachi, S. M. (2019). Reliability analysis of non-destructive testing models within a probabilistic approach. *MATEC Web of Conferences*, *281*. https://doi.org/10.1051/matecconf/201928104003

Aicher, S., & Stapf, G. (2016). Compressive strength parallel to the fiber of spruce with high moisture content. *European Journal of Wood and Wood Products*, *74*(4). https://doi.org/10.1007/s00107-015-1004-z

Ajabshir, S., Gupta, R., Lum, C., & Mazloomi, M. S. (2023). Wave Propagation Techniques for the Condition Assessment of Timber Structures: A Review. *Lecture Notes in Civil Engineering*, *348 LNCE*. https://doi.org/10.1007/978-3-031-34159-5_20

Aktharuzzaman, M., Anwar, S., Borisov, D., & He, J. (2024). Experimental full waveform inversion for elastic material characterization with accurate transducer modeling. *Mechanical Systems and Signal Processing*, *213*. https://doi.org/10.1016/j.ymssp.2024.111320

Amafabia, D. A. M., Montalvão, D., David-West, O., & Haritos, G. (2017). A review of structural health monitoring techniques as applied to composite structures. In *SDHM Structural Durability and Health Monitoring* (Vol. 11, Issue 2). https://doi.org/10.3970/sdhm.2017.011.091

André Luis, C., Tulio Hallak, P., Diogo Aparecido Lopes, S., Juliano, F., & Francisco Antonio Rocco, L. (2014). Shear and Longitudinal Modulus of Elasticity in Structural Lumber Beams. *International Journal of Materials Engineering*, *4*(1). https://doi.org/10.5923/j.ijme.20140401.04

Andreev, V. A., Bourdine, A. V., Burdin, V. A., & Dashkov, M. V. (2022). A method for non-destructive testing of the strength of a silica optical fiber. *Computer Optics*, *46*(2). https://doi.org/10.18287/2412-6179-CO-1015

António, C., & Rui, P. (2022). Performance Analysis of Thermographic Cameras Applied to Wood Damage Detection. *International Journal of Thermal and Environmental Engineering*, *19*(2), 55–62. https://doi.org/10.5383/ijtee.19.02.001

Arnold, W., Goebbels, K., & Kumar, A. (2023). Ultrasonic Non-destructive Materials Characterization. In *Springer Series in Materials Science* (Vol. 329). https://doi.org/10.1007/978-3-662-66489-6_1

Arriaga, F., Wang, X., Íñiguez-González, G., Llana, D. F., Esteban, M., & Niemz, P. (2023). Mechanical Properties of Wood: A Review. In *Forests* (Vol. 14, Issue 6). https://doi.org/10.3390/f14061202

Arzola-Villegas, X., Lakes, R., Plaza, N. Z., & Jakes, J. E. (2019). Wood moisture-induced swelling at the cellular scale-Ab intra. *Forests*, *10*(11). https://doi.org/10.3390/f10110996

Asante, B., Ye, H., Nopens, M., Schmidt, G., & Krause, A. (2022). Influence of wood moisture content on the hardened state properties of geopolymer wood composites. *Composites Part A: Applied Science and Manufacturing*, *152*. https://doi.org/10.1016/j.compositesa.2021.106680

Asokkumar, A., Jasiūnienė, E., Raišutis, R., & Kažys, R. J. (2021). Comparison of ultrasonic non-contact air-coupled techniques for characterization of impact-type defects in pultruded gfrp composites. *Materials*, *14*(5). https://doi.org/10.3390/ma14051058

Aydin, M., & Ciritcioğlu, H. H. (2022). COMPARATIVE STUDY OF DESTRUCTIVE, NON-DESTRUCTIVE, AND NUMERICAL METHODS ON THE DETERMINATION OF MOISTURE-DEPENDENT SHEAR MODULI OF CALABRIAN PINE. *Materials Evaluation*, *80*(5). https://doi.org/10.32548/2022.me-04228

Azzi, Z., Al Sayegh, H., Metwally, O., & Eissa, M. (2025). Review of Nondestructive Testing (NDT) Techniques for Timber Structures. *Infrastructures*, *10*(2), 28. https://doi.org/10.3390/infrastructures10020028

Baar, J., Tippner, J., & Gryc, V. (2012). The influence of wood density on longitudinal wave velocity determined by the ultrasound method in comparison to the resonance longitudinal method. *European Journal of Wood and Wood Products*, *70*(5). https://doi.org/10.1007/s00107-011-0550-2

Baar, J., Tippner, J., & Rademacher, P. (2015). Prediction of mechanical properties - modulus of rupture and modulus of elasticity - of five tropical species by nondestructive methods. *Maderas: Ciencia y Tecnologia*, *17*(2). https://doi.org/10.4067/S0718-221X2015005000023

Bai, L., Velichko, A., & Drinkwater, B. W. (2018). Ultrasonic defect characterisation—Use of amplitude, phase, and frequency information. *The Journal of the Acoustical Society of America*, *143*(1). https://doi.org/10.1121/1.5021246

Baker, G. S., Jordan, T. E., & Pardy, J. (2007). An introduction to ground penetrating radar (GPR). *Special Paper of the Geological Society of America*, *432*. https://doi.org/10.1130/2007.2432(01)

Bamber, R. K., & Fukazawa, K. (1985). Sapwood and heartwood: a review. *Forestry Abstracts*, *46*(9).

Ban, M., Inagaki, T., Ma, T., & Tsuchikawa, S. (2018). Effect of cellular structure on the optical properties of wood. *Journal of Near Infrared Spectroscopy*, *26*(1). https://doi.org/10.1177/0967033518757233

Barbosh, M., Dunphy, K., & Sadhu, A. (2022). Acoustic emission-based damage localization using wavelet-assisted deep learning. *Journal of Infrastructure Preservation and Resilience*, *3*(1). https://doi.org/10.1186/s43065-022-00051-8

Bartolucci, B., De Rosa, A., Bertolin, C., Berto, F., Penta, F., & Siani, A. M. (2020). Mechanical properties of the most common european woods: A literature review. In *Frattura ed Integrita Strutturale* (Vol. 14, Issue 54). https://doi.org/10.3221/IGF-ESIS.54.18

Bekhta, P., & Niemz, P. (2003). Effect of high temperature on the change in color, dimensional stability and mechanical properties of spruce wood. *Holzforschung*, *57*(5). https://doi.org/10.1515/HF.2003.080

Benítez, V., Franco, J., Camargo, Á., Raimonda, P., Mantero, C., & Ibáñez, C. M. (2021). INFLUENCE OF INITIAL WOOD MOISTURE ON DECAY PROCESS BY TWO BROWN-ROT FUNGI. *Maderas: Ciencia y Tecnologia*, *23*. https://doi.org/10.4067/s0718-221x2021000100434

Berndt, H., & Johnson, G. C. (1995). Examination of Wave Propagation in Wood from a Microstructural Perspective. In *Review of Progress in Quantitative Nondestructive Evaluation*. https://doi.org/10.1007/978-1-4615-1987-4_213

Bhattacharya, S., Carrington, T. M., & Aldridge, T. R. (2005). Buckling considerations in pile design. *Frontiers in Offshore Geotechnics, ISFOG 2005 - Proceedings of the 1st International Symposium on Frontiers in Offshore Geotechnics*. https://doi.org/10.1201/noe0415390637.ch93

Bhattacharyya, A., Thyagarajan, K., Yan, J., Pintong, K., Chen, Q., Lee, J., Kiesel, P., & Goebel, K. (2024). Elastodynamics based Modelling of Acoustic Emission for Earlier Bearing Damage Detection. *ANNUAL CONFERENCE OF THE PROGNOSTICS AND HEALTH MANAGEMENT SOCIETY*, 1–16. https://doi.org/https://doi.org/10.36001/phmconf.2024.v16i1.3971

Binda, L., & Saisi, A. (2009). Application of NDTs to the diagnosis of Historic Structures. *Non-Destructive Testing in Civil Engineering*.

Björdal, C. G., & Dayton, P. K. (2020). First evidence of microbial wood degradation in the coastal waters of the Antarctic. *Scientific Reports*, *10*(1). https://doi.org/10.1038/s41598-020-68613-y

Blomberg, J. (2006). Mechanical and physical properties of semi-isostatically densified Wood. In *Division of Wood Science and Technology*.

Bondre, R., & Gaikwad, S. (2016). ANALYSIS OF STRUCTURES WITH RESPECT TO LINEAR STATIC ANALYSIS USING P-DELTA EFFECT. *International Journal of Advance Research and Innovative Ideas in Education (IJARIIE)*, *2*(4), 3231–3236. www.ijariie.com838

Boonstra, M. J., Van Acker, J., Tjeerdsma, B. F., & Kegel, E. V. (2007). Strength properties of thermally modified softwoods and its relation to polymeric structural wood constituents. *Annals of Forest Science*, *64*(7). https://doi.org/10.1051/forest:2007048

Bornemann, T., Brischke, C., & Alfredsen, G. (2014). Decay of wooden commodities - moisture risk analysis, service life prediction and performance assessment in the field. *Wood Material Science and Engineering*, *9*(3). https://doi.org/10.1080/17480272.2014.904431

Bouras, F., Chaplain, M., & Nafa, Z. (2010). Experimental and modelling buckling of wood-based columns under repeated loading. *EPJ Web of Conferences*, *6*. https://doi.org/10.1051/epjconf/20100628003

Bourne-Webb, P. J., Potts, D. M., & Rowbottom, D. (2007). Plastic bending of steel sheet piles. *Proceedings of the Institution of Civil Engineers: Geotechnical Engineering*, *160*(3). https://doi.org/10.1680/geng.2007.160.3.129

Bozonnet, C., Saudreau, M., Badel, E., Amglio, T., & Charrier, G. (2024). Freeze dehydration vs supercooling in tree stems: Physical and physiological modelling. *Tree Physiology*, *44*(1). https://doi.org/10.1093/treephys/tpad117

Bratasz, Ł., & Kozłowski, R. (2005). Laser sensors for continuous in-situ monitoring of the dimensional response of wooden objects. *Studies in Conservation*, *50*(4). https://doi.org/10.1179/sic.2005.50.4.307

Brémaud, I., Gril, J., & Thibaut, B. (2011). Anisotropy of wood vibrational properties: Dependence on grain angle and review of literature data. In *Wood Science and Technology* (Vol. 45, Issue 4). https://doi.org/10.1007/s00226-010-0393-8

Brischke, C., Soetbeer, A., & Meyer-Veltrup, L. (2017). The minimum moisture threshold for wood decay by basidiomycetes revisited. A review and modified pile experiments with Norway spruce and European beech decayed by Coniophora puteana and Trametes versicolor. *Holzforschung*, *71*(11). https://doi.org/10.1515/hf-2017-0051

Brougui, M., Andor, K., & Szabó, P. (2025). Evaluation of Timber Mechanical Properties Through Non-Destructive Testing: A Bibliometric Analysis. In *Buildings* (Vol. 15, Issue 13). Multidisciplinary Digital Publishing Institute (MDPI). https://doi.org/10.3390/buildings15132192

Bucur, V. (1988). Wood structural anisotropy estimated by acoustic invariants. In *IAWA Journal* (Vol. 9, Issue 1). https://doi.org/10.1163/22941932-90000471

Bucur, V. (2006). Acoustics of wood. *13th International Congress on Sound and Vibration 2006, ICSV 2006*, *1*. https://doi.org/10.1121/1.1350453

Bucur, V. (2023). A Review on Acoustics of Wood as a Tool for Quality Assessment. *Forests*, *14*(8). https://doi.org/10.3390/f14081545

Bucur, V., & Archer, R. R. (1984). Elastic constants for wood by an ultrasonic method. *Wood Science and Technology*, *18*(4). https://doi.org/10.1007/BF00353361

Bucur, V., & Böhnke, I. (1994). Factors affecting ultrasonic measurements in solid wood. *Ultrasonics*, *32*(5). https://doi.org/10.1016/0041-624X(94)90109-0

Bucur, V., & Declercq, N. F. (2006). The anisotropy of biological composites studied with ultrasonic technique. *Ultrasonics*, *44*(SUPPL.). https://doi.org/10.1016/j.ultras.2006.05.203

Buddy, J. ", & Showalter, ". (2012). Round Timber Poles and Piles. *WOOD DESIGN FOCUS*, *22*(4), 14–18.

Budig, M., & Mlote, D. S. (2022). Fiber reinforced timber: Designing structural beams for sustainable buildings with enhanced load-bearing capacity. In *Structures and Architecture A Viable Urban Perspective?* https://doi.org/10.1201/9781003023555-17

Cai, C. (2020). Effects of long-term moisture and weather exposure on the structure and properties of thermally modified wood. *Dissertationes Forestales*, *2020*(298). https://doi.org/10.14214/df.298

Cao, H., Gao, X., Chen, J., Xi, G., Yin, Y., & Guo, J. (2023). Changes in Moisture Characteristics of Waterlogged Archaeological Wood Owing to Microbial Degradation. *Forests*, *14*(1). https://doi.org/10.3390/f14010009

Carbol, L., Kusak, I., Martinek, J., & Vojkuvkova, P. (2015). Influence of transducer coupling in ultrasonic testing. *NDT in Progress 2015 - 8th International Workshop of NDT Experts, Proceedings*.

Ceccato, F., Simonini, P., & Lionello, A. (2013). Long-term mechanical behavior of wooden pile foundation in Venice. *Geotechnical Engineering for the Preservation of Monuments and Historic Sites - Proc. of the 2nd Int. Symp. on Geotechnical Engineering for the Preservation of Monuments and Historic Sites*. https://doi.org/10.1201/b14895-29

Chandrasekaran, S. (2019). Structural Health Monitoring: An Overview. In *Structural Health Monitoring with Application to Offshore Structures*. https://doi.org/10.1142/9789811201097_0001

Chang, L., Qian, W., Chang, H., Chang, X., & Ye, T. (2021). Nondestructive testing based compressive bearing capacity prediction method for damaged wood components of ancient timber buildings. *Materials*, *14*(19). https://doi.org/10.3390/ma14195512

Chang, L. Y., Wang, J. C., & Zhu, X. R. (2010). Elastoplastic analytical computation of long piles under combined lateral loads. *Yantu Gongcheng Xuebao/Chinese Journal of Geotechnical Engineering*, *32*(6).

Chauhan, S., & Sethy, A. (2016). Differences in dynamic modulus of elasticity determined by three vibration methods and their relationship with static modulus of elasticity. *Maderas: Ciencia y Tecnologia*, *18*(2). https://doi.org/10.4067/S0718-221X2016005000034

Chavenetidou, M., & Kamperidou, V. (2024). Impact of Wood Structure Variability on the Surface Roughness of Chestnut Wood. *Applied Sciences (Switzerland)*, *14*(14). https://doi.org/10.3390/app14146326

Chawhan, B. S. (2012). Behavior of Lateral Resistance of Flexible Piles in Layered Soils. *IOSR Journal of Mechanical and Civil Engineering*, *2*(5). https://doi.org/10.9790/1684-0250711

Chen, H. X., Fan, D. L., Fang, L., Zhang, G. Y., Cao, C. H., Huang, W. J., Huang, J. M., & Yang, L. (2019). Finite element numerical simulation analysis based on ultrasonic phased array. *IOP Conference Series: Materials Science and Engineering*, *657*(1). https://doi.org/10.1088/1757-899X/657/1/012011

Chen, L., Chen, Y. hui, Shi, J. wei, & Chen, G. (2017). Buckling Analysis of an Axially Loaded Slender Pile Considering the Promotion Effect of Soil Pressure. *Soil Mechanics and Foundation Engineering*, *54*(3). https://doi.org/10.1007/s11204-017-9451-7

Chi Wai, L. (2013). Parametric studies on buckling of piles in cohesionless soils by numerical methods. *HKIE Transactions Hong Kong Institution of Engineers*, *20*(1). https://doi.org/10.1080/1023697X.2013.785077

Cieszko, M., & Kriese, W. (2008). INTERACTION OF ULTRASONIC WAVES WITH CONTINUOUS INHOMOGENEITY OF POROUS MATERIALS. *36th Solid Mechanics Conference*, 16–17. http://rcin.org.pl

Dackermann, U., Elsener, R., Li, J., & Crews, K. (2016). A comparative study of using static and ultrasonic material testing methods to determine the anisotropic material properties of wood. *Construction and Building Materials*, *102*. https://doi.org/10.1016/j.conbuildmat.2015.07.195

Dahle, G., Carpenter, A., & DeVallance, D. (2016). Non-destructive measurement of the modulus of elasticity of wood using acoustical stress waves. *Arboriculture and Urban Forestry*, *42*(4). https://doi.org/10.48044/jauf.2016.021

Darvishi Alamouti, S., Bahaari, M. R., & Moradi, M. (2017). Effect of Pile Bending Stiffness on Static Lateral Behavior of a Short Monopile in Dry Sand. *INTERNATIONAL JOURNAL OF COASTAL& OFFSHORE ENGINEERING*, *2*(5), 25. https://doi.org/http://ijcoe.org/article-1-88-en.html

David Redman, J., Hans, G., & Diamanti, N. (2016). Impact of Wood Sample Shape and Size on Moisture Content Measurement Using a GPR-Based Sensor. *IEEE Journal of Selected Topics in Applied Earth Observations and Remote Sensing*, *9*(1). https://doi.org/10.1109/JSTARS.2016.2517601

De Francesco, G., & Sullivan, T. J. (2023). Improved estimation of P-delta effects on the response of bilinear SDOF systems. *Earthquake Spectra*, *39*(2). https://doi.org/10.1177/87552930221146569

De Freitas, V. P., Delgado, J. M. P. Q., & Machado, N. (2015). Wood dimensional changes due to hygrothermal behaviour. *Defect and Diffusion Forum*, *365*. https://doi.org/10.4028/www.scientific.net/DDF.365.172

De Ridder, M., Van Den Bulcke, J., Vansteenkiste, D., Van Loo, D., Dierick, M., Masschaele, B., De Witte, Y., Mannes, D., Lehmann, E., Beeckman, H., Van Hoorebeke, L., & Van Acker, J. (2011). High-resolution proxies for wood density variations in Terminalia superba. *Annals of Botany*, *107*(2). https://doi.org/10.1093/aob/mcq224

Deb, D., & Roy, P. (2021). Wood and bark lignin contents of trees from deciduous forests of eastern India. *Experimental Results*, *2*. https://doi.org/10.1017/exp.2021.18

Dickens, J. R., Bender, D. A., & Bray, D. E. (1996). A critical-angle ultrasonic technique for the inspection of wood parallel-to-grain. *Wood and Fiber Science*, *28*(3).

Dietsch, P., Franke, S., Franke, B., Gamper, A., & Winter, S. (2015). Methods to determine wood moisture content and their applicability in monitoring concepts. *Journal of Civil Structural Health Monitoring*, *5*(2). https://doi.org/10.1007/s13349-014-0082-7

Dinwoodie, J. M. M. (2000). Timber: Its nature and behaviour. In *Taylor & Francis e-Library* (Vol. 1999, Issue December).

Divós, F., & Tanaka, T. (2005). Relation Between Static and Dynamic Modulus of Elasticity of Wood. *Acta Silvatica et Lignaria Hungarica*, *1*(1), 105–110. https://doi.org/10.37045/aslh-2005-0009

Doaré, O., & de Langre, E. (2006). The role of boundary conditions in the instability of one-dimensional systems. *European Journal of Mechanics, B/Fluids*, *25*(6). https://doi.org/10.1016/j.euromechflu.2006.01.001

Dubois, F., Randriambololona, H., & Petit, C. (2005). Creep in wood under variable climate conditions: Numerical modeling and experimental validation. In *Mechanics of Time-Dependent Materials* (Vol. 9, Issues 2–3). https://doi.org/10.1007/s11043-005-1083-z

Duong, D. Van, & Hasegawa, M. (2024a). RELATIONSHIP BETWEEN ACOUSTIC WAVE VELOCITY AND MECHANICAL PROPERTIES IN Acacia mangium WOOD. *Maderas: Ciencia y Tecnologia*, *26*(33), 1–10. https://doi.org/10.22320/s0718221x/2024.33

Duong, D. Van, & Hasegawa, M. (2024b). RELATIONSHIP BETWEEN ACOUSTIC WAVE VELOCITY AND MECHANICAL PROPERTIES IN Acacia mangium WOOD. *Maderas: Ciencia y Tecnologia*, *26*. https://doi.org/10.22320/s0718221x/2024.33

Dwivedi, S. K., Vishwakarma, M., & Soni, P. A. (2018). Advances and Researches on Non Destructive Testing: A Review. *Materials Today: Proceedings*, *5*(2). https://doi.org/10.1016/j.matpr.2017.11.620

Dyka, I., & Klempka, K. (2023). Influence of Pile Foundation Stiffness on Column Design in One-Story Reinforced Concrete Frames. *Applied Sciences (Switzerland)*, *13*(5). https://doi.org/10.3390/app13052915

Ebrahiminejad, A., Mardanshahi, A., & Kazemirad, S. (2022). Nondestructive evaluation of coated structures using Lamb wave propagation. *Applied Acoustics*, *185*. https://doi.org/10.1016/j.apacoust.2021.108378

Edman, M., Hagos, S., & Carlsson, F. (2021). Warming effects on wood decomposition depend on fungal assembly history. *Journal of Ecology*, *109*(4). https://doi.org/10.1111/1365-2745.13617

Eitzen, D. G., & Wadley, H. N. G. (1984). ACOUSTIC EMISSION: ESTABLISHING THE FUNDAMENTALS. *Journal of Research of the National Bureau of Standards (United States)*, *89*(1). https://doi.org/10.6028/jres.089.008

Elam, J. (2022). *Microbial degradation of wooden foundation piles in urban context – causes and concerns* [Doctor of Philosophy]. University of Gothenburg. Faculty of Science.

Elam, J., & Björdal, C. (2020). A review and case studies of factors affecting the stability of wooden foundation piles in urban environments exposed to construction work. In *International Biodeterioration and Biodegradation* (Vol. 148). https://doi.org/10.1016/j.ibiod.2020.104913

El-Hadad, A., Brodie, G. I., & Ahmed, B. S. (2018). The Effect of Wood Condition on Sound Wave Propagation. *Open Journal of Acoustics*, *08*(03). https://doi.org/10.4236/oja.2018.83004

Emms, G. W., Nanayakkara, B., & Harrington, J. J. (2013). Application of longitudinal-wave time-of-flight sound speed measurement to Pinus radiata seedlings. *Canadian Journal of Forest Research*, *43*(8). https://doi.org/10.1139/cjfr-2012-0482

Espinosa, L., Bacca, J., Prieto, F., Lasaygues, P., & Brancheriau, L. (2018). Accuracy on the time-of-flight estimation for ultrasonic waves applied to non-destructive evaluation of standing

trees: A comparative experimental study. *Acta Acustica United with Acustica*, *104*(3). https://doi.org/10.3813/AAA.919186

Espinosa, L., Brancheriau, L., Prieto, F., & Lasaygues, P. (2018). Sensitivity of ultrasonic wave velocity estimation using the christoffel equation for wood non-destructive characterization. *BioResources*, *13*(1). https://doi.org/10.15376/biores.13.1.918-928

Espinosa, L., Prieto, F., Brancheriau, L., & Lasaygues, P. (2019). Effect of wood anisotropy in ultrasonic wave propagation: A ray-tracing approach. *Ultrasonics*, *91*. https://doi.org/10.1016/j.ultras.2018.07.015

Ettelaei, A., Layeghi, M., Zarea Hosseinabadi, H., & Ebrahimi, G. (2019). Prediction of modulus of elasticity of poplar wood using ultrasonic technique by applying empirical correction factors. *Measurement: Journal of the International Measurement Confederation*, *135*. https://doi.org/10.1016/j.measurement.2018.11.076

Fabiana Goia Rosa, de O., & Sales, A. (2006). Relationship between density and ultrasonic velocity in Brazilian tropical woods. *Bioresource Technology*, *97*(18). https://doi.org/10.1016/j.biortech.2005.04.050

Fang, S., Li, M., Deng, T., & Du, K. (2022). STUDY ON THE TIME-FREQUENCY CHARACTERISTICS AND PROPAGATION LAW OF ACOUSTIC EMISSION LONGITUDINAL WAVES IN WOOD GRAIN DIRECTION. *Wood Research*, *67*(4). https://doi.org/10.37763/wr.1336-4561/67.4.582597

Farrar, C. R., Dervilis, N., & Worden, K. (2024). The Past, Present and Future of Structural Health Monitoring: An Overview of Three Ages. *Strain*, *61*(1), 1–24. https://doi.org/10.1111/str.12495

Farrar, C. R., & Worden, K. (2007). An introduction to structural health monitoring. *Philosophical Transactions of the Royal Society A: Mathematical, Physical and Engineering Sciences*, *365*(1851). https://doi.org/10.1098/rsta.2006.1928

Fathi, H., Kazemirad, S., & Nasir, V. (2020). A nondestructive guided wave propagation method for the characterization of moisture-dependent viscoelastic properties of wood materials. *Materials and Structures/Materiaux et Constructions*, *53*(6). https://doi.org/10.1617/s11527-020-01578-6

Fathi, H., Kazemirad, S., & Nasir, V. (2021). Lamb wave propagation method for nondestructive characterization of the elastic properties of wood. *Applied Acoustics*, *171*. https://doi.org/10.1016/j.apacoust.2020.107565

Feng, H. L., Li, G. H., Fang, Y. M., & Li, J. (2010). Stress wave propagation modeling and application in wood testing. *Xitong Fangzhen Xuebao / Journal of System Simulation*, *22*(6).

Fenu, L., Congiu, E., Deligia, M., Giaccu, G. F., Hosseini, A., & Serra, M. (2021). Buckling analysis of piles in multi-layered soils. *Applied Sciences (Switzerland)*, *11*(22). https://doi.org/10.3390/app112210624

Fernández-Escobar, C. J., Vega-Posada, C. A., & Garcia-Aristizábal, E. F. (2023). Lateral deformation and buckling analysis of piles including shear effects: Numerical analysis. *Engineering Structures*, *277*. https://doi.org/10.1016/j.engstruct.2022.115416

Filgueira, T. S., França, A., Jose, F., França, N., Ross, R. J., Wang, X., Donaria, M., Arantes, C., & Seale, R. D. (2015). African mahogany wood defects detected by ultrasound waves. *19th International Nondestructive Testing and Evaluation of Wood Symposium*, 22–28.

Forest Products Laboratory - USDA. (2010). Wood Handbook: Wood as an Engineering Material. In *USDA - General Technical Report*.

Fredriksson, M. (2019). On wood-water interactions in the over-hygroscopic moisture range-mechanisms, methods, and influence of wood modification. In *Forests* (Vol. 10, Issue 9). https://doi.org/10.3390/f10090779

French, S., & Whittaker, A. (2023). Pile integrity testing. In *ICE Manual of Geotechnical Engineering Volume 2: Geotechnical design, construction and verification*. https://doi.org/10.1680/icemge.66830.1561

Fu, Z., Chen, J., Zhang, Y., Xie, F., & Lu, Y. (2023). Review on Wood Deformation and Cracking during Moisture Loss. In *Polymers* (Vol. 15, Issue 15). https://doi.org/10.3390/polym15153295

Gabr, M. A., Wang, J. J., & Zhao, M. (1997). Buckling of Piles with General Power Distribution of Lateral Subgrade Reaction. *Journal of Geotechnical and Geoenvironmental Engineering*, *123*(2). https://doi.org/10.1061/(asce)1090-0241(1997)123:2(123)

Gallardo, D., Réyes, N., Monasterio, D., & Finger, R. (2018). Measurement of Wood Moisture Content Using Microwaves. *2018 IEEE MTT-S Latin America Microwave Conference, LAMC 2018 - Proceedings*. https://doi.org/10.1109/LAMC.2018.8699049

Gally, T., Kuttich, A., Pfetsch, M. E., Schaeffner, M., & Ulbrich, S. (2018). Optimal Placement of Active Bars for Buckling Control in Truss Structures under Bar Failures. *Applied Mechanics and Materials*, *885*. https://doi.org/10.4028/www.scientific.net/amm.885.119

Gatto, M. P. A., & Montrasio, L. (2021). Analysis of the Behaviour of Very Slender Piles: Focus on the Ultimate Load. *International Journal of Civil Engineering*, *19*(2). https://doi.org/10.1007/s40999-020-00547-y

Ge, Z., Chen, L., Luo, R., Wang, Y., & Zhou, Y. (2018). The Detection of Structure in Wood by X-Ray CT Imaging Technique. *BioResources*, *13*(2). https://doi.org/10.15376/biores.13.2.3674-3685

Gérard, L., Arsenault, C., Kettler, M., & Boissonnade, N. (2018). The influence of geometrical and material imperfections on the stability and resistance of I and H sections. *Proceedings of the Structural Stability Research Council Annual Stability Conference 2018*.

Gerhards, C. C. (1982a). Effect of Moisture Content and Temperature on the Mechanical Properties of Wood: An Analysis of Immediate Effects. *Wood and Fiber*, *14*(1).

Gerhards, C. C. (1982b). LONGITUDINAL STRESS WAVES FOR LUMBER STRESS GRADING: FACTORS AFFECTING APPLICATIONS: STATE OF THE ART. *Forest Products Journal*, *32*(2).

Gerolymos, N., Kassas, K., Bouzoni, E., & Brinkgreve, R. B. J. (2014). Dynamic analysis of piles subjected to axial and lateral loading with emphasis on soil and interface nonlinearities. *Numerical Methods in Geotechnical Engineering - Proceedings of the 8th European Conference on Numerical Methods in Geotechnical Engineering, NUMGE 2014*, *2*, 1117–1122. https://doi.org/10.1201/b17017-198

Ghosh, P., Bhaumik, S., & Mukherjee, S. (2023). Behavior of Vertical and Battered Piles Under Combined Axial and Lateral Load. *Lecture Notes in Civil Engineering*, *295*. https://doi.org/10.1007/978-981-19-6359-9_20

Giaccu, G. F., Meloni, D., Valdès, M., & Fragiacomo, M. (2017). Dynamic determination of the modulus of elasticity of maritime pine cross-laminated panels using vibration methods. *WIT Transactions on Ecology and the Environment*, *226*(1). https://doi.org/10.2495/SDP170501

Giese, J., Beckmann, B., Schladitz, F., Marx, S., & Curbach, M. (2023). Effect of Load Eccentricity on CRC Structures with Different Slenderness Ratios Subjected to Axial Compression. *Buildings*, *13*(10). https://doi.org/10.3390/buildings13102489

Gil-Moreno, D., Ridley-Ellis, D., & McLean, P. (2016). Using the right modulus of elasticity to get the best grades out of softwood timber species in Great Britain. *WCTE 2016 - World Conference on Timber Engineering*.

Githiomi, J K; Dougal, E. (2012). Analysis of Heartwood - Sapwood Demarcation Methods and Variation of Sapwood and Heartwood within and Between 15 Year Old Plantation Grown Eucalyptus Regnans. *International Journal of Applied Scince and Technology*, *2*(8).

Glass, Samuel V, Zelinka, & Samuel L. (2010). Moisture Relations and Physical Properties of Wood. In *Wood Handbook*.

Godoy, V. B., Schnaid, F., Cirio, E., Filho, H. S., Leonhardt, A., & Pestana, I. A. (2024). Influence of Rate Effects, Temperature, and Moisture Content on the Geomechanical Behavior of Marine Clays. *Journal of Offshore Mechanics and Arctic Engineering*, *146*(3). https://doi.org/10.1115/1.4063699

Goncalves, R., & da Costa, O. A. L. (2008). Influence of Moisture Content on Longitudinal, Radial, and Tangential Ultrasonic Velocity for Two Brazilian Wood Species. *Wood and Fiber Science*, *40*(4).

Gongalves, R., Trinca, A. J., & Cerri, D. G. P. (2011). Comparison of elastic constants of wood determined by ultrasonic wave propagation and static compression testing. *Wood and Fiber Science*, *43*(1).

Güntekin, E., & Aydın, T. Y. (2013). Effects of Moisture Content on Some Mechanical Properties of Turkish Red Pine (Pinus brutia Ten.). *International Caucasian Forestry Symposium*, *Oktober*.

Gupta, B. K., & Basu, D. (2018). Applicability of Timoshenko, Euler-Bernoulli and rigid beam theories in analysis of laterally loaded monopiles and piles. *Geotechnique*, *68*(9). https://doi.org/10.1680/jgeot.16.P.244

Gupta, M., & Khan, M. A. (2021). Advances in applications of non-destructive testing (NDT): a review. *International Research Journal of Engineering, IT & Scientific Research*, *7*(3). https://doi.org/10.21744/irjeis.v7n3.1003

Hajdo, E., Hadzalic, E., & Ibrahimbegovic, A. (2024). Buckling analysis of piles in weak single-layered soil with consideration of geometric nonlinearities. *Coupled Systems Mechanics*, *13*(3), 187–200. https://doi.org/10.12989/csm.2024.13.3.187

Halabe, U. B., Bidigalu, G. M., GangaRao, H. V. S., & Ross, R. J. (1997). Nondestructive evaluation of green wood using stress wave and transverse vibration techniques. *Materials Evaluation*, *55*(9).

Halimi, A., & Kouloughli, S. (2021). Mathematical Modelling in Civil Engineering BUCKLING LOADS OF FULLY EMBEDDED PILE IN CLAYEY SOIL BASED ON THE FINITE ELEMENT METHOD. *Mathematical Modelling in Civil Engineering*, *16*(3). https://doi.org/10.2478/mcee-2021-0013

Han, J., & Frost, J. D. (2000). Load-deflection response of transversely isotropic piles under lateral loads. *International Journal for Numerical and Analytical Methods in Geomechanics*, *24*(5). https://doi.org/10.1002/(SICI)1096-9853(20000425)24:5<509::AID-NAG79>3.0.CO;2-9

Hariswaran, S., & Premalatha, K. (2021). Experimental Investigation on the Behavior of a Defective Pile Subject to a Lateral Load. *Soil Mechanics and Foundation Engineering*, *58*(4). https://doi.org/10.1007/s11204-021-09747-7

Harris, R. A., Follett, D. H., Halliwell, M., & Wells, P. N. T. (1991). Ultimate limits in ultrasonic imaging resolution. In *Ultrasound in Medicine and Biology* (Vol. 17, Issue 6). https://doi.org/10.1016/0301-5629(91)90025-R

Hasan, A. Q. (2019a). Buckling Analysis of Piles: A Review. *Scholars Journal of Engineering and Technology*, *7*(11), 278–283. https://doi.org/10.36347/sjet.2019.v07i11.001

Hasan, A. Q. (2019b). Buckling Analysis of Piles: A Review. *Scholars Journal of Engineering and Technology*, *11*(7), 278–283. https://doi.org/DOI:10.36347/sjet.2019.v07i11.001

Hasegawa, M., Mori, M., & Matsumura, J. (2015). Relations of fiber length to within-tree variation of ultrasonic wave velocity in fast-growing trees. *Wood and Fiber Science*, *47*(3).

Hasegawa, M., Mori, M., & Matsumura, J. (2016). Non-Contact Velocity Measurement of Japanese Cedar Columns Using Air-Coupled Ultrasonics. *World Journal of Engineering and Technology*, *04*(01). https://doi.org/10.4236/wjet.2016.41005

Hasegawa, M., Takata, M., Matsumura, J., & Oda, K. (2011). Effect of wood properties on within-tree variation in ultrasonic wave velocity in softwood. *Ultrasonics*, *51*(3). https://doi.org/10.1016/j.ultras.2010.10.001

Hassan, & Osama A.B. (2021). The effect of flexural–torsional buckling on the stability of timber members: a case study. *SN Applied Sciences*, *3*(6). https://doi.org/10.1007/s42452-021-04604-6

Hatefipour, S., Ahlberg, J., & Wren, J. (2014). Thermal non-destructive testing : Modeling , simulation and experiments for improved localization of hidden defects. *QIRT2014 Conférence*.

He, H. (2020). Multiple scattering theory for strong scattering heterogeneous elastic continua with triaxial inhomogeneities: theoretical fundamentals and applications. *ArXiv: Geophysics.*, 1–27. https://arxiv.org/abs/2005.00590

He, L., Chen, X., Wang, Z., Han, Y., Su, T., Dai, G., Zhang, E., & Long, Z. (2022). A case study on the bearing characteristics of a bottom uplift pile in a layered foundation. *Scientific Reports*, *12*(1). https://doi.org/10.1038/s41598-022-27105-x

He, L., Li, Z., Xie, Y., Liu, Y., & Liu, M. (2023). Buckling failure mechanism and critical buckling load prediction method of super-long piles in soft-clay ground in deep water. *Ocean Engineering*, *276*. https://doi.org/10.1016/j.oceaneng.2023.114216

Hernández, R. E. (2007). SWELLING PROPERTIES OF HARDWOODS AS AFFECTED BY THEIR EXTRANEOUS SUBSTANCES, WOOD DENSITY, AND INTERLOCKED GRAIN. *Wood and Fiber Science*, *39*(1), 146–158.

Hirsekorn, S. (2014). Theoretical Description of Ultrasonic Propagation and Scattering Phenomena in Polycrystalline Structures Aiming for Simulations on Nondestructive Materials Characterization and Defect Detection. *11th European Conference on Non-Destructive Testing (ECNDT 2014)*, 1–10. www.ndt.net/?id=16595

Holt, J. D., Chen, S., & Douglas, R. A. (1994). Determining lengths of installed timber piles by dispersive wave propagation. *Transportation Research Record*, *1447*.

Holzer, S. M., Loferski, J. R., & Dillard, D. A. (1989). A review of creep in wood: concepts relevant to develop long-term behavior predictions for wood structures. *Wood and Fiber Science*, *21*(4).

Hu, Y., Nakao, T., Nakai, T., Gu, J., & Wang, F. (2005). Effects of grain angles of face veneer on surface wave velocities and dynamic shear moduli of wood-based composites. *Journal of Wood Science*, *51*(3). https://doi.org/10.1007/s10086-004-0673-8

Huan, Z., Jiao, Z., Li, G., & Wu, X. (2018). Velocity error correction based tomographic imaging for stress wave nondestructive evaluation of wood. *BioResources*, *13*(2). https://doi.org/10.15376/biores.13.2.2530-2545

Huang, C.-L., & Floyd, S. L. (2009). Method for predicting the modulus of elasticity of a timber based raw material group by determination of the stress wave velocity. *WEYERHAEUSER CO (Federal Way, WA 98063-9777, US)*.

Huke, P., Klattenhoff, R., von Kopylow, C., & Bergmann, R. B. (2013). Novel trends in optical non-destructive testing methods. *Journal of the European Optical Society*, *8*. https://doi.org/10.2971/jeos.2013.13043

Ibarra-Castanedo, C., Tarpani, J. R., & Maldague, X. P. V. (2013). Nondestructive testing with thermography. *European Journal of Physics*, *34*(6). https://doi.org/10.1088/0143-0807/34/6/S91

Iida, Y., Poorter, L., Sterck, F. J., Kassim, A. R., Kubo, T., Potts, M. D., & Kohyama, T. S. (2012). Wood density explains architectural differentiation across 145 co-occurring tropical tree species. *Functional Ecology*, *26*(1). https://doi.org/10.1111/j.1365-2435.2011.01921.x

Ike, C. C. (2024). Critical buckling load analysis of Euler-Bernoulli beam on two-parameter foundations using Galerkin method. *Journal of Mechatronics and Artificial Intelligence in Engineering*, *5*(2), 158–172. https://doi.org/10.21595/jmai.2024.24285

Ilic, J. (2001). Relationship among the dynamic and static elastic properties of air-dry Eucalyptus delegatensis R. Baker. *Holz Als Roh- Und Werkstoff 59*, 169–175.

Íñiguez, G., Arriaga, F., Bobadilla, I., & Esteban, M. (2008). Grading by non-destructive techniques and assessment of the mechanical properties of large cross section coniferous sawn timber for structural use. *10th World Conference on Timber Engineering 2008*, *2*.

Íñiguez-González, G., Montón, J., Arriaga, F., & Segués, E. (2015). In-situ assessment of structural timber density using non-destructive and semi-destructive testing. *BioResources*, *10*(2). https://doi.org/10.15376/biores.10.2.2256-2265

Intui, S., Soralump, S., & Inazumi, S. (2018). BEHAVIOR OF BEARING CAPACITY ON PILE FOUNDATION DURING FLUCTUATING GROUNDWATER LEVEL. *Geotechnical Engineering Journal of the SEAGS & AGSSEA, 2024*, 1–8. https://doi.org/10.21660/Year.Issue.PaperID

Irbe, I., Bikovens, O., Fridrihsone, V., & Dzenis, M. (2019). Impact of biodeterioration on structure and composition of waterlogged foundation piles from Riga Cathedral (1211 CE), Latvia. *Journal of Archaeological Science: Reports*, *23*. https://doi.org/10.1016/j.jasrep.2018.11.002

Ishiguri, F., Matsui, R., Iizuka, K., Yokota, S., & Yoshizawa, N. (2008). Prediction of the mechanical properties of lumber by stress-wave velocity and Pilodyn penetration of 36-year-old Japanese larch trees. *Holz Als Roh - Und Werkstoff*, *66*(4). https://doi.org/10.1007/s00107-008-0251-7

Işık, N., Halifeoğlu, F. M., & İpek, S. (2020). Nondestructive testing techniques to evaluate the structural damage of historical city walls. *Construction and Building Materials*, *253*. https://doi.org/10.1016/j.conbuildmat.2020.119228

Izekor, D. (2010). Effects of density on variations in the mechanical properties of plantation grown Tectona grandis wood. *Appl. Sci. Res*, *2*(6).

Jacquin, P., Longuetaud, F., Leban, J. M., & Mothe, F. (2017). X-ray microdensitometry of wood: A review of existing principles and devices. *Dendrochronologia*, *42*. https://doi.org/10.1016/j.dendro.2017.01.004

Jais, I. B. M., Lat, D. C., Alasan, A. I., & Abas, F. Z. M. (2024). Effect of Soil Restraint to Long Slender Pile. *Lecture Notes in Civil Engineering*, *386*. https://doi.org/10.1007/978-981-99-6026-2_1

James G. Collin. (2016). Timber Pile Design and Construction Manual. In *Design and Construction Manual*. Timber Piling Council American Wood Preservers Institute.

Jamil, J., Yusup, E. M., & Osman, S. A. (2024). Non-Destructive Testing (NDT) Method for Defect Detection in Glass Fibre-Reinforced Plastic/Polymer (GFRP/GRP) Composite Materials Structures: A Review. *Journal of Advanced Research in Micro and Nano Engineering*, *17*(1), 76–95. https://doi.org/10.37934/armne.17.1.7695

Jawad, A. S., & Albusoda, B. S. (2024). Numerical Evaluation of Pile Group Behavior Subject to Earthquake Loads. *Journal of Engineering*, *30*(05), 70–85. https://doi.org/10.31026/j.eng.2024.05.05

Jiang, J., Bachtiar, E. V., Lu, J., & Niemz, P. (2017). Moisture-dependent orthotropic elasticity and strength properties of Chinese fir wood. *European Journal of Wood and Wood Products*, *75*(6). https://doi.org/10.1007/s00107-017-1166-y

Jingran, G., Jian, L., Jian, Q., & Menglin, G. (2014). Degradation assessment of waterlogged wood at haimenkou site. *Frattura Ed Integrita Strutturale*, *30*. https://doi.org/10.3221/IGF-ESIS.30.60

Jodhani, J., Handa, A., Gautam, A., Ashwni, & Rana, R. (2023). Ultrasonic non-destructive evaluation of composites: A review. *Materials Today: Proceedings*, *78*. https://doi.org/10.1016/j.matpr.2022.12.055

Jol, H. M. (2008). Ground Penetrating Radar Theory and Applications. In *Ground Penetrating Radar Theory and Applications*. https://doi.org/10.1016/b978-0-444-53348-7.x0001-4

Jolly, M., Prabhakar, A., Sturzu, B., Hollstein, K., Singh, R., Thomas, S., Foote, P., & Shaw, A. (2015). Review of Non-destructive Testing (NDT) Techniques and their Applicability to Thick Walled Composites. *Procedia CIRP*, *38*. https://doi.org/10.1016/j.procir.2015.07.043

Jones, J. M., Heath, K. D., Ferrer, A., Brown, S. P., Canam, T., & Dalling, J. W. (2018). Wood decomposition in aquatic and terrestrial ecosystems in the tropics: Contrasting biotic and abiotic processes. *FEMS Microbiology Ecology*, *95*(1). https://doi.org/10.1093/femsec/fiy223

Kabir, M. F., & Araman, P. a. (2003). Nondestructive Evaluation of Defects in Wood Pallet Parts by Ultrasonic Scanning. *Proceedings of the 13th International Symposium on Nondestructive Testing of Wood*.

Kang, H., & Booker, R. E. (2002). Variation of stress wave velocity with MC and temperature. *Wood Science and Technology*, *36*(1). https://doi.org/10.1007/s00226-001-0129-x

Karampour, H., Bourges, M., Gilbert, B. P., Bismire, A., Bailleres, H., & Guan, H. (2020). Compressive behaviour of novel timber-filled steel tubular (TFST) columns. *Construction and Building Materials*, *238*. https://doi.org/10.1016/j.conbuildmat.2019.117734

Kareem, A. H. (2024). Buckling analysis of isotropic Euler-Bernoulli beam resting on Winkler elastic foundation. *International Journal of Structural Design and Engineering*, *5*(1), 1–6. http://www.civilengineeringjournals.com/ijsde

Kasal, B., & Anthony, R. W. (2004). Advances in in situ evaluation of timber structures . *Progress in Structural Engineering and Materials*, *6*(2). https://doi.org/10.1002/pse.170

Kazemi, S. M., Dickinson, D. J., & Murphy, R. J. (2001a). Effects of Initial Moisture Content on Wood Decay at Different Levels of Gaseous Oxygen Concentrations. *J. Agric. Sci. Technol*, *3*.

Kazemi, S. M., Dickinson, D. J., & Murphy, R. J. (2001b). Effects of Initial Moisture Content on Wood Decay at Different Levels of Gaseous Oxygen Concentrations. In *J. Agric. Sci. Technol* (Vol. 3).

Kerr, A. D., & Soifer, M. T. (1964). The linearization of the prebuckling state and its effect on the determined instability loads. *Journal of Applied Mechanics, Transactions ASME*, *36*(4). https://doi.org/10.1115/1.3564770

Keunecke, D., Sonderegger, W., Pereteanu, K., Lüthi, T., & Niemz, P. (2007). Determination of Young's and shear moduli of common yew and Norway spruce by means of ultrasonic waves. *Wood Science and Technology*, *41*(4). https://doi.org/10.1007/s00226-006-0107-4

Khazaei, J. (2008). Water Absorption Characteristics of three wood varieties. *Agronomical Research in Moldavia*, *XLI*(2).

Kherais, M., Csébfalvi, A., Len, A., Fülöp, A., & Pál-Schreiner, J. (2024). The effect of moisture content on the mechanical properties of wood structure. *Pollack Periodica*, *19*(1). https://doi.org/10.1556/606.2023.00917

Khon, H., Bashkov, O. V., Zolotareva, S. V., & Solovev, D. B. (2018). Modeling the propagation of elastic ultrasonic waves in isotropic and anisotropic materials when excited by various sources. *Materials Science Forum*, *945 MSF*. https://doi.org/10.4028/www.scientific.net/MSF.945.926

Kim, J., Cho, Y., Lee, J., & Kim, Y. (2022). Defect Detection and Characterization in Concrete Based on FEM and Ultrasonic Techniques. *Materials*, *15*(22). https://doi.org/10.3390/ma15228160

Kim, Y. S., & Singh, A. P. (2000). Micromorphological characteristics of wood biodegradation in wet environments: A review. In *IAWA Journal* (Vol. 21, Issue 2). https://doi.org/10.1163/22941932-90000241

Klaassen, R. K. W. M. (2014). Speed of bacterial decay in waterlogged wood in soil and open water. *International Biodeterioration and Biodegradation*, *86*. https://doi.org/10.1016/j.ibiod.2013.06.030

Klarbring, A. (2002). Stability and Critical Points in Large Displacement Frictionless Contact Problems. In P. Krause (Ed.), *Nonlinear Finite Element Analysis in Structural Mechanics* (pp. 15–34). Springer. https://doi.org/10.1007/978-3-7091-2534-2_2

Kocaefe, D., Poncsak, S., & Boluk, Y. (2008). Effect of thermal treatment on the chemical composition and mechanical properties of birch and aspen. In *BioResources* (Vol. 3, Issue 2). https://doi.org/10.15376/biores.3.2.517-537

Koch, G., Melcher, E., Lenz, M. T., & Bauch, J. (2018). Biological and topochemical studies on the resistance of excavated oak piles (Quercus sp.) from a historical bridge in Bavaria. *Holzforschung*, *72*(2). https://doi.org/10.1515/hf-2017-0105

Korkmaz, O., & Büyüksari, Ü. (2019). Effects of moisture content on mechanical properties of micro-size oak wood. *BioResources*, *14*(4). https://doi.org/10.15376/biores.14.4.7655-7663

Kotzamanis, V., & Kalliontzis, D. (2023). Understanding Flexibility Effects in the Interaction of Light-Frame Wood Structures with Wave Action. *Journal of Structural Engineering*, *149*(12). https://doi.org/10.1061/jsendh.steng-12283

Kránitz, K., Deublein, M., & Niemz, P. (2014). Determination of dynamic elastic moduli and shear moduli of aged wood by means of ultrasonic devices. *Materials and Structures/Materiaux et Constructions*, *47*(6). https://doi.org/10.1617/s11527-013-0103-8

Krause, M., Dackermann, U., & Li, J. (2015). Elastic wave modes for the assessment of structural timber: ultrasonic echo for building elements and guided waves for pole and pile structures. *Journal of Civil Structural Health Monitoring*, *5*(2). https://doi.org/10.1007/s13349-014-0087-2

Krauss, A., & Kúdela, J. (2011a). Ulrasonic wave propagation and Young ' s modulus of elasticity along the grain of Scots pine wood (Pinus sylvestris l.) varying with distance from the pith. *Wood Research*, *56*(4).

Krauss, A., & Kúdela, J. (2011b). Ultrasonic wave propagation and Young's modulus of elasticity along the grain of Scots pine wood (Pinus sylvestris L.) varying with distance from the pith. *WOOD RESEARCH*, *56*(4), 479–488.

Kretschmann, D. E. (2010). Chapter 5 - Mechanical Properties of Wood. *Wood Handbook - Wood as an Engineering Material*.

Kromoser, B., Spitzer, A., Ritt, M., & Grabner, M. (2024). Wooden Bridges: Strategies for Design, Construction and Wood Species–From Tradition to Future. *International Journal of Architectural Heritage*, *18*(4). https://doi.org/10.1080/15583058.2023.2181719

Kroworz, A., & Katunin, A. (2018). Non-destructive testing of structures using optical and other methods: A review. *SDHM Structural Durability and Health Monitoring*, *12*(1). https://doi.org/10.3970/sdhm.2018.012.001

Kubojima, Y., Okano, T., & Ohta, M. (2000). Bending strength and toughness of heat-treated wood. *Journal of Wood Science*, *46*(1). https://doi.org/10.1007/BF00779547

Kubovský, I., Kačíková, D., & Kačík, F. (2020). Structural changes of oak wood main components caused by thermal modification. *Polymers*, *12*(2). https://doi.org/10.3390/polym12020485

Kulasinski, K., Derome, D., & Carmeliet, J. (2017). Impact of hydration on the micromechanical properties of the polymer composite structure of wood investigated with atomistic simulations. *Journal of the Mechanics and Physics of Solids*, *103*. https://doi.org/10.1016/j.jmps.2017.03.016

Kumar, A. E., Professor, A., Diwakar, V., & Nagaraju, M. (2015). Buckling Analysis of Composite Cylinders Subjected to Axial Compressive Loads. *International Journal of Engineering Research & Technology (IJERT)*, *04*(04), 558–561. www.ijert.org

Kumpenza, C., Matz, P., Halbauer, P., Grabner, M., Steiner, G., Feist, F., & Müller, U. (2018). Measuring Poisson's ratio: mechanical characterization of spruce wood by means of non-contact optical gauging techniques. *Wood Science and Technology*, *52*(6). https://doi.org/10.1007/s00226-018-1045-7

Küttenbaum, S., Taffe, A., Braml, T., & Maack, S. (2018). Reliability assessment of existing bridge constructions based on results of non-destructive testing. *MATEC Web of Conferences*, *199*. https://doi.org/10.1051/matecconf/201819906001

Lachowicz, J., & Rucka, M. (2016). Experimental and numerical investigations for GPR evaluation of reinforced concrete footbridge. *Proceedings of 2016 16th International Conference of Ground Penetrating Radar, GPR 2016*. https://doi.org/10.1109/ICGPR.2016.7572675

Lee, Y., Ahn, J., Kim, C., Kim, S., & Hong, S. (2015). A Study on the Estimation of Compressive Strength of Structural Timber using Ultrasonic Pulse Velocity Method. In *IOSR Journal of Engineering (IOSRJEN) www.iosrjen.org ISSN* (Vol. 05). www.iosrjen.org

Lee, Y., Mahoor, M., & Hall, W. (2020). A 2D numerical model of ultrasonic wave propagation in wooden utility poles using embedded waveguide excitation technique. *Wood and Fiber Science*, *52*(1). https://doi.org/10.22382/wfs-2020-008

Leiderman, R., & Castello, D. (2014). Scattering of ultrasonic waves by heterogeneous interfaces: Formulating the direct scattering problem as a least-squares problem. *The Journal of the Acoustical Society of America*, *135*(1). https://doi.org/10.1121/1.4845615

Li, J., Zhang, Y., Yuan, G., & Bian, T. (2024). Numerical study on the lateral behavior of pile groups in Toyoura sand using the hypoplastic constitutive model. *Scientific Reports*, *14*(1). https://doi.org/10.1038/s41598-024-74494-2

Li, M., Huang, C., Fang, S., Zhao, Y., Xu, N., Qin, G., & Mao, F. (2023). Study on the effect of different angles on the propagation characteristics of acoustic emission signals in wood. *Science Progress*, *106*(2). https://doi.org/10.1177/00368504231168532

Li, M. yue, Ren, H. qing, Wang, Y. rong, Gong, Y. chun, & Zhou, Y. dong. (2021). Comparative studies on the mechanical properties and microstructures of outerwood and corewood in Pinus radiata D. Don. *Journal of Wood Science*, *67*(1). https://doi.org/10.1186/s10086-021-01992-6

Lian, Y., Du, F., Xie, L., Hu, Q., Jin, P., Wang, Y., & Lu, Z. (2024). Application of laser ultrasonic testing technology in the characterization of material Properties: A review. *Measurement*, *234*, 114855. https://doi.org/10.1016/J.MEASUREMENT.2024.114855

Lin, W. S., & Wu, J. Z. (2013). Non-destructive testing of wood defects based on ultrasonic technology. *Applied Mechanics and Materials*, *401–403*. https://doi.org/10.4028/www.scientific.net/AMM.401-403.1124

Lin, W., & Wu, J. (2013). Non-destructive testing of wood defects for Korean pine in northeast China based on ultrasonic technology. *2013 IEEE International Conference on Signal Processing, Communications and Computing, ICSPCC 2013*. https://doi.org/10.1109/ICSPCC.2013.6664057

Linpei, D. Y. T. F. Z. Q. M. H. N. X. H. (2024). Research on Identification and Localization of Internal Defects in Insulation Components Based on Ultrasonic Non-Destructive Testing Technology. *10th International Conference on Condition Monitoring and Diagnosis (CMD)*, 320–323. https://doi.org/10.23919/CMD62064.2024.10766220.

Liu, J., Shao, X., Cheng, B., Cao, G., & Li, K. (2020). Study on Buckling Behavior of Tapered Friction Piles in Soft Soils with Linear Shaft Friction. *Advances in Civil Engineering*, *2020*. https://doi.org/10.1155/2020/8865656

Liu, S.-W., Wan, J.-H., Zhou, C.-Y., Liu, Z., & Yang, X. (2020). Efficient Beam–Column Finite-Element Method for Stability Design of Slender Single Pile in Soft Ground Mediums. *International Journal of Geomechanics*, *20*(1). https://doi.org/10.1061/(asce)gm.1943-5622.0001542

Liu, T., Vinck, K., Ushev, E. R., & Jardine, R. J. (2024). In-situ and laboratory characterisation of stiff and dense geomaterials for driven pile analysis and design. *Soils and Rocks*, *47*(3). https://doi.org/10.28927/SR.2024.009323

Liu, W., Rasmussen, K. J. R., Zhang, H., Xie, Y., Liu, Q., & Dai, L. (2023). Probabilistic study and numerical modelling of initial geometric imperfections for 3D steel frames in advanced structural analysis. *Structures*, *57*. https://doi.org/10.1016/j.istruc.2023.105190

Llana, D. F., Íñiguez-González, G., Díez, M. R., & Arriaga, F. (2020). Nondestructive testing used on timber in Spain: A literature review. *Maderas: Ciencia y Tecnologia*, *22*(2). https://doi.org/10.4067/S0718-221X2020005000201

López, G., Basterra, L. A., & Acuña, L. (2013). Estimation of wood density using infrared thermography. *Construction and Building Materials*, *42*. https://doi.org/10.1016/j.conbuildmat.2013.01.001

López, G., Basterra, L. A., & Acuña, L. (2018). Infrared thermography for wood density estimation. *Infrared Physics and Technology*, *89*. https://doi.org/10.1016/j.infrared.2018.01.015

López-Castro, B., Haro-Baez, A. G., Arcos-Aviles, D., Barreno-Riera, M., & Landázuri-Avilés, B. (2022). A Systematic Review of Structural Health Monitoring Systems to Strengthen Post-Earthquake Assessment Procedures. In *Sensors* (Vol. 22, Issue 23). https://doi.org/10.3390/s22239206

Lucas Filho, F. C. (2012). EFEITO COMBINADO DO TEOR DE UMIDADE E DA MASSA ESPECÍFICA NA RESISTÊNCIA E RIGIDEZ DA MADEIRA DE Pinus elliottii. *FLORESTA*, *42*(3). https://doi.org/10.5380/rf.v42i3.16973

Lynes, J., & Mamaghani, I. H. P. (2021a). Strength Properties of Hardwood Timber Species Exposed to Decay and Marine Borer Attack in Tidal Zones. *International Conference on Civil, Structural and Transportation Engineering*. https://doi.org/10.11159/iccste21.145

Lynes, J., & Mamaghani, I. H. P. (2021b). Strength Properties of Hardwood Timber Species Exposed to Decay and Marine Borer Attack in Tidal Zones. *International Conference on Civil, Structural and Transportation Engineering*. https://doi.org/10.11159/iccste21.145

Ma, S., Ren, S., Chen, Z., Wu, C., & Jiang, S. (2023). Wooden beam damage evaluation under bending loading based on the integration of acoustic emission and principal component analysis. *Measurement: Journal of the International Measurement Confederation*, *222*. https://doi.org/10.1016/j.measurement.2023.113569

MacChioni, N., Palanti, S., & Rozenberg, P. (2007). Measurements of fungal wood decay on Scots pine and beech by means of X-ray microdensitometry. *Wood Science and Technology*, *41*(5). https://doi.org/10.1007/s00226-007-0128-7

Madhoushi, M., & Boskabadi, Z. (2019). Relationship between the dynamic and static modulus of elasticity in standing trees and sawn lumbers of Paulownia fortune planted in Iran. *Maderas: Ciencia y Tecnologia*, *21*(1). https://doi.org/10.4067/S0718-221X2019005000104

Madhoushi, M., & Daneshvar, S. (2016). Predicting the static modulus of elasticity in eastern cottonwood (Populus deltoides) using stress wave non-destructive testing in standing trees. *European Journal of Wood and Wood Products*, *74*(6). https://doi.org/10.1007/s00107-016-1043-0

Mahalil, R. A., Mydin, M. A. O., & Omar, R. (2024). Exploration of Timber Dry and Wet Rot Defects in Buildings: Types, Causes, Effects and Mitigation Methods. *Journal of Advanced Research in Fluid Mechanics and Thermal Sciences*, *119*(1), 196–217. https://doi.org/10.37934/arfmts.119.1.196217

Malan, F. S. (2004). Some notes on the effect of wet-storage on timber. *Southern African Forestry Journal*, *202*(1). https://doi.org/10.1080/20702620.2004.10431793

Mantanis, G. I., Young, R. A., & Rowell, R. M. (1994). Swelling of wood - Part 1. Swelling in water. *Wood Science and Technology*, *28*(2). https://doi.org/10.1007/BF00192691

Manuel, K. (2017). Die Fichte – Baum des Jahres 2017 und Baum des Anstoßes. *FVA-Einblick*, *1*(2017), 21–25.

Mao, H., Lan, S., Mao, H., Ren, J., Yi, X., Huang, Z., & Li, X. (2022). Experimental Study on Properties of Ultrasonic Coupling Agent with Graphene in NDT. *Applied Sciences (Switzerland)*, *12*(3). https://doi.org/10.3390/app12031236

Marais, B. N., Brischke, C., Militz, H., Peters, J. H., & Reinhardt, L. (2020). Studies into fungal decay of wood in ground contact—part 1: The influence of water-holding capacity, moisture content, and temperature of soil substrates on fungal decay of selected timbers. *Forests*, *11*(12). https://doi.org/10.3390/f11121284

Mardanshahi, A., Nasir, V., Kazemirad, S., & Shokrieh, M. M. (2020). Detection and classification of matrix cracking in laminated composites using guided wave propagation and artificial neural networks. *Composite Structures*, *246*. https://doi.org/10.1016/j.compstruct.2020.112403

Martín, J. A., & López, R. (2023). Biological Deterioration and Natural Durability of Wood in Europe. In *Forests* (Vol. 14, Issue 2). https://doi.org/10.3390/f14020283

Mason, E. G., Hayes, M., & Pink, N. (2017). Validation of ultrasonic velocity estimates of wood properties in discs of radiata pine. *New Zealand Journal of Forestry Science*, *47*(1). https://doi.org/10.1186/s40490-017-0098-y

Masoumi, H. R., Degrande, G., & Holeyman, A. (2009). Pile response and free field vibrations due to low strain dynamic loading. *Soil Dynamics and Earthquake Engineering*, *29*(5). https://doi.org/10.1016/j.soildyn.2008.08.008

Mastela, L. da C., Segundinho, P. G. de A., Gonçalves, F. G., Souza, C. G. F. de, Lahr, F. A. R., & Taquetti, V. B. (2023). The use of non-destructive testing methods on glued laminated wood to obtain data. In *A LOOK AT DEVELOPMENT*. https://doi.org/10.56238/alookdevelopv1-011

Meeker, T. R., & Meitzler, A. H. (1961). Determination of Elastic Constants of Isotropic Materials at Megacycle Frequencies. *The Journal of the Acoustical Society of America*, *33*(6_Supplement). https://doi.org/10.1121/1.1936912

Melin, C. B. (2019). *The Influence of Low Temperature on Moisture Transport and Deformation in Wood: A Neglected Area of Research*. https://doi.org/10.1007/978-3-030-11054-3_9

Milke, M., Fang, Y., & John, S. (2010). Anaerobic biodegradability of wood: a preliminary review. *2010 Water New Zealand Annual Conference*.

Mishiro, A. (1995). Ultrasonic velocity in wood and its moisture content .1. Effects of moisture gradients on ultrasonic velocity in wood. *Mokuzai Gakkaishi*, *41*(12).

Missanjo, E., & Matsumura, J. (2016). Wood density and mechanical properties of Pinus kesiya royle ex Gordon in Malawi. *Forests*, *7*(7). https://doi.org/10.3390/f7070135

Miyoshi, Y., Kojiro, K., & Furuta, Y. (2018). Effects of density and anatomical feature on mechanical properties of various wood species in lateral tension. *Journal of Wood Science*, *64*(5). https://doi.org/10.1007/s10086-018-1730-z

Mohammadi, J. (2004). An Overview of Non-Destructive Test Methods in Fatigue and Fracture Reliability Assessment. In *NDT Methods Applied to Fatigue Reliability Assessment of Structures*. https://doi.org/10.1061/9780784407424.ch01

Moita, J. S., Araújo, A. L., Correia, V. F., Mota Soares, C. M., & Herskovits, J. (2020). Buckling behavior of composite and functionally graded material plates. *European Journal of Mechanics, A/Solids*, *80*. https://doi.org/10.1016/j.euromechsol.2019.103921

Montero, M. J., de La Mata, J., Esteban, M., & Hermoso, E. (2015a). Influence of moisture content on the wave velocity to estimate the mechanical properties of large cross-section pieces for structural use of scots pine from Spain. *Maderas: Ciencia y Tecnologia*, *17*(2), 407–420. https://doi.org/10.4067/S0718-221X2015005000038

Montero, M. J., de La Mata, J., Esteban, M., & Hermoso, E. (2015b). Influence of moisture content on the wave velocity to estimate the mechanical properties of large cross-section pieces for structural use of scots pine from Spain. *Maderas: Ciencia y Tecnologia*, *17*(2). https://doi.org/10.4067/S0718-221X2015005000038

Morris, P. (1998). Understanding biodeterioration of wood in structures. *... ./Canadian Wood Council, Http://Www. Durable-Wood. ...*.

Murat, A., & Yasin, F. G. (2024). Structural Investigation of Wood-Inspired Cell Wall Geometries Using Additive Manufacturing: Compression Testing and Finite Element Analysis Validation. *BioResources*, *19*(4), 7493–7512. DOI: 10.15376/biores.19.4.7493-7512

Nadeem, M., Chakraborty, T., & Matsagar, V. (2015). Nonlinear Buckling Analysis of Slender Piles with Geometric Imperfections. *Journal of Geotechnical and Geoenvironmental Engineering*, *141*(1). https://doi.org/10.1061/(asce)gt.1943-5606.0001189

Nallar, M., Bernier, A. P., & Potter, J. T. (2023). *Evaluation of Non-Destructive Testing (NDT) Methods for Wood Power Poles*. https://erdclibrary.on.worldcat.org/discovery.

N'Guessan, J. L. L., Niamké, B. F., Yao, N. J. C., & Amusant, N. (2023). Wood Extractives: Main Families, Functional Properties, Fields of Application and Interest of Wood Waste. *Forest Products Journal*, *73*(3). https://doi.org/10.13073/FPJ-D-23-00015

Niemz, P., & Mannes, D. (2012). Non-destructive testing of wood and wood-based materials. *Journal of Cultural Heritage*, *13*(3 SUPPL.). https://doi.org/10.1016/j.culher.2012.04.001

Niemz, P., & Sonderegger, W. (2003). Untersuchungen zur Korrelation ausgewählter Holzeigenschaften untereinander und mit der Rohdichte unter Verwendung von 103 Holzarten | Analysis of the correlation between selected wood properties among each other and the density of 103 wood species. *Schweizerische Zeitschrift Fur Forstwesen*, *154*(12). https://doi.org/10.3188/szf.2003.0489

Nofal, M., & Kumaran, M. K. (1999). Durability assessments of wood-frame construction using the concept of damage-functions. *Durability of Building Materials and Components 8, Vols 1-4, Proceedings*.

Oberle, B., Ogle, K., Zanne, A. E., & Woodall, C. W. (2018). When a tree falls: Controls on wood decay predict standing dead tree fall and new risks in changing forests. *PLoS ONE*, *13*(5). https://doi.org/10.1371/journal.pone.0196712

Oliveira, de F. G. R., Candian, M., Lucchette, F. F., Luis Salgon, J., & Sales, A. (2005). A technical note on the relationship between ultrasonic velocity and moisture content of Brazilian hardwood (Goupia glabra). *Building and Environment*, *40*(2). https://doi.org/10.1016/j.buildenv.2004.06.002

Ortiz Mansilla, R., Baradit, E., & Navarrete, J. (2009). Analysing variance for determining humidity content and measuring directional effect on ultrasound speed in Pinus radiata D. Don wood samples. In *DICIEMBRE DE* (Vol. 29, Issue 3).

Ottosen, L. M., Kunther, W., Ingeman-Nielsen, T., & Karatosun, S. (2024). Non-Destructive Testing for Documenting Properties of Structural Concrete for Reuse in New Buildings: A Review. *Materials*, *17*(15), 1–21. https://doi.org/10.3390/ma17153814

Ozyhar, T., Hering, S., & Niemz, P. (2012). Moisture-dependent elastic and strength anisotropy of European beech wood in tension. *Journal of Materials Science*, *47*(16). https://doi.org/10.1007/s10853-012-6534-8

Ozyhar, T., Hering, S., Sanabria, S. J., & Niemz, P. (2013). Determining moisture-dependent elastic characteristics of beech wood by means of ultrasonic waves. *Wood Science and Technology*, *47*(2). https://doi.org/10.1007/s00226-012-0499-2

Paajanen, A., Zitting, A., Rautkari, L., Ketoja, J. A., & Penttilä, P. A. (2022). Nanoscale Mechanism of Moisture-Induced Swelling in Wood Microfibril Bundles. *Nano Letters*, *22*(13). https://doi.org/10.1021/acs.nanolett.2c00822

Pahnabi, N., Schumacher, T., & Sinha, A. (2024). Imaging of Structural Timber Based on In Situ Radar and Ultrasonic Wave Measurements: A Review of the State-of-the-Art. In *Sensors*

(Vol. 24, Issue 9). Multidisciplinary Digital Publishing Institute (MDPI). https://doi.org/10.3390/s24092901

Palma, S. S. A., Gonçalves, R., Trinca, A. J., Costa, C. P., Reis, M. N., & Martins, G. A. (2018). Interference from knots, wave propagation direction, and effect of juvenile and reaction wood on velocities in ultrasound tomography. *BioResources*, *13*(2). https://doi.org/10.15376/biores.13.2.2834-2845

Pandharpatte Priyanka, A., Adake Ashutosh, D., Sapkal Neha, R., & Maske, M. M. (2022). Review of Applications of Ground Penetrating Radar as an NDT Tool. *ASEAN Journal of Science and Engineering*, *2*(2). https://doi.org/10.17509/ajse.v2i2.37975

Park, J.-W., Choo, J.-H., Park, G.-R., Hwang, I.-B., & Shin, Y.-S. (2015). The Evaluation of Non-Destructive Formulas on Compressive Strength Using the Reliability Based on Probability. *Journal of the Korea Institute for Structural Maintenance and Inspection*, *19*(4). https://doi.org/10.11112/jksmi.2015.19.4.025

Patel, R., Patel, D., & Meshram, D. (2022). A Review on Non-Destructive Testing (NDT) Techniques: Advances, Researches and Applicability. *International Journal of Current Science Research and Review*, *05*(04). https://doi.org/10.47191/ijcsrr/V5-i4-59

Pattillo, P. D. (2018). External Pressure Resistance. *Elements of Oil and Gas Well Tubular Design*, 215–243. https://doi.org/10.1016/B978-0-12-811769-9.00008-6

Pavlo, B., & Niemz, P. (2003). Effect of temperature on color and strength of spruce wood. *Holzforschung* , *57*, 539–546.

Peruń, G. (2024). Advances in Non-Destructive Testing Methods. In *Materials* (Vol. 17, Issue 3). https://doi.org/10.3390/ma17030554

Pietsch, K. A., Eichenberg, D., Nadrowski, K., Bauhus, J., Buscot, F., Purahong, W., Wipfler, B., Wubet, T., Yu, M., & Wirth, C. (2019). Wood decomposition is more strongly controlled by temperature than by tree species and decomposer diversity in highly species rich subtropical forests. *Oikos*, *128*(5). https://doi.org/10.1111/oik.04879

Pitarma, R., Crisóstomo, J., & Pereira, L. (2019). Detection of wood damages using infrared thermography. *Procedia Computer Science*, *155*. https://doi.org/10.1016/j.procs.2019.08.067

P.Morlier. (1994). *Creep in Timber Structures*.

Pourali, N., Khosravi, H., & Dehestani, M. (2019). An investigation of P-delta effect in conventional seismic design and direct displacement-based design using elasto-plastic SDOF systems. *Bulletin of Earthquake Engineering*, *17*(1). https://doi.org/10.1007/s10518-018-0460-3

Pouya, A. T. (2019). P-Delta Effects on Tall Concrete Buildings. *Kardan Journal of Engineering and Technology*. https://doi.org/10.31841/kjet.2021.6

Praveen, H. M., & Suresh, R. D. (2021). Influence of p-y curves on buckling capacity of pile foundation. *International Journal of Geotechnical and Geological Engineering*, *15*(8), 238–242. https://www.researchgate.net/publication/356253684

Puaad, M. B. F. M., Ahmad, Z., & Muhamad Azlan, H. (2014). Ultrasonic Wave Non-Destructive Method for Predicting the Modulus of Elasticity of Timber. In *InCIEC 2013*. https://doi.org/10.1007/978-981-4585-02-6_8

Qu, Z., Jiang, P., & Zhang, W. (2020). Development and application of infrared thermography non-destructive testing techniques. In *Sensors (Switzerland)* (Vol. 20, Issue 14). https://doi.org/10.3390/s20143851

Quan, C., Walport, F., & Gardner, L. (2024). Equivalent geometric imperfections for the design of steel and stainless steel beam-columns by GMNIA. *Journal of Constructional Steel Research*, *215*. https://doi.org/10.1016/j.jcsr.2024.108502

Radha, P., Selvakumar, N., Sekar, J. R., & Johnsonselva, J. V. (2021). A Novel Ultrasonic based NDT for smart analysis of material defects using IoT. *Proceedings of the 6th International Conference on Inventive Computation Technologies, ICICT 2021*. https://doi.org/10.1109/ICICT50816.2021.9358723

Rainieri, C., Marra, A., Rainieri, G. M., Gargaro, D., Pepe, M., & Fabbrocino, G. (2015). Integrated non-destructive assessment of relevant structural elements of an Italian heritage site: The Carthusian monastery of Trisulti. *Journal of Physics: Conference Series*, *628*(1). https://doi.org/10.1088/1742-6596/628/1/012018

Rais, A., Pretzsch, H., & van de Kuilen, J. W. G. (2020). European beech log and lumber grading in wet and dry conditions using longitudinal vibration. *Holzforschung*, *74*(10). https://doi.org/10.1515/hf-2019-0227

Rajagopalam, P. R., & Prakash, J. (1975). NON-DESTRUCTIVE TESTING OF PILE FOUNDATIONS. *Indian Concrete Journal*, *49*(12). http://worldcat.org/issn/00194565

Randolph, M. F. (1981). The response of flexible piles to lateral loading. *Geotechnique*, *31*(2). https://doi.org/10.1680/geot.1981.31.2.247

Ravi Prakash, P., & Prashant, A. (2016). *Instability of a Mono Pile in Flexural and Buckling Modes Due to Lateral Spreading*. https://doi.org/10.1061/9780784480106.016

Reci, H., Chinh Maï, T., Mehdi Sbartaï, Z., Pajewski, L., & Kiri, E. (2016). Non-destructive evaluation of moisture content in wood using ground-penetrating radar. *Geoscientific Instrumentation, Methods and Data Systems*, *5*(2), 575–581. https://doi.org/10.5194/gi-5-575-2016

Reinprecht, L., & Pánek, M. (2012). Ultrasonic technique for evaluation of biodefects in wood: Part 1 - Influence of the position, extent and degree of internal artificial rots. *International Wood Products Journal*, *3*(2), 107–115. https://doi.org/10.1179/2042645311Y.0000000019

Roman, K., Grzegorzewska, E., Leszczyński, M., Pycka, S., Barwicki, J., Golisz, E., & Zatoń, P. (2023). Effect of Seawater with Average Salinity on the Moisture Content, Ash Content and Tensile Strength of Some Coniferous Wood. *Materials*, *16*(8). https://doi.org/10.3390/ma16082984

Roman, K., Leszczyński, M., Pycka, S., & Wardal, W. J. (2023). The Effects of Seawater Treatment on Selected Coniferous Wood Types. *Materials*, *16*(17). https://doi.org/10.3390/ma16175831

Ross, R. J., & Pellerin, R. F. (1991). NDE of green material with stress waves: preliminary results using dimension lumber. *Forest Products Journal*, *41*(6).

Ross, R. J., & Pellerin, R. F. (1994). Nondestructive testing for assessing wood members in structures: A review. *The Forest Products Laboratory, University of Wiusconsin*, 1–40.

Rucka, M., Wojtczak, E., & Zielińska, M. (2020). Interpolation methods in GPR tomographic imaging of linear and volume anomalies for cultural heritage diagnostics. *Measurement: Journal of the International Measurement Confederation*, *154*. https://doi.org/10.1016/j.measurement.2020.107494

Saadat-Nia, M. A., Brancheriau, L., Gallet, P., Enayati, A. A., Pourtahmasi, K., & Honarvar, F. (2011). Ultrasonic wave parameter changes during propagation through poplar and spruce reaction wood. *BioResources*, *6*(2). https://doi.org/10.15376/biores.6.2.1172-1185

Sabaliauskaite, G., Divall, S., Mcnamara, A. M., Stallebrass, S. E., & Taylor, R. N. (2024). An investigation into the effects of pile stiffness on pile working load capacity in clay utilising

novel modelling techniques. *5th European Conference on Physical Modelling in Geotechnics*, 1–6.
Sabina, H. (2019). *Moisture-Induced Strains and Stresses in Wood* [Dissertation for Doctor of Philosophy., Uppsala University]. http://urn.kb.se/resolve?urn=urn:nbn:se:uu:diva-375148
Sahin, H. T. (2010). Experimental determination of the anisotropic swelling and water sorption properties of chestnut wood. *Wood Research*, *55*(1).
Sahin, H. T., & Mantanis, G. I. (2011). Nano-based surface treatment effects on swelling, water sorption and hardness of wood. *Maderas: Ciencia y Tecnologia*, *13*(1). https://doi.org/10.4067/S0718-221X2011000100004
Sakai, H., Minamisawa, A., & Takagi, K. (1990). Effect of moisture content on ultrasonic velocity and attenuation in woods. *Ultrasonics*, *28*(6). https://doi.org/10.1016/0041-624X(90)90060-2
Sanchez, L. F. M. (2024). Visual inspection and non-destructive testing (NDT). In *Internal Swelling Reactions in Concrete*. https://doi.org/10.1201/9781003188155-4
Sandberg, K. (2009). *Norway Spruce Heartwood Properties Related to Outdoor use* [Doctoral thesis]. Luleå University of Technology, Skellefteå.
Sandoz, J. L. (1989). Grading of construction timeber by ultrasound. *Wood Science and Technology*, *23*(1). https://doi.org/10.1007/BF00350611
Sandoz, J. L. (1993). Moisture content and temperature effect on ultrasound timber grading. *Wood Science and Technology*, *27*(5). https://doi.org/10.1007/BF00192223
Santos, R. B., Capanema, E. A., Balakshin, M. Y., Chang, H. M., & Jameel, H. (2012). Lignin structural variation in hardwood species. *Journal of Agricultural and Food Chemistry*, *60*(19). https://doi.org/10.1021/jf301276a
Sargent, R. (2022). Evaluating Dimensional Stability in Modified Wood: An Experimental Comparison of Test Methods. *Forests*, *13*(4). https://doi.org/10.3390/f13040613
Schajer, G. S., & Orhan, F. B. (2006). Measurement of wood grain angle, moisture content and density using microwaves. *Holz Als Roh - Und Werkstoff*, *64*(6). https://doi.org/10.1007/s00107-006-0109-9
Schimleck, L., Dahlen, J., Apiolaza, L. A., Downes, G., Emms, G., Evans, R., Moore, J., Pâques, L., Van den Bulcke, J., & Wang, X. (2019). Non-destructive evaluation techniques and what they tell us about wood property variation. In *Forests* (Vol. 10, Issue 9). https://doi.org/10.3390/f10090728
Schot, F. (1999). Determination of the shear modulus of wood based panels. *1st International Rilem Symposium on Timber Engineering*, *8*.
Schroll, M., Lenhart, K., Bender, T., Hötten, P., Rudolph, A., Sörensen, S., & Keppler, F. (2024). Fungal Methane Production Controlled by Oxygen Levels and Temperature. *Methane*, *3*(2), 257–275. https://doi.org/10.3390/methane3020015
Secco, C. B., Gonçalves, R., Cerri, D. G. P., Vasques, É. C., & Batista, F. A. F. (2012). Behavior of ultrasonic waves in wood with presence of holes. *CERNE*, *18*(3). https://doi.org/10.1590/s0104-77602012000300019
Sedighi Gilani, M., Fife, J. L., Boone, M. N., & Ghazi Wakili, K. (2013). Dynamics of microcrack propagation in hardwood during heat treatment investigated by synchrotron-based X-ray tomographic microscopy. *Wood Science and Technology*, *47*(5), 889–896. https://doi.org/10.1007/s00226-013-0545-8
SEIDU, H., BROUGUI, M., ABDUL RAHIM, N. R., & NÉMETH, R. (2024). EVALUATION OF DYNAMIC AND STATIC MODULI OF ELASTICITY OF HYBRID EUCALYPTUS

WOOD FROM DIFFERENT LOCATIONS IN GHANA. *Wood Research*, 132–142. https://doi.org/10.37763/wr.1336-4561/69.1.132142

Seim, A., Marquer, L., Bisson, U., Hofmann, J., Herzig, F., Kontic, R., Lechterbeck, J., Muigg, B., Neyses-Eiden, M., Rzepecki, A., Rösch, M., Walder, F., Weidemüller, J., & Tegel, W. (2022). Historical Spruce Abundance in Central Europe: A Combined Dendrochronological and Palynological Approach. *Frontiers in Ecology and Evolution*, *10*. https://doi.org/10.3389/fevo.2022.909453

Senalik, C. A., Schueneman, G., & Ross, R. J. (2014). *Ultrasonic-Based Nondestructive Evaluation Methods for Wood: A Primer and Historical Review*. www.fpl.fs.fed.us.

Senalik, C. A., Wacker, J. P., & Wang, X. (2022). Evaluating the Efficacy of Ground-Penetrating Radar as an Inspection Tool for Timber Bridges. *Conference Proceedings 4th ICTB*.

Shaji, T., Somayaji, S., & Mathews, M. S. (2000). Ultrasonic Pulse Velocity Technique for Inspection and Evaluation of Timber. *Journal of Materials in Civil Engineering*, *12*(2). https://doi.org/10.1061/(asce)0899-1561(2000)12:2(180)

Shan, H., Yang, J., Hu, Z., & He, S. (2022). Buckling stability analysis of underpinning piles during basement excavation beneath existing buildings. *Scientific Reports*, *12*(1). https://doi.org/10.1038/s41598-022-11791-8

Sharapov, E., Brischke, C., Militz, H., & Smirnova, E. (2019). Prediction of modulus of elasticity in static bending and density of wood at different moisture contents and feed rates by drilling resistance measurements. *European Journal of Wood and Wood Products*, *77*(5). https://doi.org/10.1007/s00107-019-01439-2

Sharma, S., & Bhandari, M. (2021). Analysis of Load Capacity of Functionally Graded Material Structures. *Lecture Notes in Mechanical Engineering*. https://doi.org/10.1007/978-981-16-0909-1_20

Sharma, S. K., & Shukla, S. R. (2012). Properties evaluation and defects detection in timbers by ultrasonic non-destructive technique. *Journal of the Indian Academy of Wood Science*, *9*(1). https://doi.org/10.1007/s13196-012-0064-5

Shatri, V., Bozo, L., Shatri, B., & Shefkiu, B. (2013). BUCKLING OF FULLY EMBEDDED PILES IN THE GROUND SUBJECT TO AXIAL COMPRESSION FORCE. *2nd International Balkans Conference on Challenges of Civil Engineering,* 1170–1181.

Shen, J., & Wadee, M. A. (2019). Local–global mode interaction in thin-walled inelastic rectangular hollow section struts part 1: Nonlinear finite element analysis. *Thin-Walled Structures*, *145*. https://doi.org/10.1016/j.tws.2019.106183

Sherif, A. (1989). INSPECTION OF BRIDGE TIMBER PILING OPERATIONS AND ANALYSIS MANUAL. *The National Technical Information,Springfield, Virginia 22161*.

Sherif, A. (1991). Nondestructive Testing of Timber Piles for Structures. *TRANSPORTATION RESEARCH RECORD (1331),Civil Engineering Department, University of Maryland, College Park, Md.*, 36–44.

Siddig Ibrahim, M., & Rahman Elzubair Mohamed, A. (2016). A Simplified P-Delta Second Order Numerical Analysis of High Rise Buildings: Formulation and Validation. In *SUST Journal of Engineering and Computer Sciences (JECS)* (Vol. 17, Issue 3).

Sik, H. S., Choo, K. Ten, Zakaria, S., Ahmad, S., How, S. S., Chia, C. H., & Yusoff, M. (2010). Dimensional stability of high temperature-dried rubberwood solid lumber at two equilibrium moisture content conditions. *Drying Technology*, *28*(9). https://doi.org/10.1080/07373937.2010.506162

Simpson, W. T., & Wang, X. (2001). Relationship between longitudinal stress wave transit time and moisture content of lumber during kiln-drying. *Forest Products Journal*, *51*(10).

Simpson, W., & TenWolde, a. (1999). Physical properties and moisture relations of wood. *Wood Handbook: Wood as an Engineering Material*.

Sirohi, R. S. (2001). Optical methods in non-destructive testing. *Insight: Non-Destructive Testing and Condition Monitoring*, *43*(4).

Sklarczyk, C., Porsch, F., Wolter, B., Boller, C., & Kurz, J. H. (2013). Nondestructive characterization of and defect detection in timber and wood. *Advanced Materials Research*, *778*. https://doi.org/10.4028/www.scientific.net/AMR.778.295

Smulski, S. J. (1991). RELATIONSHIP OF STRESS WAVE-AND STATIC BENDING-DETERMINED PROPERTIES OF FOUR NORTHEASTERN HARDWOODS. *Wood and Fiber Science*, *23*(1), 44–57.

Soares, L. S. Z. R., Fraga, I. F., E Paula, L. de S., Arroyo, F. N., Ruthes, H. C., Aquino, V. B. de M., Molina, J. C., Panzera, T. H., Branco, L. A. M. N., Chahud, E., Christoforo, A. L., & Lahr, F. A. R. (2021). Influence of Moisture Content on Physical and Mechanical Properties of Cedrelinga catenaeformis Wood. *BioResources*, *16*(4). https://doi.org/10.15376/biores.16.4.6758-6765

Soffietti, F. P., Turello, D. F., & Pinto, F. (2024). Analytical solution for the kinematic response of end-bearing piles subjected to SH waves in a homogeneous layer by an improved beam-foundation model. *Soil Dynamics and Earthquake Engineering*, *186*, 108924. https://doi.org/10.1016/J.SOILDYN.2024.108924

Sotomayor-Castellanos, J. R., & Villaseñor-Aguilar, J. M. (2014). Mechanical characteristics of historical beams of Picea abies wood: Assessment by ultrasound. *Materials Research Society Symposium Proceedings*, *1618*. https://doi.org/10.1557/opl.2014.475

Stalin, V. K., Priyadharshini, A., Deepan, P., & Abudaheer, A. (2021). Study on Piles Subjected to Axial and Lateral Loading. *Lecture Notes in Civil Engineering*, *133 LNCE*. https://doi.org/10.1007/978-981-33-6346-5_46

Stanciu, M. D., Teodorescu, H. D., & Vlase, S. (2020). Degradation of mechanical properties of pine wood under symmetric axial cyclic loading parallel to grain. *Polymers*, *12*(10). https://doi.org/10.3390/POLYM12102176

Sugimoto, H., Kawabuchi, S., Sugimori, M., & Gril, J. (2018). Reflection and transmission of visible light by sugi wood: effects of cellular structure and densification. *Journal of Wood Science*, *64*(6). https://doi.org/10.1007/s10086-018-1751-7

Szymczak, C., & Kujawa, M. (2017). Buckling of thin-walled columns accounting for initial geometrical imperfections. *International Journal of Non-Linear Mechanics*, *95*. https://doi.org/10.1016/j.ijnonlinmec.2017.06.003

Tabarestani, N. P., & Naghipour, M. (2022). Numerical and analytical investigation of square timber columns confined with steel and carbon fiber reinforced polymer external jacket. *Journal of Composite Materials*, *56*(27). https://doi.org/10.1177/00219983221127754

Tallavo, F. J., Pandey, M. D., Cascante, G., & Lara, C. A. (2022). Ultrasonic and acoustic pulse velocity methods for nondestructive detection of early decay in wood poles. *Canadian Journal of Civil Engineering*, *49*(6). https://doi.org/10.1139/cjce-2020-0658

Taylor, A. M., Gartner, B. L., & Morrell, J. J. (2002). Heartwood formation and natural durability - A review. *Wood and Fiber Science*, *34*(4).

Teder, M., Pilt, K., Miljan, M., Pallav, V., & Miljan, J. (2012). Investigation of the physical-mechanical properties of timber using ultrasound examination. *Journal of Civil Engineering and Management*, *18*(6), 795–801. https://doi.org/10.3846/13923730.2012.736233

Teixeira, D. E. (2016). Evaluation of Maximum Strength and Modulus of Elasticity of Douglas-Fir Lumber in Axial to Grain Tension by Two Nondestructive Techniques. *Revista Ciência Da Madeira - RCM*, *7*(1). https://doi.org/10.12953/2177-6830/rcm.v7n1p1-6

Tenoudji, F. C., Citerne, J. M., Dutilleul, H., & Busquet, D. (2016). Non-contact ultrasonic defect imaging in composites. *AIP Conference Proceedings*, *1706*. https://doi.org/10.1063/1.4940535

Thomas Lee Wilkinson. (1968). STRENGTH EVALUATION OF ROUND TIMBER PILES. *FOREST SERVICE RESEARCH PAPER, U.S. Department of Agriculture, Forest Service ,Forest Products Laboratory Madison, Wis.*, 1–44.

Thybring, E. E., Fredriksson, M., Zelinka, S. L., & Glass, S. V. (2022). Water in Wood: A Review of Current Understanding and Knowledge Gaps. In *Forests* (Vol. 13, Issue 12). https://doi.org/10.3390/f13122051

Tippner, J., Gryc, V., & Baar, J. (2013). The relation of fibre length and ray dimensions to sound propagation velocity in wood of selected tropical hardwoods. *IAWA Journal*, *34*(1). https://doi.org/10.1163/22941932-00000005

Topaloglu, E., & Erisir, E. (2018). Longitudinal variation in selected wood properties of oriental beech and caucasian fir. *Maderas: Ciencia y Tecnologia*, *20*(3), 403–416. https://doi.org/10.4067/S0718-221X2018005031101

Tran, H. T. K., Manh, T., & Hoff, L. (2016). Measurements of acoustic material properties using ultrasonic through transmission technique. *IMAPS Nordic Annual Conference 2016 Proceedings*. https://doi.org/10.4071/2016-nor-tran

Treu, A., Zimmer, K., Brischke, C., Larnøy, E., Gobakken, L. R., Aloui, F., Cragg, S. M., Flaete, P.-O., Humar, M., Westin, M., Borges, L., & Williams, J. (2019). Durability and Protection of Timber Structures in Marine Environments in Europe: An Overview. *BioResources*, *14*(4), 10161–10184.

Tu, J., Yu, L., Zhao, J., Zhang, J., & Zhao, D. (2022). Damage Modes Recognition of Wood Based on Acoustic Emission Technique and Hilbert–Huang Transform Analysis. *Forests*, *13*(4). https://doi.org/10.3390/f13040631

Tuğba Yılmaz, A., & Murat, A. (2018). Effect of Density and Propagation Length on Ultrasonic Longitudinal Wave Velocity in Some Important Wood Species Grown in Turkey. *Turkish Journal of Forestry | Türkiye Ormancılık Dergisi*. https://doi.org/10.18182/tjf.459005

Tumšys, O., & Mažeika, L. (2023). Determining the Elastic Constants of Isotropic Materials by Measuring the Phase Velocities of the A0 and S0 Modes of Lamb Waves. *Sensors*, *23*(15). https://doi.org/10.3390/s23156678

Ukyo, S., Ido, H., Nagao, H., & Kato, H. (2010). Simultaneous determination of shear strength and shear modulus in glued-laminated timber using a full-scale shear block specimen. *Journal of Wood Science*, *56*(3). https://doi.org/10.1007/s10086-009-1083-8

Umap, V. S., & Rao, Y. R. M. (2023). Application of Non-destructive Testing (NDT) Techniques on Reinforced Concrete Structure: A Review. *International Journal for Research in Applied Science and Engineering Technology*, *11*(1). https://doi.org/10.22214/ijraset.2023.47231

Uncuoğlu, E., & Laman, M. (2012). Numerical modelling of short pile behaviour subjected to lateral load. *European Journal of Environmental and Civil Engineering*, *16*(2). https://doi.org/10.1080/19648189.2012.667697

van de Kuilen, J. W., Beketova-Hummel, O., Pagella, G., Ravenshorst, G., & Gard, W. (2021). An integral approach for the assessment of timber pile foundations. *World Conference on Timber Engineering 2021, WCTE 2021*.

Van De Kuilen, J. W. G. (2007). Service life modelling of timber structures. *Materials and Structures/Materiaux et Constructions*, *40*(1), 151–161. https://doi.org/10.1617/s11527-006-9158-0

Van De Kuilen, J.-W. G. ;, Ravenshorst, G. J. P. ;, & Gard, W. F. (2024). Wooden pile foundations Structural analysis and assessment of remaining load carrying capacity. *2nd Annual Conference on Foundation Decarbonization and Re-Use*, 1–10.

Van Dyk, H., & Rice, R. W. (2005). An assessment of the feasibility of ultrasound as a defect detector in lumber. *Holzforschung*, *59*(4). https://doi.org/10.1515/HF.2005.072

Varnier, M., Sauvat, N., Ulmet, L., Montero, C., Dubois, F., & Gril, J. (2020). Influence of temperature in a mass transfer simulation: application to wood. *Wood Science and Technology*, *54*(4). https://doi.org/10.1007/s00226-020-01197-y

Verbist, M., Branco, J. M., & Nunes, L. (2020). Characterization of the mechanical performance in compression perpendicular to the grain of insect-deteriorated timber. *Buildings*, *10*(1). https://doi.org/10.3390/buildings10010014

Vikberg, T., Oja, J., & Antti, L. (2012). MOISTURE CONTENT MEASUREMENT IN SCOTS PINE BY MICROWAVE AND X-RAYS. *WOOD AND FIBER SCIENCE*, *44*(3), 1–6.

Vogt, N., Vogt, S., & Kellner, C. (2009). Buckling of slender piles in soft soils. *Bautechnik*, *86*(SUPPL. 1). https://doi.org/10.1002/bate.200910046

Vukelic, G., Murawski, L., Recho, N., & Vizentin, G. (2017). Marine structural failures: Causes and analysis tools. *18th Annual General Assembly of the International Association of Maritime Universities - Global Perspectives in MET: Towards Sustainable, Green and Integrated Maritime Transport, IAMU 2017*, *2*.

Wang, C. hsiang, Leicester, R. H., & Nguyen, M. (2008). Probabilistic procedure for design of untreated timber poles in-ground under attack of decay fungi. *Reliability Engineering and System Safety*, *93*(3). https://doi.org/10.1016/j.ress.2006.12.007

Wang, F., & Sigmund, O. (2023). Architecting materials for extremal stiffness, yield, and buckling strength. *Programmable Materials*, *1*. https://doi.org/10.1017/pma.2023.5

Wang, J., & DeGroot, R. (1996). Treatability and durability of heartwood. *National Conference on Wood Transportation …*.

Wang, N., & Wang, L. (2011). Response of ultrasonic wave velocity to wood structure defect of Korean pine. *Advanced Materials Research*, *311–313*. https://doi.org/10.4028/www.scientific.net/AMR.311-313.1609

Wang, S. Y., & Chuang, S. T. (2000). Experimental data correction of the dynamic elastic moduli, velocity and density of solid wood as a function of moisture content above the fiber saturation point. *Holzforschung*, *54*(3). https://doi.org/10.1515/HF.2000.052

Wang, X., Meng, Z., Lv, X., & Wei, G. (2024). Dynamic Testing and Finite Element Model Adjustment of the Ancient Wooden Structure Under Traffic Excitation. *Buildings*, *14*(11). https://doi.org/10.3390/buildings14113527

Wang, Y., Su, M., Sun, H., & Ren, H. (2018). Comparative studies on microstructures and chemical compositions of cell walls of two solid wood floorings. *Journal of Wood Science*, *64*(5). https://doi.org/10.1007/s10086-018-1743-7

Wang, Z., Gao, C., Zheng, L., Ren, J., Wang, W., Zhang, Y., & Han, S. (2021). FEM Simulation and Test Verification of PD Ultrasonic Signal Propagation in a Power Transformer Model.

Journal of Electrical Engineering and Technology, *16*(1). https://doi.org/10.1007/s42835-020-00545-z

Wei, J., Rao, F., Huang, Y., Zhang, Y., Qi, Y., Yu, W., & Hse, C. Y. (2019). Structure, mechanical performance, and dimensional stability of radiata pine (Pinus radiata D. Don) scrimbers. *Advances in Polymer Technology*, *2019*. https://doi.org/10.1155/2019/5209624

Xue, Y., Gao, J., Liu, J., Shen, X., Zhang, B., & Feng, Q. (2024). Nondestructive testing of internal defects by ring-laser-excited ultrasonic. *Nondestructive Testing and Evaluation*, *39*(8). https://doi.org/10.1080/10589759.2023.2297081

Yaitskova, N., & van de Kuilen, J. W. (2014). Time-of-flight modeling of transversal ultrasonic scan of wood. *The Journal of the Acoustical Society of America*, *135*(6). https://doi.org/10.1121/1.4873519

Yang, H., Yu, L., & Wang, L. (2015). Effect of moisture content on the ultrasonic acoustic properties of wood. *Journal of Forestry Research*, *26*(3). https://doi.org/10.1007/s11676-015-0079-z

Yang, J. L., & Evans, R. (2003). Prediction of MOE of eucalypt wood from microfibril angle and density. *Holz Als Roh - Und Werkstoff*, *61*(6). https://doi.org/10.1007/s00107-003-0424-3

Yang, N. C. (1966). Buckling Strength of Pile. *Paper Sponsored by Committee on Substructures, Retaining Walls and Foundations and Presented at the 45th Annual Meeting.*, 35–51.

Yang, Q., Gao, C., Liu, K., Zhu, Y., & Wang, J. (2022). Compressive Strength of Aged Timber Members in Traditional Building: Considering Differences in Heartwood and Sapwood. *Applied Sciences (Switzerland)*, *12*(15). https://doi.org/10.3390/app12157719

Yang, Z., Ren, H. Q., & Jiang, Z. H. (2010). Effects of biological decay on mechanical properties of slash pine wood. *Beijing Linye Daxue Xuebao/Journal of Beijing Forestry University*, *32*(3).

Yassine, R., Mustapha, S., Fakih, M. A., & Malinowski, P. H. (2024). Non-Contact Laser Doppler Vibrometer for Characterization of Guided Waves in Timber Structures with Varying Moisture Content and Grain Orientations. *11th European Workshop on Structural Health Monitoring, EWSHM 2024*. https://doi.org/10.58286/29680

Yazdani, N., Beneberu, E., Baniya, A., & Efaz, I. H. (2020). Performance of Light-Frame Wooden Structures (LFWSs) Subjected to Combined Wind and Flood Hazards. *Journal of Coastal Research*, *36*(4). https://doi.org/10.2112/JCOASTRES-D-19-00098.1

Yu, Y., Dackermann, U., Li, J., & Yan, N. (2014, December 9). GUIDED-WAVE-BASED DAMAGE DETECTION OF TIMBER POLES USING A HIERARCHICAL DATA FUSION ALGORITHM. *23rd Australasian Conference on the Mechanics of Structures and Materials (ACMSM23)*.

Yu, Y., & Yan, N. (2017). Numerical study on guided wave propagation in wood utility poles: Finite element modelling and parametric sensitivity analysis. *Applied Sciences (Switzerland)*, *7*(10). https://doi.org/10.3390/app7101063

Yue, K., Song, X., Cheng, Lai, Y., Jia, C., Lu, W., & Liu, W. (2019). Study on moisture stresses in Chinese fir glued laminated timber. *Journal of Forestry Engineering*, *4*, 35–40.

Zanne, A. E., Flores-Moreno, H., Powell, J. R., Cornwell, W. K., Dalling, J. W., Austin, A. T., Classen, A. T., Eggleton, P., Okada, K. I., Parr, C. L., Carol Adair, E., Adu-Bredu, S., Alam, M. A., Alvarez-Garzón, C., Apgaua, D., Aragón, R., Ardon, M., Arndt, S. K., Ashton, L. A., … Zalamea, P. C. (2022). Termite sensitivity to temperature affects global wood decay rates. *Science*, *377*(6613). https://doi.org/10.1126/science.abo3856

Zechel, F., Kunze, R., König, N., & Schmitt, R. H. (2020). Optical coherence tomography for non-destructive testing. *Tm - Technisches Messen*, *87*(6). https://doi.org/10.1515/teme-2019-0098

Zelinka, S. L., Glass, S. V., Jakes, J. E., & Stone, D. S. (2016). A solution thermodynamics definition of the fiber saturation point and the derivation of a wood–water phase (state) diagram. *Wood Science and Technology*, *50*(3). https://doi.org/10.1007/s00226-015-0788-7

Zhan, T., Kuai, B., Lyu, C., Wang, X., Xu, K., & Zhang, Y. (2019). Moisture dependence of the tensile strength perpendicular to grain of poplar and Chinese fir. *Journal of Forestry Engineering*, *4*(5). https://doi.org/10.13360/j.issn.2096-1359.2019.05.005

Zhang, J., Wang, Y. C., Yang, X. J., Ma, S. W., Xu, Q. F., & Li, X. M. (2011). Research on test and theory analysis of long service-beyond timber pillar reinforced with GFRP. *2011 International Conference on Electric Technology and Civil Engineering, ICETCE 2011 - Proceedings*. https://doi.org/10.1109/ICETCE.2011.5774361

Zhang, R., Li, C., & Jin, D. (2021a). Buckling Stability Analysis for Piles in the Slope Foundation Based on Cusp Catastrophe Theory. *Mathematical Problems in Engineering*, *2021*. https://doi.org/10.1155/2021/5560790

Zhang, R., Li, C., & Jin, D. (2021b). Buckling Stability Analysis for Piles in the Slope Foundation Based on Cusp Catastrophe Theory. *Mathematical Problems in Engineering*, *2021*. https://doi.org/10.1155/2021/5560790

Zhang, X., Wang, S., Liu, H., Cui, J., Liu, C., & Meng, X. (2024). Assessing the impact of inertial load on the buckling behavior of piles with large slenderness ratios in liquefiable deposits. *Soil Dynamics and Earthquake Engineering*, *176*. https://doi.org/10.1016/j.soildyn.2023.108322

Zielińska, M., & Rucka, M. (2021). Non-destructive Testing of Wooden Elements. *IOP Conference Series: Materials Science and Engineering*, *1203*(3), 032058. https://doi.org/10.1088/1757-899x/1203/3/032058

Zoidis, N., Tatsis, E., Vlachopoulos, C., Clausen, J. S., Matikas, T. E., Aggelis, D. G., & Gkotzamanis, A. (2012). Visual inspection and evaluation using NDT testing methods of extensively cracked concrete floor. *Emerging Technologies in Non-Destructive Testing V - Proceedings of the 5th Conference on Emerging Technologies in NDT*. https://doi.org/10.1201/b11837-92

Zoormand, H., Lnu, S., Dorn, M., & Johannesson, B. (2024). *Mechanical Effects of Moisture Content Variations in CLT-Structures*. Linnaeus University, Faculty of Technology Department of Building Technology.

List of publications

Brougui, M., Andor, K., & Szabó, P. (2023). Wood concrete for high thermal efficiency compared to concrete. *In XXVI. Tavaszi Szél Konferencia*, 5-7 May 2023, University of Miskolc, Hungary. **https://m2.mtmt.hu/api/publication/36166415**

Brougui, M., & Andor, K. (2024). Investigating the stability of wooden lake piles: The influence of dynamic MOE and pile length on buckling behavior. In *Wood 4 Sustainability: Processing, Construction, Products and Design* (pp. 161–174). Sopron University Press. ISBN 978-963-334-541-2. **https://doi.org/10.35511/978-963-334-541-2-16**

Seidu, H., Brougui, M., Abdul Rahim, N. R., & Németh, R. (2024). Evaluation of dynamic and static moduli of elasticity of hybrid eucalyptus wood from different locations in Ghana. *Wood Research*, 69(1), 132–142. **https://doi.org/10.37763/wr.1336-4561/69.1.132142**

Brougui, M., Andor, K., & Szabó, P. (2025). Assessment of Defect Severity in Wooden Pillars Using Ultrasonic Testing. *Periodica Polytechnica Civil Engineering*, published by the Faculty of Civil Engineering, Budapest University of Technology and Economics, Hungary. Available at: **https://pp.bme.hu/ci/article/view/40197**

Brougui, M., Andor, K., & Szabó, P. (2025). Evaluation of Timber Mechanical Properties Through Non-Destructive Testing: A Bibliometric Analysis. *Buildings*, 15(13), 2192. **https://doi.org/10.3390/buildings15132192**

Brougui, M., Andor, K., & Szabó, P. (2025). Integrated Risk Classification and Buckling Resistance Prediction in Timber Piles Using Ultrasonic Wave Velocity and Dynamic Modulus of Elasticity, *JOURNAL OF NONDESTRUCTIVE EVALUATION,*11 p. **https://doi.org/10.21203/rs.3.rs-6813815/v1**

Brougui, M., Andor, K., & Szabó, P**.** (2025). Sensitivity of Buckling Resistance to Pile Length and Structural Imperfections in Submerged Timber Piles. *International Wood Products Journal*, 24 p. **https://m2.mtmt.hu/api/publication/ 36450180**

Brougui, M., Andor, K., & Szabó, P. (2025). Finite Element Modeling of Submerged Timber Piles: Validation of Ultrasonic Non-Destructive Testing for Buckling Resistance. *Structural Health Monitoring Journal*, 19 p. **https://m2.mtmt.hu/api/publication/ 36450184**

Brougui, M., Andor, K., & Szabó, P. (2025). Wood-concrete for high thermal efficiency compared to the concrete II. *In TAUCC25: 1st national seminar* - abstract book (pp. 5-5). University Larbi Ben M'hidi Oum El Bouaghi, Oum El Bouaghi, Algeria. **https://m2.mtmt.hu/api/publication/ 36166597**

Brougui, M., & Szabó, P. (2025). Integrating micro-algae facades in Algerian building: A sustainable approach to energy efficiency. *Periodica Polytechnica Architecture*, 6 p. **https://m2.mtmt.hu/api/publication/36166695**

Appendices

Appendix A: Comprehensive Dataset of Geometric Properties, Material Moduli, and Critical Buckling Loads from Euler and Granholm Analytical Models

Pile ID	length (m)	Slenderness Ratio (λ)	Longitudinal MOE (MPa)	Radial MOE (MPa)	Shear Moduli GLR (MPa)	Shear Moduli GLT (MPa)	Shear Moduli GRT (MPa)	effective shear modulus (MPa)	ϕ Granholm correction factor	Euler P_{cr} (kN)	Granholm P_{cr} (kN)
1	15,63	312,6	8389	838,9	2 902,77	2759,54	391,10	6053,40	0,99986	26,59	26,586
2	16,13	322,6	8345	834,5	2 887,54	2745,07	389,04	6021,65	0,999861	24,88	24,877
3	9,25	185	6420	642	2 221,45	2111,84	299,30	4632,60	0,999746	58,17	58,155
4	8,20	164	7612	761,2	2 633,91	2503,95	354,87	5492,73	0,999484	87,71	87,665
5	10,03	200,6	6548	654,8	2 265,74	2153,95	305,27	4724,96	0,999663	50,42	50,403
6	12,37	247,4	8096	809,6	2 801,38	2663,16	377,44	5841,98	0,999777	41,02	41,011
7	14,57	291,4	9400	940	3 252,60	3092,11	438,23	6782,93	0,999832	34,280	34,275
8	11,48	229,6	6602	660,2	2 284,43	2171,71	307,79	4763,93	0,999677	38,81	38,797
9	9,21	184,2	6799	679,9	2 352,60	2236,51	316,97	4906,08	0,99959	62,1	62,075
10	10,43	208,6	6241	624,1	2 159,52	2052,96	290,96	4503,43	0,999684	44,48	44,447
11	10,01	200,2	6953	695,3	2 405,88	2287,17	324,15	5017,20	0,99966	53,81	53,792
12	9,73	194,6	6069	606,9	2 100,00	1996,38	282,94	4379,32	0,999659	49,68	49,663
13	15,15	303	6804	680,4	2 354,33	2238,16	317,20	4909,69	0,999851	22,98	53,792
14	11,25	225	7081	708,1	2 450,17	2329,28	330,12	5109,57	0,999734	43,33	49,652
15	13,19	263	5919	591,9	2 048,10	1947,04	275,94	4271,08	0,999837	26,33	26,326
16	12,96	259,2	5699	569,9	1 971,97	1874,67	265,69	4112,33	0,999835	26,28	26,276
17	9,76	195,2	8191	819,1	2 834,26	2694,41	381,86	5910,53	0,999629	66,64	66,615
18	8,40	168,00	7338	733,8	2 539,10	2413,82	342,10	5295,01	0,99951	80,48	80,441
19	9,11	182,20	9198	919,8	3 182,70	3025,66	428,81	6637,17	0,99962	86,12	86,087
20	8,88	177,60	6716	671,6	2 323,88	2209,21	313,10	4846,19	0,999557	66,29	66,254
21	6,99	139,80	8675	867,5	3 001,73	2853,62	404,43	6259,78	0,999378	138,35	138,264
22	10,25	205,00	8570	857	2 965,40	2819,08	399,53	6184,01	0,999486	63,6	63,567
23	11,17	223,40	9827	982,7	3 400,35	3232,57	458,14	7091,05	0,999572	61,4	61,374
24	12,72	254,40	9078	907,8	3 141,18	2986,18	423,22	6550,58	0,999742	43,71	43,699
25	7,81	156,20	10751	1075,1	3 720,07	3536,51	501,21	7757,79	0,999444	136,63	136,554
26	10,73	214,60	6641	664,1	2 297,92	2184,54	309,60	4792,07	0,999707	44,61	44,597
27	10,86	217,20	10072	1007,2	3 485,12	3313,16	469,56	7267,84	0,999707	66,19	66,171
28	9,41	188,20	4727	472,7	1 635,64	1554,93	220,37	3410,95	0,998806	41,33	41,281

29	8,05	161,00	8901	890,1	3 079,93	2927,96	414,97	6422,86	0,999482	106,39	106,335
30	12,59	251,80	11186	1118,6	3 870,59	3679,61	521,49	8071,69	0,999571	54,7	54,677
31	14,41	288,20	7817	781,7	2 704,84	2571,38	364,43	5640,65	0,999836	29,16	29,155
32	8,89	177,80	5747	574,7	1 988,58	1890,46	267,93	4146,97	0,998999	56,37	56,314
33	14,25	285,00	8702	870,2	3 011,07	2862,50	405,69	6279,26	0,999735	33,23	33,221
34	5,65	113,00	10155	1015,5	3 513,84	3340,46	473,43	7327,73	0,999332	246,65	246,485
35	20,83	416,60	7346	734,6	2 541,87	2416,45	342,47	5300,79	0,999922	13,12	13,119
36	11,34	226,80	8890	889	3 076,12	2924,34	414,45	6414,92	0,99948	53,46	53,434
37	9,09	181,80	7727	772,7	2 673,70	2541,78	360,23	5575,71	0,999586	72,41	72,380
38	10,24	204,80	9150	915	3 166,09	3009,87	426,57	6602,53	0,999589	67,62	67,592
39	17,00	340,00	6744	674,4	2 333,56	2218,42	314,41	4866,39	0,999814	18,01	18,007
40	7,81	156,20	5943	594,3	2 056,40	1954,93	277,06	4288,40	0,999569	75,33	75,294

Appendix B: Summary statistics of pile properties and critical buckling loads predicted by FEM and ultrasonic methods

		Modulus of Elasticity (MPa)			From ultrasonic test	From COMSOL simulation		
Pile ID	**Length (m)**	**Longitudinal Elastic Modulus (E_L)**	**Radial Elastic Modulus (E_R)**	**Tangential Elastic Modulus (E_T)**	**Ultrasonic Buckling Load (N)**	**FEM Buckling Load (N)**	**Critical Load factor**	**Difference %**
1	15,63	8389	838,9	419,45	26590	25233,91	2,523	5,39
2	16,13	8345	834,5	417,25	24880	23760,4	2,376	4,71
3	9,25	6420	642	321	58170	53981,76	5,398	7,76
4	8,20	7612	761,2	380,6	87710	84201,6	8,420	4,17
5	10,03	6548	654,8	327,4	50420	47596,48	4,760	5,92
6	12,37	8096	809,6	404,8	41020	39584,33	3,958	3,64
7	14,57	9400	940	470	34280	32771,68	3,277	4,61
8	11,48	6602	660,2	330,1	38810	36287,35	3,629	6,94
9	9,21	6799	679,9	339,95	62100	58187,7	5,819	6,72
10	10,43	6241	624,1	312,05	44480	42611,84	4,261	4,39
11	10,01	6953	695,3	347,65	53810	52249,51	5,225	2,99
12	9,73	6069	606,9	303,45	49680	47990,88	4,799	3,52
13	15,15	6804	680,4	340,2	22980	21876,96	2,188	5,03
14	11,25	7081	708,1	354,05	43330	41640,13	4,164	4,06
15	13,19	5919	591,9	295,95	26330	24592,22	2,459	7,08
16	12,96	5699	569,9	284,95	26280	24755,76	2,476	6,14
17	9,76	8191	819,1	409,55	66640	61908,56	6,191	7,64

18	8,40	7338	733,8	366,9	80480	78146,08	7,815	2,98
19	9,11	9198	919,8	459,9	86120	79402,64	7,940	8,46
20	8,88	6716	671,6	335,8	66290	62378,89	6,238	6,27
21	6,99	8675	867,5	433,75	138350	133231,05	13,323	3,84
22	10,25	8570	857	428,5	63600	59911,2	5,991	6,16
23	11,17	9827	982,7	491,35	61400	56979,2	5,698	7,76
24	12,72	9078	907,8	453,9	43710	42442,41	4,244	2,99
25	7,81	10751	1075,1	537,55	136630	130618,28	13,062	6,4
26	10,73	6641	664,1	332,05	44610	41844,18	4,184	6,62
27	10,86	10072	1007,2	503,6	66190	63608,59	6,361	4,04
28	9,41	4727	472,7	236,35	41330	39346,16	3,935	5,03
29	8,05	8901	890,1	445,05	106390	100751,33	10,075	5,6
30	12,59	11186	1118,6	559,3	54700	52293,2	5,229	4,61
31	14,41	7817	781,7	390,85	29160	28168,56	2,817	3,51
32	8,89	5747	574,7	287,35	56370	52762,32	5,276	6,84
33	14,25	8702	870,2	435,1	33230	31502,04	3,150	5,49
34	5,65	10155	1015,5	507,75	246650	236290,7	23,629	4,38
35	20,83	7346	734,6	367,3	13120	12621,44	1,262	3,96
36	11,34	8890	889	444,5	53460	50947,38	5,095	4,93
37	9,09	7727	772,7	386,35	72410	69223,96	6,922	4,61
38	10,24	9150	915	457,5	67620	65659,02	6,566	2,99
39	17,00	6744	674,4	337,2	18010	16785,32	1,679	7,27
40	7,81	5943	594,3	297,15	75330	71789,49	7,179	4,93

Appendix C: Stress Distribution Analysis in FEM COMSOL

		Case 01: Initial load of 1000 N				**Case 02: High load (approaching buckling condition) 10000 N**			
		Stress distribution (MPa)				**Stress distribution (MPa)**			
Pile ID	**Length (m)**	**Axial Stress**	**Bending Stress**	**The max Compressive Stress**	**The max Tensile Stress**	**Axial Stress**	**Bending Stress**	**The max Compressive Stress**	**The max Tensile Stress**
1	15,63	0.0318	0.0204	0.0522	0.0114	0.318	7.91	8.23	−7.59
2	16,13	0.0318	0.0217	0.0535	0.0102	0.318	8.51	8.82	−8.19
3	9,25	0.0318	0.0115	0.0433	0.0204	0.318	3.46	3.78	−3.14

4	8,20	0.0318	0.0102	0.0420	0.0216	0.318	2.84	3.16	−2.52
5	10,03	0.0318	0.0127	0.0446	0.0191	0.318	3.88	4.20	−3.56
6	12,37	0.0318	0.0166	0.0484	0.0153	0.318	5.05	5.37	−4.74
7	14,57	0.0318	0.0191	0.0509	0.0127	0.318	6.41	6.73	−6.09
8	11,48	0.0318	0.0153	0.0471	0.0165	0.318	4.84	5.16	−4.52
9	9,21	0.0318	0.115	0.146	0.083	0.318	3.40	3.72	−3.08
10	10,43	0.0318	0.0140	0.0458	0.0178	0.318	4.16	4.48	−3.85
11	10,01	0.0318	0.0127	0.0446	0.0191	0.318	3.78	4.10	−3.46
12	9,73	0.0318	0.0127	0.0446	0.0191	0.318	3.76	4.08	−3.44
13	15,15	0.0318	0.0204	0.0522	0.0115	0.318	8.53	8.85	−8.22
14	11,25	0.0318	0.0153	0.0471	0.0166	0.318	4.52	4.84	−4.20
15	13,19	0.0318	0.0178	0.0497	0.0140	0.318	6.79	7.11	−6.47
16	12,96	0.0318	0.0178	0.0497	0.0140	0.318	6.65	6.97	−6.33
17	9,76	0.0318	0.0127	0.0446	0.0191	0.318	3.55	3.87	−3.23
18	8,40	0.0318	0.0115	0.0433	0.0204	0.318	2.94	3.26	−2.62
19	9,11	0.0318	0.0115	0.0433	0.0204	0.318	3.18	3.50	−2.86
20	8,88	0.0318	0.0115	0.0433	0.0204	0.318	3.23	3.55	−2.92
21	6,99	0.0318	0.0089	0.0407	0.0229	0.318	2.31	2.62	−1.99
22	10,25	0.0318	0.0127	0.0446	0.0191	0.318	3.76	4.08	−3.44
23	11,17	0.0318	0.0140	0.0458	0.0178	0.318	4.14	4.46	−3.82
24	12,72	0.0318	0.0166	0.048	0.0153	0.318	5.08	5.40	−4.76
25	7,81	0.0318	0.010	0.042	0.022	0.318	2.59	2.91	−2.27
26	10,73	0.0318	0.014	0.046	0.018	0.318	4.31	4.62	−3.99
27	10,86	0.0318	0.0140	0.0458	0.0178	0.318	3.93	4.25	−3.62
28	9,41	0.0318	0.0127	0.0446	0.0191	0.318	3.86	4.18	−3.54
29	8,05	0.0318	0.0102	0.0420	0.0216	0.318	2.73	3.04	−2.41
30	12,59	0.0318	0.0166	0.0484	0.0153	0.318	4.75	5.07	−4.43
31	14,41	0.0318	0.0191	0.0509	0.0127	0.318	6.83	7.15	−6.51
32	8,89	0.0318	0.0115	0.0433	0.0204	0.318	3.35	3.67	−3.03
33	14,25	0.0318	0.019	0.051	0.013	0.318	6.38	6.70	−6.06
34	5,65	0.0318	0.008	0.039	0.024	0.318	1.81	2.13	−1.49
35	20,83	0.0318	0.029	0.061	0.003	0.318	30.66	30.97	−30.34
36	11,34	0.0318	0.015	0.047	0.017	0.318	4.32	4.64	−4.00
37	9,09	0.0318	0.011	0.043	0.020	0.318	3.25	3.57	−2.93
38	10,24	0.0318	0.013	0.045	0.019	0.318	3.69	4.01	−3.37

39	17,00	0.0318	0.023	0.055	0.009	0.318	12.85	13.17	−12.53
40	7,81	0.0318	0.010	0.042	0.022	0.318	2.78	3.09	−2.46

Appendix D: Lateral Displacement Behavior in FEM COMSOL

		Case 01: Initial load of 1000 N		Case 02: High load (approaching buckling condition) 10000 N	
Pile ID	**Length (m)**	**Lateral Displacement (m)**	**λ=P/Pcr**	**Lateral Displacement (m)**	**λ=P/Pcr**
1	15,63	0,0160	0,040	0,621	0,396
2	16,13	0,0170	0,042	0,668	0,421
3	9,25	0,0090	0,019	0,272	0,185
4	8,20	0,0080	0,012	0,621	0,396
5	10,03	0,0100	0,021	0,668	0,421
6	12,37	0,0130	0,025	0,272	0,185
7	14,57	0,0150	0,031	0,223	0,119
8	11,48	0,0120	0,028	0,305	0,210
9	9,21	0,0900	0,017	0,397	0,253
10	10,43	0,0110	0,023	0,503	0,305
11	10,01	0,0100	0,019	0,380	0,276
12	9,73	0,0100	0,021	0,267	0,172
13	15,15	0,0160	0,046	0,327	0,235
14	11,25	0,0120	0,024	0,297	0,191
15	13,19	0,0140	0,041	0,295	0,208
16	12,96	0,0140	0,040	0,670	0,457
17	9,76	0,0100	0,016	0,355	0,240
18	8,40	0,0090	0,013	0,533	0,407
19	9,11	0,0090	0,013	0,522	0,404
20	8,88	0,0090	0,016	0,279	0,162
21	6,99	0,0070	0,008	0,231	0,128
22	10,25	0,0100	0,017	0,250	0,126
23	11,17	0,0110	0,018	0,254	0,160
24	12,72	0,0130	0,024	0,181	0,075
25	7,81	0,0080	0,008	0,295	0,167
26	10,73	0,0110	0,024	0,325	0,176
27	10,86	0,0110	0,016	0,399	0,236

28	9,41	0,0100	0,025	0,203	0,077
29	8,05	0,0080	0,010	0,338	0,239
30	12,59	0,0130	0,019	0,309	0,157
31	14,41	0,0150	0,036	0,303	0,254
32	8,89	0,0090	0,019	0,214	0,099
33	14,25	0,0150	0,032	0,373	0,191
34	5,65	0,0060	0,004	0,536	0,355
35	20,83	0,0230	0,079	0,263	0,19
36	11,34	0,0120	0,020	0,339	0,196
37	9,09	0,0090	0,014	0,255	0,144
38	10,24	0,0100	0,015	0,290	0,152
39	17,00	0,0180	0,060	1,009	0,596
40	7,81	0,0080	0,014	0,218	0,139